①

**DTIC**
**ELECTE**
**S** FEB 2 3 1983 **D**

B

**UNITED STATES AIR FORCE**
**AIR UNIVERSITY**

# AIR FORCE INSTITUTE OF TECHNOLOGY

**Wright-Patterson Air Force Base, Ohio**

83   02   023   115

AFIT/GAE/AA/81D-19

APPLICATION OF
THE VORTEX-LATTICE METHOD
TO PROPELLER PERFORMANCE ANALYSIS

THESIS

AFIT/GAE/AA/81D-19    Marc L. Masquelier
                      1st Lt        USAF

DTIC
ELECTE
FEB 2 3 1983

B

**Approved for public release; distribution unlimited**

| REPORT DOCUMENTATION PAGE | | READ INSTRUCTIONS<br>BEFORE COMPLETING FORM |
|---|---|---|
| 1. REPORT NUMBER<br><br>AFIT/GAE/AA/81D-19 | 2. GOVT ACCESSION NO.<br>AD A124837 | 3. RECIPIENT'S CATALOG NUMBER |
| 4. TITLE *(and Subtitle)*<br><br>APPLICATION OF THE VORTEX-LATTICE METHOD<br>TO PROPELLER PERFORMANCE ANALYSIS | | 5. TYPE OF REPORT & PERIOD COVERED<br><br>Masters Thesis |
| | | 6. PERFORMING ORG. REPORT NUMBER |
| 7. AUTHOR(s)<br><br>1Lt Marc L. Masquelier | | 8. CONTRACT OR GRANT NUMBER(s) |
| 9. PERFORMING ORGANIZATION NAME AND ADDRESS<br><br>Air Force Institute of Technology (AFIT-EN)<br>Wright-Patterson AFB, Ohio 45433 | | 10. PROGRAM ELEMENT, PROJECT, TASK<br>AREA & WORK UNIT NUMBERS |
| 11. CONTROLLING OFFICE NAME AND ADDRESS<br>Aerodynamics & Performance Branch<br>Aeronautical Systems Division (ASD/ENFTA)<br>Wright-Patterson AFB, Ohio 45433 | | 12. REPORT DATE<br>July, 1982 |
| | | 13. NUMBER OF PAGES<br>102 |
| 14. MONITORING AGENCY NAME & ADDRESS*(if different from Controlling Office)* | | 15. SECURITY CLASS. *(of this report)*<br><br>Unclassified |
| | | 15a. DECLASSIFICATION/DOWNGRADING<br>SCHEDULE |

16. DISTRIBUTION STATEMENT *(of this Report)*

Approved for public release; distribution unlimited

17. DISTRIBUTION STATEMENT *(of the abstract entered in Block 20, if different from Report)*

18. SUPPLEMENTARY NOTES

Approved for public release; IAW AFR 190-17.

LYNN E. WOLAVER
Dean for Research and Professional Development
Air Force Institute of Technology (AIC)
Wright-Patterson AFB OH 45433

4 JAN 1988

19. KEY WORDS *(Continue on reverse side if necessary and identify by block number)*

Propellers
Vortex Lattice Method
Potential Flow Methods

20. ABSTRACT *(Continue on reverse side if necessary and identify by block number)*

The objective of this thesis is to examine the feasibility of
applying a vortex lattice method to propeller performance analysis.
This method allows the calculation of spanwise and chordwise pres-
sure distributions on thin propeller blades of arbitrary planform.
The research for this project involves the application of a
vortex lattice method to a propeller with twisted, non-cambered,
constant chord blades. The analysis assumes incompressible,

DD <sub>1 JAN 73</sub> FORM 1473    EDITION OF 1 NOV 65 IS OBSOLETE

20.   ABSTRACT

inviscid flow over thin sections.   The helical wake is modeled as
a series of straight vortex filament segments.

     A computer code has been developed which uses a vortex lattice
method to predict performance for propellers.   Results are shown
for several operating conditions, using various angle of attack
distributions, numbers of blades on the propeller, and advance
ratios.   Similar results are shown using the blade-element theory
for comparison.   Results indicate that this vortex lattice method
is applicable to initial propeller performance analysis.

AFIT/GAE/AA/81D-19

APPLICATION OF THE VORTEX-LATTICE METHOD

TO PROPELLER PERFORMANCE ANALYSIS

THESIS

Presented to the Faculty of the School of Engineering

of the Air Force Institute of Technology

Air University

in Partial Fulfillment of the

Requirements for the Degree of

Master of Science

by

Marc L. Masquelier, B.S.

1st Lt                    USAF

Graduate Aeronautical Engineering

July 1982

## Preface

This report is my attempt to expand the knowledge available in the area of propeller performance. My principal concern has been in adapting the Vortex-Lattice Method to the unique conditions found in the propeller problem.

The completion of this investigation required the assistance of the Aeronautical Systems Division, and the Air Force Institute of Technology. Without the support of these organizations, this report would not have been possible. Specifically, I would like to thank Mr. D. P. LeMaster of the Aeronautical Systems Division for providing computer support; Captain H. C. Briggs for his continual software assistance; and Major M. L. Smith for his guidance.

# Contents

# Contents

## List of Figures

## List of Tables

# List of Symbols

| | |
|---|---|
| A | panel area |
| AR | aspect ratio, $= b^2/A$ |
| b | panel span |
| B | number of blades on the propeller |
| B | blade span |
| c | section chord |
| $C_d$ | drag coefficient, $= D/qA$ |
| $C_l$ | lift coefficient, $= L/qA$ |
| $C_{li}$ | — section design lift coefficient (=0 for no camber) |
| $C_p$ | power coefficient, $= 2\pi C_q = P/\rho n^3 D^5$ |
| $C_q$ | torque coefficient, $= Q/\rho n^2 D^5$ |
| $C_t$ | thrust coefficient, $= T/\rho n^2 D^4$ |
| D | section drag |
| D | propeller diameter |
| h | blade thickness (=C) |
| J | propeller advance ratio, $= V/nD$ |
| L | section lift |
| n | propeller rotational speed, rps |
| N | propeller rotational speed, rpm |
| P | power output from the engine, also SHP |
| q | dynamic pressure, $= 1/2\rho\, V_{tot}^2$ |
| Q | torque due to aerodynamic loading |
| r | section radius, or radial position |
| R | propeller radius, $= D/2$ |

| | |
|---|---|
| T | thrust |
| $U_\infty$ | forward (axial) velocity, or flight speed |
| $V_{tot}$ | total section velocity due to $U_\infty$ & $r\omega$ |
| x | spanwise fraction, $= r/R$ |
| $\alpha$ | angle of attack, degrees |
| $\beta$ | blade angle, degrees |
| $\eta$ | propeller efficiency, $= T\, U_\infty / Q\omega$ |
| $\Lambda$ | sweep angle, degrees |
| $\rho$ | air density |
| $\sigma$ | section solidity, $= C \cdot B / \pi \cdot x \cdot D$ |
| $\phi$ | section wind angle, $= \arctan(U_\infty / r\omega)$ |
| $\omega$ | rotational speed, rad/s |

## Abstract

The objective of this thesis is to examine the feasibility of applying a vortex lattice method to propeller performance analysis. This method allows the calculation of spanwise and chordwise pressure distributions on thin propeller blades of arbitrary planform.

The research for this project involves the application of a vortex lattice method to a propeller with twisted, noncambered, constant chord blades. The analysis assumes incompressible, inviscid flow over thin sections. The helical wake is modeled as a series of straight vortex filament segments.

A computer code has been developed which uses a vortex lattice method to predict performance for propellers. Results are shown for several operating conditions, using various angle of attack distributions, numbers of blades on the propeller, and advance ratios. Similar results are shown using the blade-element theory for comparison. Results indicate that this vortex lattice method is applicable to initial propeller performance analysis.

# APPLICATION OF THE VORTEX-LATTICE METHOD
## TO PROPELLER PERFORMANCE ANALYSIS

## I. Introduction

### Background

Recent increases in the cost of fuel have revived interest in the propeller for next-generation aircraft propulsion. Advanced propeller designs for turboprop applications are being investigated by NASA-Lewis (Ref 1). These newer designs have low aspect ratios (less than five), swept blades, and six or more blades per propeller. The relative merits of the newer designs have been investigated through wind tunnel and flight tests. The method most often used for propeller analysis (blade element, or strip theory) is not accurate for these propeller configurations.

### Problem Statement

A need exists for an analytical method which will give an approximate pressure distribution on an arbitrary planform. The vortex lattice method is chosen for this role because of its widely demonstrated accuracy in wing applications.

The vortex lattice method developed here permits determination of both spanwise and chordwise distributions of lift over blade surfaces, and thus it is possible to find the bending and twisting moments of the individual blades.

Similarly, it is possible to use this method iteratively to find the blade camber surface which will generate a desired pressure distribution. This method has a great deal of potential to become a powerful design tool, from both an aerodynamic as well as a structural standpoint.

Modifications to the vortex lattice method for modelling propellers primarily consist of changes associated with the wake. The wake produced by a wing is nearly planar, while the wake of a propeller is helical. The wind velocity seen by a wing is assumed to be constant over the entire wing. The magnitude of the wind velocity is equal to the flight speed. The wind velocity seen by a propeller at any point on a blade is a vector sum of both the rotational and flight speed of the blade. These changes require some approximations and computational routines which are not necessary in the vortex lattice method for wings. With the advent of the high-speed digital computer, the execution of these routines becomes feasible.

To examine the accuracy of the vortex lattice method, a comparison is made with a proven method of propeller analysis - blade element theory. This method uses airfoil section theory applied to spanwise sections (strips) of a propeller blade to establish performance figures, these being thrust, torque and efficiency. Empirical corrections are made in order to compensate for three-dimensional (aspect ratio) effects,

compressibility, thickness and camber. Blade element theory is widely accepted in predicting performance for blades with traditional configurations (large aspect ratio, no sweepback). Comparison cases are presented using configurations for which the blade element method performs well.

Vortex lattice methods have been extensively applied to thin lifting surfaces, typically wings. In the propeller application, vortex lattice methods have several major advantages over blade element theory. These are due primarily to the method of modelling of the blade and the flow field. Vortex lattice methods account for both interference effects due to other blades and three dimensional effects due to a finite aspect ratio without any empirical correction factors required. No panel-specific aerodynamic parameters (such as $Cl_i$ and $\alpha_{OL}$) are required, since the camber can be approximated by placing a series of flat panels along the camber line. This flexibility allows a great deal of freedom in choosing propeller profiles, in that the user is not restricted to known airfoil profiles.

Several problems exist with the vortex lattice methods which are not encountered with blade element theory. A much more detailed geometry description is required to accurately model a configuration. An extensive program must be written and verified. Finally, computational runs are more expensive than those using strip theory. A vortex lattice solution should not be used if strip theory may be adequately applied.

3

This analysis is potentially most useful for studying non-standard propeller designs without requiring expensive and time-consuming flight or w_nd tunnel tests. The newer propellers, with many blades and large chords, cannot be effectively modeled by older methods. The objective of this study is to evaluate a method that can be used to rapidly investigate new propeller designs.

## Assumptions

This vortex lattice method assumes potential incompressible flow. On each panel, the total velocity (equal to the vector sum of flight speed and rotational speed) is calculated at a central position and is taken as a constant over the entire panel. The geometric parameters relating to flight conditions are applied in different parts of the solution: Zero angle-of-attack geometry (including blade twist) is represented in the main coefficient matrix, while angle of attack is represented in the forcing function vector. The blade is assumed to be rigid, with no deformation due to pressure variations along the blade. The wake is assumed to be fixed, with a constant helix angle (Fig 1).

## II. Development of Vortex Lattice Methods for Wings

### Background

Vortex lattice methods have been developed for calculating performance of thin, swept wings. The methods are used to find chordwise and spanwise distributions of lift and induced drag. They are a member of the class of discrete singularity methods. In this section, the basic concepts of a vortex lattice method are described as applied to a wing.

### Assumptions and Limitations

Most of the assumptions and limitations of the vortex lattice method for wings are associated with the modeling of the wake. The actual wake position for a wing at an angle of attack is a curved stream surface, but is assumed to lie along the wing chord line for analytical purposes. This assumption is acceptable at small angles of attack, where the deflection of the wake is small enough to be ignored. The model of the wing takes the wing camber line as a rigid, fixed fluid boundary.

### Governing Equations

Vortex lattice methods involve the construction and solution of a series of simultaneous linear equations to find a distribution of circulation on a lifting surface. The unknowns in these equations represent the circulation distribution on the lifting surface. The coefficients are geometrically

5

determined influence coefficients, each of which represents the downwash at a given point (control point) per unit circulation due to a given vortex. The forcing function represents the total downwash at a given control point. The general form of the equation is given in Eq 1, where A is the influence coefficient matrix, $\Gamma$ is the circulation distribution vector, and W is the downwash velocity distribution vector.

$$[A] \ \{\Gamma\} = \{W\} \tag{1}$$

The influence coefficient matrix A is determined by the blade geometry. The downwash velocity vector is determined by flight conditions. Equation 1 then becomes a statement of the flow tangency boundary condition at control points on the blade surface. A linear equation solver is used to solve for the circulation vector $\Gamma$. Once $\Gamma$ is known, the desired performance parameters are calculated. The major task is to determine this circulation vector.

## Influence Coefficient Matrix Assembly

The first portion of the analysis that will be discussed is the construction of the influence coefficient matrix, A.

In a vortex lattice method, a lifting surface that sheds a continuous vortex sheet is approximated by a finite number of horseshoe vortices. Each of these vortices is composed of a bound vortex and a pair of semi-infinite trailing vortices.

6

The wing to be analyzed is initially divided into a grid structure, or lattice. A complete description of the lattice is found in Appendix A. The bound vortex is placed along the quarter-chord of each element, on the mean camber line of the wing. Vortex filaments are shed from the ends of each bound vortex. The trailing vortices are shed along the stream surface coincident with the wake due to the lifting surface. For the physical wing, this wake follows a curved path, initially parallel to the bisector of the trailing edge of the wing, and asymptotically approaching the free-stream direction (Fig 2). For analytical purposes, the wake position is assumed to be always parallel to the wing axis. This makes the wake position independent of angle of attack. Since A depends only on the locations of the wake and the control points, A is also independent of angle of attack. In order to find a solution for any angle of attack, only the forcing function vector W must be altered. At small angles of attack, this wake position assumption is acceptable, since the solution is insensitive to any reasonable wake location for wings.

The Biot-Savart Law is used to calculate A. The Biot-Savart Law states that the velocity induced at any point due to a vortex filament of strength $\Gamma$ and length $dL$ is:

$$\overline{dV} = \frac{\Gamma}{4\pi} \frac{\overline{dL} \times \overline{r}}{|\overline{r}|^3} \tag{2}$$

where $\overline{dV}$ is the incremental velocity vector induced at an

7

arbitrary point due to a vortex filament segment dL; $\Gamma$ is the strength of the vortex filament segment; and $\bar{r}$ is the vector whose tail is located at the center of the filament segment, and whose head is located at the given point (control point). This equation is evaluated over all incremental line segments dL and the total velocity ($W_{ij}$) at point i due to horseshoe vortex j is found. This produces Eq 3, where

$$A_{ij} = \sum_{K=1}^{K} \frac{\overline{dL}_K \times {}_K\bar{r}_i}{|{}_K\bar{r}_i|^3}$$

and K is the total number of dL-segments associated with horseshoe vortex j. ${}_K r_i$ is the vector from filament segment K to control point i. $A_{ij}$ is a summation of this series of vector cross product operations. For straight vortex filaments, this summation can be evaluated using integrals whose limits are established by the filament endpoints, and the control point coordinates. This development is shown in Appendix B. Thus,

$$A_{ij} \cdot \Gamma_j = W_{ij} \tag{3}$$

The influence of an entire horseshoe vortex is found by integrating over all three portions of the horseshoe (bound vortex plus two semi-infinite legs), and adding the results. These results constitute the elements of the influence coefficient matrix A.

8

Each wing usually has a symmetric counterpart. This symmetry may be exploited if the flight conditions do not include yaw. For the port wing, only the y-axis coordinate values are different than those of the starboard wing, and only by a sign. Using this symmetry, the input geometry of one wing is used to produce the coordinates of its mirror image, which are used in the calculation of A.

## Calculation of the Boundary Condition Vector

To find a distribution of circulation on a wing, A must be calculated at points where the flow conditions are known. These are control points, located mid-panel span on the three-quarter panel chord line on the camber surface of the wing (Fig 3). If N horseshoe vortices exist in a flow field, N control points are required to enable the solution of the N simultaneous equations.

The right hand side of Eq 1 is the boundary condition vector, representing the component of the free stream velocity that is normal to the lifting surface at the control point. The boundary condition requires that there be no flow through the lifting surface. This condition is satisfied at the control point of each panel. The component of free stream velocity normal to the lifting surface at the control point must be cancelled by the velocity normal to the surface at the control point that is induced by all of the horseshoe vortices in the flow field (Fig 2). Therefore,

9

the boundary condition becomes

$$W_i + U_\infty(\sin(\alpha_i - \tan^{-1}(\frac{dz}{dx}_i))) = 0$$

where $W_i$ is the induced downwash velocity, $U_\infty$ is the free-stream velocity, $\alpha_i$ is the known angle of attack of the panel, and $(dz/dx)_i$ is the local slope of the camber line (Fig 4). For the case of the flat-plate at small angle of attack, $(dz/dx)_i = 0$, and $\sin(\alpha_i) = \alpha_i$. Then,

$$W_i = -U_\infty \cdot \alpha_i \qquad (4)$$

This vector is the right hand side of the general equation 1. The form of the equation becomes

$$[A_{ij}]\{\Gamma_j\} = -\{U_\infty \cdot \alpha_i\} \qquad (5)$$

The boundary condition vector is a product only of the free stream (which is spanwise constant for a wing) and the panel angle of attack (which is constant for a flat, non-twisted wing).

## Determination of Performance

Once A and the boundary condition vector are determined, the circulation distribution is calculated. A routine is used to solve the system of linear equations, determining the strength of each horseshoe vortex. From a distribution of horseshoe vortex strengths, and flight conditions, overall wing performance is calculated.

Each horseshoe vortex is composed of a bound vortex and two semi-infinite trailing vortices that are shed along the wing axis. The Kutta-Joukowski Theorem states that lifting force per unit span is equivalent to density multiplied by the cross product of the circulation vector and the free stream velocity vector. The cross product of a trailing vortex vector and a free stream vector is zero since they are parallel within the approximations made, so only the bound vortex produces a force. This force is a vector sum of lift and induced drag. The proportion of lift to induced drag is determined solely by local angle of attack.

Total wing configuration lift and induced drag is the summation of lift and drag for all of the panels in the flow field, which is twice the value of the starboard wing for the symmetrical case.

Wing pressure distribution is found knowing the total panel lifting force, and assuming constant pressure over each panel. The panel pressure is found by dividing the lifting force by the panel area.

## III.  Application of Vortex Lattice
### Methods to Propellers

The propeller introduces some unique conditions into
the problem which require a more complex set of assumptions
*regarding both the wake and the boundary condition vector.*

## Background

The vortex lattice method is selected as a solution
method to the propeller problem based upon the accuracy shown
in solving wing problems.  The other primary advantage of
implementing a vortex lattice method is the adaptability of
the method to solution by digital computer.

## Assumptions

A propeller can be viewed as a wing in a rotational flow
field.  Since the vortex filaments are shed parallel to the
local total velocity, the wake that is shed by a propeller
is helical.  In the case of the wing, the integration of the
Biot-Savart Law over an entire vortex filament can be per-
formed analytically because the modelled filament is straight.
The propeller wake cannot be easily solved in this manner
because of the helical wake.  The complete solution for the
construction of the influence coefficient matrix is found in
Appendix C.

In the analytical procedure for the wing, the solution
is calculated with the trailing vortex filaments extending

12

to infinity.  For the helical wake of the propeller, this is neither practical nor possible because this requires an infinite number of calculations.  To establish where the helical wake no longer significantly influences the solution, trial runs are required.

## Influence Coefficient Matrix Assembly

The influence coefficient matrix A is found using a procedure similar to that used for the wing.  The integration of the Biot-Savart Law is performed using a numerical representation of each vortex filament as a series of discrete line segments.  Each line segment dL is a small arc which is represented by a straight line (Fig 5).  The integral must be evaluated for every line segment-control point pairing in the flow field.  The velocity per unit of circulation induced at a given control point due to a horseshoe vortex is calculated by summing the Biot-Savart integrations of every dL for that given horseshoe.

Multiple blades on a propeller configuration are arranged symmetrically.  A two-bladed propeller sheds two wakes, each wake $\pi$ radians out of phase with the other.  In modelling a symmetrical configuration only the base blade geometry is entered.  This base blade establishes the locations of the control points and the horseshoe vortices.  By symmetry, the other (N-1) blades on an N bladed configuration will shed trailing vortices at intervals of $2\pi/N$ radians.  After per-

13

forming the summation of integrations over all of the vortex
filaments of the base blade, the procedure is repeated with
vortex filaments displaced $2\pi/N$ radians. This is repeated
for the vortex filaments from all (N-1) other blades. The
geometry of the remaining blades must not be implicitly
entered.

### Boundary Condition Vector

The boundary requirements for the propeller problem are
the same as those for the wing, in that no flow is allowed to
pass through the control points. The components of the bound-
ary condition vector for the propeller are more complex than
those of the wing boundary condition vector.

The right hand side of the B.L. eq. is the vector
$\{-U_\infty * \alpha_i\}$. In the case of the flat, untwisted wing, this
is constant for all panels. For the propeller, $U_\infty$ becomes
the local total velocity $(V_{tot})$, equal to the vector sum of
flight velocity and panel rotational velocity. The flight
direction is normal to the plane of rotation (Fig 6), there-
fore

$$V_{tot} = [U_\infty^2 + (r \cdot \omega)^2]^{\frac{1}{2}} \tag{6}$$

This vector points in the direction of the wind seen by
the propeller blade,

$$\beta = \tan^{-1}(\frac{U_\infty}{r \cdot \omega})$$

14

Each panel is oriented parallel to this local total velocity vector at the zero local angle of attack condition. Angle of attack distribution is a design parameter. This distribution is a function of the twist distribution and flight conditions.

In the final construction of the boundary condition vector, the assigned angle of attack is multiplied by the magnitude of the local total velocity for each panel. The product represents the component of local total velocity that acts normal to the panel surface, opposite and equal to the magnitude of the downwash induced at the control point by all of the vortices in the flow field.

## Determination of Performance

With A and the boundary condition vector, the distribution of circulation is calculated using a linear equation solver.

Once the circulation distribution along the propeller blade is found, the performance parameters are calculated. Since viscous effects are not included in this method, the lifting forces act normal to the panel. Lifting force is found using the relationship

$$L_j = (\rho \cdot b_j \cdot \overline{V}_{TOT,j} \times \Gamma_j) \cdot \overline{n} \qquad (7)$$

where $\rho$ is density, $b_j$ is the length of the bound vortex of panel j, and $V_{TOT}$ is the total panel velocity, combining flight and rotational velocity of section j. At small angles

15

of attack, the local velocity parallel to the panel can be approximated by the local total velocity. For small angles of attack, lift is represented by

$$L_j = \rho \cdot b_j \cdot |\overline{V}_{TOT,j}| \cdot |\Gamma_j|$$

The lift coefficient is found using the relationship

$$c_{\ell_j} = \frac{L_j}{\frac{1}{2} \cdot \rho \cdot V^2_{TOT,j} \cdot A_j} \tag{8}$$

For the test cases, where $\overline{V}_{TOT}$ is perpendicular to the bound vortices, and the area (A) is well approximated by the product of panel span and panel chord $C_j$, lift coefficient can be calculated by the relationship

$$c_{\ell_j} = \frac{2 \cdot \Gamma_j}{V_{TOT,j} \cdot C_j} \tag{9}$$

This panel lift coefficient is normalized based on panel dynamic pressure, a function of the local total velocity. An exact solution requires dynamic pressure to be a function of the component of local total velocity parallel to the panel. For small angles of attack, this component is accurately represented by the local total velocity.

Thrust and torque are calculated from lifting force. The lift force acts normal to the surface of the blade at the control point, resulting in force components which act both in the direction of flight and in the direction of

16

rotation (Fig 6). The component of force acting along the
flight path is thrust. The panel component of force acting
in the rotation direction, when multiplied by the distance
of that panel from the axis of rotation (the radius), is the
panel torque. Bending moment is found by multiplying panel
radius by panel thrust and summing over all panels. Propeller
efficiency is found by dividing the total output power (equal
to the product of thrust and flightspeed) by the total input
power (the product of torque and rotational velocity).

$$\eta = \frac{T \cdot U_\infty}{Q \cdot \omega} \tag{10}$$

Pressure distribution on the blades is a function of
the panel lift and the panel area. Pressure is assumed to
be uniform over an entire panel, which is acceptable for
small panels. Section pressure is calculated by dividing
the panel lifting force by the wetted area of the panel.
Calculating this for every panel produces a distribution of
pressure over the entire blade.

This process is used to completely define the perfor-
mance parameters of a propeller with thin, uncambered, twisted
blades in an incompressible, inviscid flow field.

17

## IV.  Approximations Used for
## Numerical Implementation

This section discusses the approximations used in the numerical integration of the analytical solution derived in Appendix C.

An analytical solution for a line integration, such as the integration in Appendix C, uses an infinite number of infinitesmal line segments to represent a line. A numerical solution uses a finite number of small line segments to approximate the analytical solution. The size assigned to each line segment determines the level of accuracy of the solution. Integrations using very small line segments produce accurate solutions, but require more computation time than those using larger line segments.

The size of the line segments of the wake filaments is determined by the size of the differential angle $(d\theta)$ multiplied by the distance from the axis of rotation to that specific filament. For all of the test cases run in this analysis, the differential angle $(d\theta)$ is assigned a value of $2\pi/100$ (Fig 5). Several check runs show virtually no change in solution for smaller values of $d\theta$. Filament segments larger than this produce numerically inaccurate results, as the assumption of small filament segments becomes increasingly inappropriate. For all grid systems, particularly those with panels having aspect ratios significantly less than unity,

18

the user must be sure that no filament passes through a control point, or the solution will diverge.

The use of the Biot-Savart Law, as one of the inputs, a vector with magnitude equal to the distance between the line segment and control point of interest. In implementing a numerical solution of the Biot-Savart Law with finite-length line segments, an approximation must be made for the point location of a line segment. The point used in the model to represent a line segment is the midpoint of the line segment.

The spanwise axial velocity profile is assumed to be constant for the model. In actual propeller flow fields, the velocity near the hub is greater than the velocity across the rest of the propeller face. Possible direct errors which may result from neglecting this include a faulty angle of attack distribution near the hub, and incorrect dynamic pressures near the hub.

The influence of a vortex filament segment on a control point diminishes with the square of the distance between the two. The first several segments, located on or near the blade, usually have the most impact on the influence coefficient. After less than one-quarter turn of the wake, the effect of the individual line segment is very small. Since the wake position varies with advance ratio, the position at which the remaining infinity of line segments becomes insignificant is defined in terms of diameters downstream of the configuration. The lift coefficient distribution for a case in which the wake

19

is truncated five (5) diameters downstream is the same as that distribution for a case in which a wake is truncated ten diameters downstream.

## V. Outline of Program

This section discusses the layout of the program used to implement this vortex lattice method.

The mesh generator takes the input geometry which describes the planform and divides it into an M x N grid, where M is the number of spanwise strips and N is the number of chordwise divisions. It also establishes the locations of the bound vortex endpoints, and the locations of the control points.

The assembler oversees the construction of A, the influence coefficient matrix. The assembler selects a control point identifier and a horseshoe vortex identifier. The driver subroutine recovers the control point coordinates and the bound vortex endpoint coordinates from memory. A helix generating routine is commanded by the driver to provide dL (incremental filament) endpoints, which are transferred to the kernel routine. The kernel routine uses the control point coordinates and the dL endpoints to calculate the incremental velocity induced by the dL on the designated control point. These are velocities per unit circulation of the horseshoe vortex. The driver sums the induced velocities as the kernel routine calculates them. As the driver completes one control point-horseshoe vortex pair, the summed induced velocity per unit circulation value is stored in memory by the assembler as a coefficient of A. This procedure is

repeated until all values of A are calculated.

The boundary condition vector routine is the next routine called by the main routine. The flight and rotational speeds are used to find the local total velocity at each panel. These panel velocities are multiplied by the panel angles of attack (an input parameter) to determine the components of local total velocity that act normal to the panel at the control point. These values are calculated to represent the overall velocity induced at the control points, since the sum of the normal local velocity and the velocity induced must equal zero to satisfy the boundary condition. These values are stored in memory as the boundary condition vector.

The IMSL routine LEQT1F retrieves the boundary condition vector and the matrix A from memory, and solves the system of equations $\{\Gamma\} = [A]^{-1} \{W\}$ for the values of circulation.

The blade performance routine accesses the flight condition and circulation values. These are used with the blade geometry to calculate panel lifting force, and ultimately, thrust and torque values for individual panels. The panel values of thrust and torque are summed to provide configuration thrust and torque.

## VI.  Results

### Initial Verification

To test the program, it is run with inputs which simulate a wing in a uniform flow.  This is accomplished by setting hub and tip radii very large, setting axial velocity very small, and truncating the wake at one-twelfth of a revolution (Fig 7).  The local total velocity along this configuration is virtually constant, and the wake filaments essentially straight.  The resulting values of circulation match experimental and analytical values of circulation for thin wings (e.g., those of Ref 4).  This shows that the mesh generation routine, the matrix assembly routines, the boundary condition routine, and the linear equation solving routine all perform correctly.  The performance routine is not tested in this run, since torque and thrust are not relevant factors for a wing.  Manual calculations show that this routine works correctly.

### Description of Test Cases

Test cases are established which approximate the typical operating regime of propellers.  In the test cases, a base blade configuration is used which has the following characteristics.

| | |
|---|---|
| Spanwise sections | 10 |
| Chordwise sections | 1 |

| Chord | 1 ft |
|---|---|
| Propeller Diameter | 16 ft |
| Hub Diameter | 4.8 ft |

These figures were chosen for ease of comparison with the blade element method. The resulting blade is shown in Fig 8. The blade element routine used divides the blade into seven unequally spaced blade segments (skewed toward the tip), therefore a lattice with more (ten) equally-spaced elements is appropriate for comparison. No comparison cases were run with more than one chordwise section, since the blade element method is incapable of analytically producing chordwise performance information.

A comparison is desired for a variety of flight conditions and propeller configurations. These configurations are run, using both the blade element and vortex lattice methods, to represent changes in the number of blades, the advance ratio, and the angle of attack distribution, on each blade.

Two and three bladed propellers are analyzed in the test cases for two reasons. First, blade element theory is well suited to analyzing propellers of this size. Furthermore, the amount of computer time required for the vortex lattice method is proportional to the square of the number of blades in a configuration. Two and three blades were chosen in the interest of economy, and in the interest of maintaining a good level of confidence in the blade element theory.

24

The advance ratio is fixed at either 1 or 2 for all of the cases. Advance ratio (J) is a function of flight speed (U∞) and rotational speed (n) ..r a propeller; for the cases run, rotational speed is fixed at 1000 rpm, and flight speed is varied to produce the desired advance ratio. These advance ratios bracket typical operating regimes for propeller aircraft in a cruise mode. -

Conventional propeller blades have a relatively flat, parabolic angle of attack distribution, with the highest strip design angle of attack located around mid-span. Two distributions of angle of attack are used in this analysis. The first distribution assigns all strips a five (5) degree attack angle to the relative wind. The second distribution assigns each strip a spanwise-varying quadratic angle of attack distribution, with the angle of attack equal to five degrees at mid-span, and two degrees at the hub and tip.

Table 1 shows the input conditions for all of the cases.

## Discussion of Results

As previously mentioned, all of the test cases are run at advance ratios of 1 or 2. For all of the cases, the effect of the wake becomes negligible after five or less revolutions, regardless of the number of blades. The results of varying the wake truncation point is shown in Table 2. The cases shown in Table 2 are lift coefficients for a single bladed propeller run with the conditions given for Case 1. The lift

TABLE 1

Case Descriptions

| Case Number | Number of Blades | Advance Ratio | alpha Distribution |
|---|---|---|---|
| 1 | 2 | 1 | Constant |
| 2 | 3 | 1 | Constant |
| 3 | 2 | 2 | Constant |
| 4 | 3 | 2 | Constant |
| 5 | 2 | 1 | Quadratic |
| 6 | 3 | 1 | Quadratic |
| 7 | 2 | 2 | Quadratic |
| 8 | 3 | 2 | Quadratic |

coefficients converge to the fourth decimal place after four revolutions. The tip strips are marginally less sensitive to wake truncation than the strips near the hub. The hub strips are positioned closest to the axis of propeller rotation, and are the strips most sensitive to the total array of shed wake filaments. In the hub position, the difference in lift co-efficient between the single rotation and five-rotation case is less than 3%.

The overall comparisons of the blade element cases to those of the vortex lattice method are shown in Table 3. Graphic displays of the comparison of spanwise distribution of lift coefficients are shown in Figure 9. Fig 10 shows

the strip lift coefficient distribution for a Case 1 run
with 10 strips and 5 chordwise sections. Fig 11 shows the
strip lift coefficient distribution for a Case 1 run with 10
strips and 10 chordwise sections. Comparison with Fig 9a
shows that the strip lift coefficient distribution for a 10 x
1 case is the same as that for a 10 x 10 case. The conver-
gence of the solution based on number of chordwise sections
is assumed for all other test cases. A spanwise and chord-
wise lift distribution calculated for Case 1 with 10 chord-
wise sections and 10 spanwise strips is shown in Figures 12.

TABLE 2

Effect of Varying Wake Truncation on Section
Lift Coefficient for a Single Bladed Propeller

LIFT COEFFICIENT COMPARISON

RADIAL FRACTION

| #REV | .3341 | .4024 | .4707 | .5390 | .6073 | .6756 | .7439 | .8122 | .8805 | .9488 |
|------|-------|-------|-------|-------|-------|-------|-------|-------|-------|-------|
| 1 | .3281 | .4091 | .4357 | .4415 | .4370 | .4253 | .4066 | .3780 | .3320 | .2465 |
| 2 | .3260 | .4067 | .4333 | .4392 | .4349 | .4235 | .4050 | .3766 | .3308 | .2457 |
| 3 | .3255 | .4061 | .4328 | .4387 | .4344 | .4230 | .4046 | .3763 | .3305 | .2455 |
| 4 | .3254 | .4059 | .4326 | .4385 | .4342 | .4229 | .4044 | .3761 | .3304 | .2454 |
| 5 | .3253 | .4059 | .4325 | .4385 | .4342 | .4228 | .4044 | .3761 | .3303 | .2454 |

Table 3 reveals some interesting trends. The vortex lat-
tice method shows a much greater sensitivity to the presence
of multiple blades in the flow field than the blade element

27

method. This sensitivity is partially due to the wake model, which does not alter the wake shape to reflect an increase in flow velocity through the propeller face. With this unaltered wake positioned unrealistically close to the propeller, the inverse-squared distance term of the Biot-Savart Law causes inaccuracies in the results.

## TABLE 3

### Comparison of Overall Performance - VLM vs BEM

#### VORTEX - LATTICE TEST RUNS

| CASE NUMBER | THRUST COEFFICIENT | POWER COEFFICIENT | INPUT POWER (SHP) | PERCENT EFFICIENCY |
|---|---|---|---|---|
| 1 | .02580 | .03231 | 501.9 | 80.0 |
| 2 | .02936 | .03674 | 570.8 | 80.0 |
| 3 | .03062 | .07335 | 1139.4 | 83.5 |
| 4 | .03489 | .08356 | 1298.0 | 83.5 |
| 5 | .01975 | .02357 | 366.1 | 83.9 |
| 6 | .02255 | .02691 | 418.1 | 83.9 |
| 7 | .02374 | .05471 | 849.9 | 86.7 |
| 8 | .07140 | .06255 | 971.7 | 86.7 |

#### BLADE - ELEMENT COMPARISON CASES

| CASE NUMBER | THRUST COEFFICIENT | POWER COEFFICIENT | INPUT POWER (SHP) | PERCENT EFFICIENCY |
|---|---|---|---|---|
| 1 | .03268 | .03594 | 558.2 | 90.9 |
| 2 | .04751 | .05159 | 801.4 | 92.1 |
| 3 | .04096 | .08719 | 1354.5 | 94.0 |
| 4 | .05991 | .12745 | 1979.8 | 94.0 |
| 5 | .02546 | .02623 | 407.4 | 97.1 |
| 6 | .03561 | .03806 | 591.2 | 93.6 |
| 7 | .03106 | .06512 | 1011.6 | 95.4 |
| 8 | .04538 | .09541 | 1482.1 | 95.1 |

28

The blade element method predicts total power input 10 to 20 percent higher than the vortex lattice method for the two-bladed cases. The three bladed cases show differences in input power of as much as 60 percent. This can be attributed to the wake position error as well, since the inaccurately close wake acts to decrease both thrust and torque of a propeller.

One of the main problems in using the blade element method for the inviscid, incompressible, thin non-cambered propeller is that all of the tabulated data in the supporting document include all of these effects to some degree. Therefore, the accuracy in using the blade element method while attempting to suppress these effects is questionable, as can be seen in some of the ideal efficiencies in Table 3.

Comparison of the efficiencies of vortex lattice method with those of blade element theory show a significant variation. The blade element method predicts efficiencies ten or more percentage points higher than those predicted by the vortex lattice method. Two factors cause this deviation; the artificial removal of compressibility effects from blade element theory, and the inaccurate positioning of the wake for vortex lattice method. A multiplying factor which includes the effects of compressibility is indeterminate at Mach numbers less than 0.4. The incompressible (M=0) factor is extrapolated from a graph used in the blade element report.

Availability of the compressibility factor for low mach numbers and a wake location routine would help alleviate this discrepancy. In Table 3, one of the blade element theory case efficiencies was calculated to be 97 percent. This figure is optimistic and can be attributed to the fairly coarse integration approximations required to calculate total thrust and torque figures, as well as the inability of the blade element method to accurately model non-typical propeller flow conditions (thin flat blade, inviscid incompressible flow).

Comparison of the lift coefficients of each case show mixed results. For all cases, the vortex lattice method predicts lower lift coefficients than blade element theory. The overall shapes of the lift coefficient-versus-radius curves were very similar, the greatest disagreement being with the distribution near the hub. This is to be expected, as the actual hub has not been modeled in this application of the vortex lattice procedure.

## Error Analysis

The first run of the program simulated a wing, as described earlier. The results agreed very well with those using conventional vortex lattice methods for wings, as well as with experimental data (Ref 4). Some of the disagreement of trial case results with those using known methods for multiple-bladed configurations are attributable to changes in the vortex lattice method associated with the rotating of

30

the flow field. These problems can be broken down into three areas:

1. Oversimplification of the wake model

2. Making the influence coefficient matrix independent of angle of attack

3. The hub model

The error analysis section addresses each of these problems.

The wake is modelled as a rigid helix with constant helix angle $\beta$, equal to $\tan^{-1}(U_\infty/R\omega)$. In an actual propeller flow field, the momentum theory (Appendix E) indicates that the wake extends axially and constricts radially as it moves downstream of the propeller (Fig 13). The helix angle must change with axial position to correctly model the wake.

The vortex lattice model for a wing does not require an accurate wake model because the effect of the wake is negligible at those points where the wake position is very inaccurate (far downstream). The influence of the wake of the propeller does not decay as rapidly, but rather has a periodically decaying influence on the blade. The non-axially-extended wake model positions the shed vortex filament segments too close to the propeller, artificially inducing an unrealistically high level of downwash on the blade. When a multiple-bladed configuration is modeled, this error is even more pronounced, as shown by the differences in power figures.

The influence coefficient matrix is independent of angle

31

of attack. This assumption is appropriate for the planar wing at small angles of attack, but is inadequate for the propeller. In a flow field which includes a very dense assembly of blades and rotating wakes, the accurate locations of all control points and bound vortices are critical to finding accurate results. A model with many blades, low aspect ratios, and low advance ratios at high angle of attack would be very sensitive to wake position. The inverse-squared distance term of the Biot-Savart Law forces the user to input accurate blade positions in order to produce accurate results.

The performance trends near the hub show significant deviation from those of the comparison method. Two factors cause this discrepancy. The first is the lack of a model of a hub, which is a solid axisymmetrical body on the axis of rotation. The strip closest to the axis of rotation in the configuration is effectively modelled as a tip section due to the absence of the hub model, therefore the circulation is low. A model is needed which analytically places a solid body on the axis of rotation to eliminate this tip effect. The second factor is the assumption of a constant axial velocity distribution across the propeller face. The hub acts as a flow constrictor, causing the flow about the hub to accelerate. The hub generates an increase in thrust and torque from the hub strip that is not represented in the current model.

## VII. Conclusions and Recommendations

The test cases show that the vortex lattice method predicts the lift coefficient trends reasonably well. Several improvements that would enhance the accuracy of the method include the following:

1. Modify the modelling of the wake to account for extension due to the increase in the axial velocity of the freestream, as demonstrated by the momentum theory. This will force the solution to be iterative, but also attenuate the extreme sensitivity of the routine to the presence of multiple blades in the flow field. Since induced velocity is a function of the inverse-squared distance from control point to wake filament segment, small changes in the wake position produce very significant changes in lift coefficient.

2. Include camber for the modelling of realistic planforms in order to model actual propellers. Doing this would allow for comparisons with existing propellers with known performance characteristics.

3. Modify the lattice generator to include arbitrary geometry. This modification would perform a series of biquadratic coordinate transformations on an input geometry, and establish a complete lattice configuration compatible with the rest of the program. This could include the modification suggested in 2.

4. Include a hub model. Placement of an analytical

33

solid body on the rotational axis would correct the distri-
bution of velocity on the propeller face, and moderate the
dip in the lift coefficient near the hub. This solid body
could be represented by a series of ring vortices or sources
centered about the axis of rotation.

5. Add a compressibility correction that accounts for
high but subsonic tip mach numbers. A Prandtl-Glauert trans-
formation could be used.

There is a significant amount of room for growth with
this method. Initial results indicate that even the coarse
model used produces impressive correlation with blade element
theory especially for blade circulation distribution. The
method's ability to produce chordwise pressure distributions
is also valuable as an analysis tool. It is presumed that
even greater accuracy is attainable, once these improvements
have been implemented.

# Bibliography

1. Duzan, J. F. "The NASA High-Speed Turboprop Program," NASA TM81561, Lewis Research Center, Cleveland, OH, 1980.

2. Hough, G. R. "Remarks on Vortex-Lattice Methods," Journal of Aircraft, Vol 10, No 5, 1973.

3. Hough, G. R. "Lattice Arrangements for Rapid Convergence," NASA SP405, May 1976.

4. Bertin, J. J. and Smith, M. L. "Aerodynamics for Engineers," Prentice-Hall, Englewood Cliffs, NJ, 1979.

5. Weber, J. and Brebner, G. G. "Low Speed Tests on 45-deg Swept-Back Wings, Part I. Pressure Measurements on Wings of Aspect Ratio 5," Reports and Memoranda 2882, Aeronautical Research Council, 1958.

6. Smith, M. L., Personal Notes, 1981.

7. Dommasch, D. O. "Airplane Aerodynamics," Pitman Publishing, New York, 1951.

8. Cooper, J. P. "The Linearized Inflow Propeller Strip Analysis," TR56-615, Wright Air Development Center, WPAFB, OH, 1957.

9. Clancy, L. J. "Aerodynamics," J. Wiley, New York, 1975.

## Appendix A - Construction of the Lattice

In a vortex-lattice method, a lifting surface is divided into a grid for analytical purposes. The spanwise divisions are made parallel to streamlines, coincidental with the trailing vortex filaments. Chordwise divisions are made along constant-percent-chord lines. For the wing, this produces a series of parallelogram-shaped lifting panels whose sides are straight (Fig 14). Horseshoe vortices are superimposed on these lifting surfaces. Each horseshoe is composed of three vortex filament pieces. Incompressible, thin airfoil theory indicates that the aerodynamic center of a surface is at the quarter-chord. For this reason, the finite (bound) vortex is placed along the panel quarter-chord. This bound vortex has endpoints located on the panel edges. The two trailing vortices comprise the rest of the horseshoe vortex. Each of these trailing vortices has an endpoint at the bound vortex, and trails off along a streamline to infinity. The three pieces form a horseshoe vortex. Note that the actual trailing vortex filaments are coincident with the panel edges, but are shown displaced for clarity in the figures.

Each horseshoe vortex is associated with one lifting panel. In order to model the entire flow field, the horseshoe vortices from all panels are assembled, thus forming a vortex lattice (Fig 14). The vortex lattice method

36

mathematically models this lattice.

The circulation at the tip of a three-dimensional wing must go to zero. A large number of spanwise strips is required to reasonably approximate this condition, using the mesh described above. A method which provides a more accurate solution to the problem (given the same number of spanwise divisions) is implemented. Hough (Ref 2) indicates that the tip should be inset by one quarter of a panel span. This has been shown to more accurately represent the absence of lift at the tip (Ref 3).

In this method, a given configuration is initially divided into a grid in the manner previously described. The grid is assumed to have N spanwise divisions and an overall span of length B (Fig 14). The panel span, b, is equal to B/N. The modification is implemented by decreasing the size of b to b′, such that

$$B - (N \cdot b') = .25 \cdot b'$$

which satisfies the quarter-tip inset requirement. Fig 3 shows the resulting configuration. Note that $\Delta b'$ is equal to b′/4, as prescribed by Hough. Solving for b′, then,

$$b' = \frac{B}{N+.25}$$

Hough shows that convergence to an accurate solution is found with significantly fewer strips than the vortex lattice solution not using the quarter-tip inset.

Each panel has a point at which the flow tangency boundary condition is satisfied. This is the control point, located at the panel three-quarter chord point, centered between the trailing vortices. Selection of the three-quarter chord point is justified in the following discussion from Ref 4.

The bound vortex filament is placed at the panel quarter chord (Fig 14). This filament induces a velocity v, where

$$v = \frac{\Gamma}{2\pi r}$$

at the control point of the panel, which is a distance r from the bound vortex. In order for the flow to be parallel to the wing at the control point, the freestream flow must be deflected through the angle of attack. This angle of attack can be approximately described by

$$\alpha \cong \sin\alpha = \frac{v}{V_{TOT}} \cong \frac{\Gamma}{2\pi r V_{TOT}}$$

For a flat plate at small angle of attack, thin airfoil theory shows that $C_{\ell_\alpha} = 2\pi$. From this, $C_\ell = 2\pi\alpha$, and panel lift is

$$\ell = \tfrac{1}{2}\rho V_{TOT}^2 \cdot C \cdot 2\pi\alpha = \rho \cdot V_{TOT} \cdot \Gamma$$

Combining these relationships

$$\pi\rho V_{TOT}^2 \cdot C \cdot \frac{\Gamma}{2\pi r V_{TOT}} = \rho \cdot V_{TOT} \cdot \Gamma$$

Then, solving for r,

38

$$r = C/2$$

Thus, the three-quarter chord point is an appropriate location for the control point. This position is typically used in vortex lattice applications.

For the propeller case, streamlines are not rectilinear, but helical. To model the propeller in a manner consistent with a vortex lattice method the spanwise divisions must follow streamlines. Using this framework, the spanwise divisions are made such that each division line lies along a line of constant distance from the axis of propeller rotation (Fig 15). Chordwise divisions are made along lines of constant-percent chord, similar to the method applied to the wing analysis.

Control points are located at the three-quarter-chord lines, just as in the case of the wing. Each control point is placed along the mean radius of its panel in order to be properly centered between the filament legs.

Tip inset is established in a manner similar to that of the wing. In the analysis, the wing span B is replaced by the distance from the propeller center of rotation to the tip.

The entire lattice with quarter panel tip inset and trailing vortices for the propeller is shown in Fig 16. This configuration is for a propeller using three spanwise divisions and two chordwise divisions.

## Appendix B - The Planar Wing Case

In this appendix, the procedure for calculating the lift on a wing in a uniform flow field will be described. The discussion follows that in Ref 4.

The velocity induced at a point due to a vortex filament segment of strength $\Gamma_n$ and length $d\ell$ is described by the Biot-Savart law,

$$d\overline{V} = \frac{\Gamma_n (d\overline{\ell} \times \overline{r})}{4\pi |r|^3} \qquad\qquad \text{B-1}$$

where $\overline{r}$ is the vector from the filament to the point. Referring to Fig 18a, the magnitude of the induced velocity is

$$dV = \frac{\Gamma_n \sin\theta d\ell}{4\pi r^2} \qquad\qquad \text{B-2}$$

For the wing, the velocity is induced by a horseshoe vortex composed of three straight filament segments. The effect of each segment is best calculated separately. The induced velocity is found for an arbitrary line segment AB, with vorticity vector directed from A to B. Let C be an arbitrary point in space whose normal distance to line AB is $r_p$. From geometry,

$$r = \frac{r_p}{\sin\theta} \qquad , \qquad d\ell = \frac{r_p}{\sin^2\theta} d\theta \qquad\qquad \text{B-3}$$

Integrating to find the velocity magnitude,

$$V = \frac{\Gamma_n}{4\pi r_p} \int_{\theta_1}^{\theta_2} \sin\theta d\theta = \frac{\Gamma_n}{4\pi r_p}(\cos\theta_1 - \cos\theta_2) \qquad\qquad \text{B-4}$$

40

For the infinite vortex filament, $\theta_1$ goes to 0, and $\theta_2$ goes to $\pi$, so

$$V = \frac{\Gamma_n}{2\pi r_p} \qquad \text{B-5}$$

which is the two-dimensional solution for induced velocity. Using the vector designations of AB, AC, and BC as shown in Fig 18a,

$$r_p = \frac{|\bar{r}_1 x \bar{r}_2|}{r_0} \quad \cos\theta_1 = \frac{\bar{r}_0 \cdot \bar{r}_1}{r_0 \; r_1} \quad \cos\theta_2 = \frac{\bar{r}_0 \cdot \bar{r}_2}{r_0 \; r_2} \qquad \text{B-6}$$

The direction of the induced velocity is described by the unit vector

$$\frac{\bar{r}_1 \; x \; \bar{r}_2}{|\bar{r}_1 \; x \; \bar{r}_2|} \qquad \text{B-7}$$

which, when substituted into Eq B-4 produces

$$\bar{v} = \frac{\Gamma_n}{4\pi} \frac{\bar{r}_1 \; x \; \bar{r}_2}{|\bar{r}_1 \; x \; \bar{r}_2|^2} \; [\bar{r}_0 \; (\frac{\bar{r}_1}{r_1} - \frac{\bar{r}_2}{r_2})] \qquad \text{B-8}$$

This is the general equation for the induced velocity due to a line vortex in the vortex lattice method. The following description shows how this can be applied to a horseshoe vortex.

Equation B-8 is used to find the velocity induced at a point in space by the horseshoe vortex shown in Fig 18b. Segment AB is the bound vortex, coinciding with the panel quarter chord. The trailing vortices are parallel to the x - axis. The resultant induced velocity vector is found by

41

summing the effects of each vortex filament.

For the bound vortex, segment AB,

$$\bar{r}_0 = \overline{AB} = (X_{2n}-X_{1n})\bar{i} + (y_{2n}-y_{1n})\bar{j} + (Z_{2n}-Z_{1n})\bar{k}$$

$$\bar{r}_1 = (X-X_{1n})\bar{i} + (y-y_{1n})\bar{j} + (Z-Z_{1n})\bar{k}$$

$$\bar{r}_2 = (X-X_{2n})\bar{i} + (y-y_{2n})\bar{j} + (Z-Z_{2n})\bar{k}$$

Using Eq B-8 to calculate the velocity induced at some point C(x,y,z) by vortex filament AB, (see Fig 18a),

$$\bar{V}_{AB} = \frac{\Gamma_n}{4\pi}\{F_{AC}1_{AB}\}\{F_{AC}2_{AB}\} \qquad\qquad B\text{-}9$$

where

$$F_{AC}1_{AB} = \frac{\bar{r}_1 \times \bar{r}_2}{|\bar{r}_1 \times \bar{r}_2|^2}$$

$$= \{[(y-y_{1n})(Z-Z_{2n})-(y-y_{2n})(Z-Z_{3n})]\hat{i}$$

$$-[(X-X_{1n})(Z-Z_{2n})-(X-X_{2n})(Z-Z_{3n})]\hat{j}$$

$$+[(X-X_{1n})(y-y_{2n})-(X-X_{2n})(y-y_{1n})]\hat{k}\}/$$

$$\{[(y-y_{1n})(Z-Z_{2n})-(y-y_{2n})(Z-Z_{1n})]^2$$

$$+[(X-X_{1n})(Z-Z_{2n})-(X-X_{2n})(Z-Z_{3n})]^2$$

$$+[(X-X_{1n})(y-y_{2n})-(X-X_{2n})(y-y_{3n})]^2\}$$

and

$$\{F_{AC}2_{AB}\} = (\bar{r}_0 \cdot \frac{\bar{r}_1}{r_1} - \bar{r}_0 \cdot \frac{\bar{r}_2}{r_2})$$

42

$$= \{ i \, (X_{2n}-X_{1n})(X-X_{1n})+(Y_{2n}-Y_{1n})(y-y_{3n})+(Z_{2n}-Z_{3n})(Z-Z_{1n})]/$$

$$[(X-X_{1n})^2+(y-y_{1n})^2+(Z-Z_{1n})^2]^{\frac{1}{2}}$$

$$-[(X_{2n}-X_{1n})(X-X_{2n})+(Y_{2n}-Y_{1n})(y-y_{2n})+(Z_{2n}-Z_{1n})(Z-Z_{2n})]/$$

$$[(X-X_{2n})^2+(y-y_{2n})^2+(Z-Z_{2n})^2]^{\frac{1}{2}} \}$$

To find the velocity induced by the trailing vortex that extends from A, the velocity induced by the collinear, finite-length filament AD is first calculated. Since $\overline{r}_0$ is in the direction of the vorticity vector,

$$\overline{r}_0 = \overline{DA} = (X_{1n}-X_{3n})\overline{i}$$

$$\overline{r}_1 = (X-X_{3n})\overline{i} + (y-y_{1n})\overline{j} + (Z-Z_{1n})\overline{k}$$

$$\overline{r}_2 = (X-X_{1n})\overline{i} + (y-y_{1n})\overline{j} + (Z-Z_{1n})\overline{k}$$

as shown in Fig 13b. Thus, the induced velocity is

$$\overline{V}_{AD} = \frac{\Gamma_n}{4\pi} \{F_{AC}1_{AD}\}\{F_{AC}2_{AD}\}$$

where

$$\{F_{AC}1_{AD}\} = \frac{(Z-Z_{1n})\overline{j} + (y_{1n}-y)\overline{k}}{[(Z-Z_{1n})^2+(y_{1n}-y)^2](X_{3n}-X_{1n})}$$

and

$$\{F_{AC}2_{AD}\} = (X_{3n}-X_{1n}) \{ \frac{X_{3n}-X}{[(X-X_{3n})^2+(y-y_{1n})^2+(Z-Z_{1n})^2]^{\frac{1}{2}}}$$

$$+ \frac{X-X_{1n}}{[(X-X_{1n})^2+(y-y_{1n})^2+(Z-Z_{1n})^2]^{\frac{1}{2}}} \}$$

Letting $x_3$ go to infinity, the first term of $\{F_{AC}{}^2{}_{AD}\}$ goes
to 1. Therefore, the velocity induced by the vortex fila-
ment which extends from A to infinity parallel to the x axis
is given by

$$\overline{V}_{A_\infty} = \frac{\Gamma_n}{4} \left[ \frac{(z+z_{1n})\hat{d}+(y_{1n}-y)\hat{k}}{(z+z_{1n})^2+(y_{1n}-y)^2} \right] \left[ 1 + \frac{X - X_{1n}}{\{(X-X_{1n})^2+(y-y_{1n})+(z-z_{1n})^2\}^{\frac{1}{2}}} \right]$$

B-10

Similarly, the velocity induced by the vortex filament
that extends from B to infinity parallel to the x axis is

$$\overline{V}_{B_\infty} = \frac{-\Gamma_n}{4\pi} \left[ \frac{(z-z_{2n})\hat{d}+(y_{2n}-y)\hat{k}}{(z-z_{2n})^2+(y_{2n}-y)^2} \right] \left[ 1 + \frac{X - X_{2n}}{\{(X-X_{2n})^2+(y-y_{2n})^2+(z-z_{2n})^2\}^{\frac{1}{2}}} \right]$$

B-11

The total velocity at an arbitrary point $(x,y,z)$ due to
a horseshoe vortex representing a portion of a lifting sur-
face (panel) is the sum of the components given in Eqs B-9 to
B-11. The point $(x,y,z)$ is designated the control point of
panel m, with coordinates $(x_m, y_m, z_m)$. The velocity at this
mth control point due to the horseshoe vortex representing
the nth panel is designated $\overline{V}m,n$. From Eqs B-9 through B-11,

$$\overline{V}_{m,n} = \overline{C}_{m,n} \, \Gamma_n$$

B-12

where $\overline{C}_{m,n}$ is the influence coefficient which depends strictly
on the relative geometries of the nth horseshoe vortex and
the mth control point. Since the governing equation is

44

linear, the velocities induced by the 2N vortices are added together to obtain an expression for the total induced velocity at the mth control point:

$$\overline{V}_m = \sum_{n=1}^{2N} \overline{C}_{m,n} \; \Gamma_n \qquad\qquad \text{B-13}$$

There exists one such equation for each control point, or a total of 2N equations.

Using the above development, it is possible to find the velocity induced at any point in space, given the geometry of the problem and the circulation strengths of all of the vortices. These strengths are not initially known, however. To find these strengths, it is necessary to establish a boundary condition. The boundary condition is that the surface must be a stream surface, hence the flow is parallel to the surface at every control point (the control point location described in Appendix A). To satisfy this condition, the total induced velocity at a given control point must be cancelled by the component of freestream velocity that is normal to the surface. Referring to Fig 4, the tangency condition for no dihedral yields

$$-u_m \sin\delta + w_m \cos\delta + U \sin(\alpha-\delta) = 0 \qquad\qquad \text{B-14}$$

where $\delta$ is the slope of the mean camber line at the control point, or

$$\delta = \tan^{-1}\left(\frac{dz}{dx}\right)_m$$

45

For wings where the slope of the mean camber line is small
and which are at small angles of attack, this equation can
be approximated by

$$-u_m \, \delta + w_m + U_\infty(\alpha-\delta) = 0 \qquad \text{B-15}$$

For the case of the flat plate, this further reduces to

$$w_m = -U_\infty \alpha \qquad \text{B-16}$$

These approximations are consistent with the assumptions of
linearized theory.  The unknown circulation strengths required
to satisfy these boundary conditions are found by solving the
system of linear equations developed earlier in this appendix.

Eqs B-9 through B-15 are those for a VLM where the trail-
ing vortices are parallel to the x axis.  These equations can
be applied to a relatively simple geometry, a planar wing
(one that lies in the x-y plane).  For a planar wing, $z_{1n} =$
$z_{2n} = 0$ for all of the bound vortices.  Furthermore, $z_m = 0$
for all of the control points.  Thus, for the planar wing:

$$\overline{V}_{AB} = \frac{\Gamma_n}{4\pi} \left[ \frac{\hat{k}}{(X_m-X_{1n})(Y_m-Y_{2n})-(X_m-X_{2n})(Y_m-Y_{1n})} \right]$$

$$\left[ \frac{(X_{2n}-X_{1n})(X_m-X_{1n})+(Y_{2n}-Y_{1n})(Y_m-Y_{1n})}{((X_m-X_{1n})^2+(Y_m-Y_{1n}))^2} \right.$$

$$\left. - \frac{(X_{2n}-X_{1n})(X_m-X_{2n})+(Y_{2n}-Y_{1n})(Y_m-Y_{1n})}{((X_m-X_{2n})^2+(Y_m-Y_{2n})^2)^{\frac{1}{2}}} \right]$$

$$\overline{V}_{A\infty} = \frac{\Gamma_n}{4\pi} \frac{\hat{k}}{Y_{1n}-Y_m} \left[ 1 + \frac{X_m - X_{1n}}{((X_m-X_{1n})^2+(Y_m-Y_{1n})^2)^{\frac{1}{2}}} \right]$$

$$\overline{V}_{B\infty} = \frac{\Gamma_n}{4\pi} \frac{\hat{k}}{Y_{2n}-Y_m} \left[ 1 + \frac{X_m - X_{2n}}{((X_m-X_{2n})^2+(Y_m-Y_{2n})^2)^{\frac{1}{2}}} \right] \qquad \text{B-16}$$

Note that, for the planar wing, all three components of the vortex representing the nth panel induce a velocity at the control point of the mth panel which is in the z direction (i.e., a downwash). Therefore, we can simplify Eq B-16 by combining the components into one expression:

$$W_{m,n} \doteq \frac{\Gamma_n}{4\pi} \left\{ \frac{1}{(X_m-X_{1n})(Y_m-Y_{2n})-(X_m-X_{2n})(Y_m-Y_{1n})} \right.$$

$$\left[ \frac{(X_{2n}-X_{1n})(X_m-X_{1n})+(Y_{2n}-Y_{1n})(Y_m-Y_{2n})}{((X_m-X_{1n})^2+(Y_m-Y_{1n})^2)^{\frac{1}{2}}} \right.$$

$$\left. - \frac{(X_{2n}-X_{1n})(X_m-X_{2n})+(Y_{2n}-Y_{1n})(Y_m-Y_{2n})}{((X_m-X_{2n})^2+(Y_m-Y_{2n})^2)^{\frac{1}{2}}} \right]$$

$$+ \frac{1}{Y_{1n}-Y_m} \left[ 1 + \frac{X_m - X_{1n}}{((X_m-X_{1n})^2+(Y_m-Y_{1n})^2)^{\frac{1}{2}}} \right]$$

$$\left. - \frac{1}{Y_{2n}-Y_m} \left[ 1 + \frac{X_m - X_{2n}}{((X_m-X_{2n})^2+(Y_m-Y_{2n})^2)^{\frac{1}{2}}} \right] \right\} \qquad \text{B-17}$$

Summing the contributions of all the vortices to the downwash at the control point of the mth panel:

$$W_m = \sum_{n=1}^{2N} W_{m,n} \qquad \text{B-18}$$

47

The tangency conditions as defined by Eqs B-14 and B-15 will now be applied. Since the wing is planar, $(dz/dx) = 0$ everywhere and there is no dihedral. The component of the freestream velocity perpendicular to the wing is $U_\infty \sin \alpha$ at any point on the wing. Thus, the resultant flow will be tangent to the wing if the total vortex-induced downwash at the control point of the mth panel which is calculated using Eq B-18, balances the normal component of the freestream velocity:

$$w_m + U_\infty \sin \alpha = 0 \qquad\qquad\qquad \text{B-19}$$

For small angles of attack,

$$w_m \approx -U_\infty \alpha \qquad\qquad\qquad \text{B-20}$$

The following example shows how a VLM is used to find the circulation and lift about a swept, planar wing (from Ref 4).

The wing to be analyzed has an aspect ratio of five (5), a taper ratio of unity, and an uncambered panel (Fig 14). Since the taper ratio is unity, the leading edge, the quarter-chord line, the three-quarter-chord line, and the trailing edge all have the same sweep, 45 degrees. Since

$$AR = 5 = B^2/S$$

and since for a swept, untapered wing

$$S = B\, c$$

it is clear that $B = 5\, c$. Using this relation, it is possible

48

to calculate all of the necessary coordinates in terms of
the parameter B. Therefore, the solution does not require
knowledge of the physical dimensions of the configuration.

The flow field under consideration is symmetric with
respect to the x-z plane (i.e., there is no yaw). Thus, the
lift force acting at a point on the starboard wing (+y) is
equal to that at the corresponding point on the port wing
(-y). Because of symmetry, we need only to solve for the
strengths of the vortices of the starboard wing. Furthermore,
we need to apply the tangency condition only at the control
points of the starboard wing. However, we must remember to
include the contributions of the horseshoe vortices of the
port wing to the velocities induced at control points of the
starboard wing. Thus, for this planar symmetric flow, Eq
B-18 becomes

$$w_m = \sum_{n=1}^{N} w_{m,n_s} + \sum_{n=1}^{N} w_{m,n_p}$$

where the symbols s and p represent the starboard and port
wings, respectively.

The planform of the starboard wing is divided into four
panels, each panel extending from the leading edge to the
trailing edge. As before, the bound portion of each horse-
shoe vortex coincides with the quarter-chord line of its
panel and the trailing vortices are in the plane of the wing,
parallel to the x axis. The control points are designated
by the circles in Fig 15. Recall that $(x_m, y_m, 0)$ are the

49

coordinates of a given control point and that $(x_{1n}, v_{1n}, 0)$ and $(x_{2n}, v_{2n}, 0)$ are the coordinates of the ends of the bound vortex filament AB.

Using Eq B-17 to calculate the downwash velocity at the control point (CP) of panel 1 induced by the horseshoe vortex of panel 1 of the starboard wing:

$$w_{1,1_s} = \frac{\Gamma_1}{4\pi} \left\{ \frac{-1}{(.1625B)(-.0625B) - (.0375B)(.0625B)} \right.$$

$$\left[ \frac{(.125B)(.1625B) + (.125B)(.0625B)}{((.1625B)^2 + (.0625B)^2)^{\frac{1}{2}}} \right.$$

$$\left. - \frac{(.125B)(.0375B) + (.125B)(.0625B)}{((.0375B)^2 + (-.0625B)^2)^{\frac{1}{2}}} \right]$$

$$+ \frac{1}{-.0625B} \left[ 1 + \frac{.1625B}{((.1625B)^2 + (.0625B)^2)^{\frac{1}{2}}} \right]$$

$$\left. - \frac{1}{.0625B} \left[ 1 + \frac{.0375B}{((.0375B)^2 + (.0625B)^2)^{\frac{1}{2}}} \right] \right\}$$

$$= \frac{\Gamma_1}{4\pi B} \ (-16.353 - 30.934 - 24.232)$$

Note that, as one would expect, each of the vortex elements induces a negative (downward) component of velocity at the control point. In addition, the velocity induced by the vortex trailing from A to $\infty$ is greatest in magnitude. Adding the components together, we find

$$w_{1,1_s} = \frac{\Gamma_1}{4\pi B} \ (-71.5187)$$

50

The downwash velocity at the CP of panel no. 1 (of the starboard wing) induced by the horseshoe vortex of panel no. 1 of the port wing is:

$$W_{1,1_p} = \frac{\Gamma 1}{4\pi} \left\{ \frac{1}{(.0375B)(.0625B)-(.1625B)(.1875B)} \right.$$

$$\left[ \frac{(-.1250B)(.0375B)+(.1250B)(.1875B)}{((.0375B)^2+(.1875B)^2)^{\frac{1}{2}}} \right.$$

$$\left. - \frac{(-.1250B)(.1625B)+(.1250B)(.0625B)}{((.1625B)^2+(.0625B)^2)^{\frac{1}{2}}} \right]$$

$$+ \frac{1}{(-.1875B)}\left[ 1 - \frac{.0375B}{((.0375B)^2 + (.1875B)^2)^{\frac{1}{2}}} \right]$$

$$\left. - \frac{1}{(-.0625B)}\left[ 1 - \frac{.1625B}{((.1625B)^2 + (.0625B)^2)^{\frac{1}{2}}} \right] \right\}$$

$$= \frac{\Gamma_1}{4\pi B} \{18.515\}$$

Evaluating all of the various components (or influence coefficients), we find that at control point 1:

$$W_1 = \frac{1}{4\pi B} [ (-71.5187\Gamma_1+11.2933\Gamma_2+1.0757\Gamma_3+.3775\Gamma_4)_s$$

$$+ (18.5150\Gamma_1+2.0504\Gamma_2+.5887\Gamma_3+.2659\Gamma_4)_p ]$$

At CP 2:

$$W_2 = \frac{1}{4\pi B} [ (20.2174\Gamma_1-71.5187\Gamma_2+11.2933\Gamma_3+1.0757\Gamma_4)_s$$

$$+ (3.6144\Gamma_1+1.1742\Gamma_2+.4903\Gamma_3+.2503\Gamma_4)_p ]$$

At CP 3:

$$W_3 = \frac{1}{4\pi B} \left[ (3.8792\Gamma_1 + 20.2174\Gamma_2 - 71.5187\Gamma_3 + 11.2933\Gamma_4)_s \right.$$

$$\left. + (1.5480\Gamma_1 + .7227\Gamma_2 + .3776\Gamma_3 + .2179\Gamma_4)_p \right]$$

At CP 4:

$$W_4 = \frac{1}{4\pi B} \left[ (1.6334\Gamma_1 + 3.8792\Gamma_2 + 20.2174\Gamma_3 - 71.5187\Gamma_4)_s \right.$$

$$\left. + (.8609\Gamma_1 + .4834\Gamma_2 + .2895\Gamma_3 + .1836\Gamma_4)_p \right]$$

Since it is a planar wing with no dihedral, the no-flow condition of Eq B-20 requires that

$$W_1 = W_2 = W_3 = W_4 = -U_\infty \alpha$$

Thus,

$$-53.0037\Gamma_1 + 13.3437\Gamma_2 + 1.6644\Gamma_3 + .6434\Gamma_4 = -4\pi B U_\infty \alpha$$

$$23.8318\Gamma_1 - 70.3445\Gamma_2 + 11.7836\Gamma_3 + 1.3260\Gamma_4 = 4\pi B U_\infty \alpha$$

$$5.4272\Gamma_1 + 20.9401\Gamma_2 - 71.1411\Gamma_3 + 11.5112\Gamma_4 = -4\pi B U_\infty \alpha$$

$$2.4943\Gamma_1 + 4.3626\Gamma_2 + 20.5069\Gamma_3 - 71.3351\Gamma_4 = -4\pi B U_\infty \alpha$$

Solving for $\Gamma_1, \Gamma_2, \Gamma_3,$ and $\Gamma_4$, we find that

$$\Gamma_1 = .02728 \cdot (4\pi B U_\infty \alpha)$$

$$\Gamma_2 = .02869 \cdot (4\pi B U_\infty \alpha)$$

$$\Gamma_3 = .02841 \cdot (4\pi B U_\infty \alpha)$$

$$\Gamma_4 = .02490 \cdot (4\pi B U_\infty \alpha)$$

Having determined the strength of each of the vortices by satisfying the boundary conditions that the flow is tangent

to the surface at each of the control points, the lift of
the wing may be calculated. Since the panels extend from
the leading edge to the trailing edge, the lift acting on
the nth panel is

$$\ell n = \rho \cdot U_\infty \cdot \Gamma n$$

which is also the lift per unit span. Since the flow is
symmetric, the total lift for the wing is

$$L = 2 \int_0^{.5B} \rho \cdot U_\infty \cdot \Gamma(y) dy$$

or, in terms of the finite-element panels,

$$L = 2\rho U_\infty \sum_{n=1}^{4} \Gamma n \Delta yn$$

Since $\Delta y = 0.125B$ for each panel,

$$L = 2\rho U_\infty 4\pi B U_\infty \alpha (.02728+.02869+.02841+.02490) \cdot .125B$$

$$= \rho U_\infty^2 b^2 \pi \alpha (.10928)$$

To calculate the lift coefficient, recall that $A = b \cdot c$
and $b = 5 c$ for this wing. Therefore,

$$C_L = \frac{L}{qA} = 1.0928\pi\alpha$$

Furthermore,

$$C_{L_\alpha} = \frac{dC_L}{d\alpha} = .05992/degree$$

The theoretical lift curve generated using VLM is com-
pared in Fig 20 with experimental results reported in Ref 5.
The experimentally-determined values of the lift coefficient

53

are for a wing of constant chord and of constant section, which is swept 45 degrees and which has an aspect ratio of five.  The theoretical lift coefficients are in good agreement with the experimental values.

## Appendix C - Analytical Wake Integration

The Biot-Savart Law is used to find the velocity induced by a vortex filament segment at a point in space. This calculation is performed for every vortex filament segment in a horseshoe vortex to find the velocity due to the entire horseshoe vortex. In this appendix, the integration for the case of a single semi-infinite filament segment of a helical wake is developed.

Following reference 6, let P be a point on a blade surface. Let the location of P be defined in the reference frame of the rotating disk, as $(r_p, \theta_p, z_p)$. Assume P emits a helical vortex filament defined by

$$X = r_p \cos\theta \quad , \quad y = r_p \sin\theta \quad , \quad Z = -k\theta$$

This filament will induce a velocity at a point Q. Let the coordinates of Q be $(r_Q, \theta_Q, z_Q)$.

The velocity induced at Q by a segment $\overline{d\ell}$ of the helical filament emitted by P is

$$\delta\overline{V}_{Q,p} = \frac{\Gamma_p}{4\pi} \frac{\overline{d\ell} \times (\overline{r}_Q - \overline{r})}{|(\overline{r}_Q - \overline{r})|^3}$$

where $\overline{r}$ is a vector from the origin to $\overline{d\ell}$, and $\overline{r}_Q$ is a vector from the origin to Q. $\overline{d\ell}$ is an infinitesmal segment of the helical vortex filament in the direction of the vorticity vector. Therefore,

$$\overline{d\ell} = -r_p \sin\theta d\theta \overline{i} + r_p \cos\theta d\theta \overline{j} - kd\theta \overline{k}$$

$$\overline{r}_Q = X_Q \overline{i} + y_Q \overline{j} + z_Q \overline{k}$$

$$\overline{r} = X_p \overline{i} + y_p \overline{j} + z_p \overline{k} = r\cos\theta \overline{i} + r\sin\theta \overline{j} - k\theta \overline{k}$$

Inserting these relationships into the expression of the Biot-Savart Law,

$$\delta \overline{V}_{Q,p} = \frac{\Gamma p}{4\pi} \frac{[-r\sin\theta d\theta \overline{i} + r\cos\theta d\theta \overline{j} - kd\theta \overline{k}] \times [(X_Q-X)\overline{i} + (y_Q-y)\overline{j} + (Z_Q)\overline{k}]}{[(X_Q-X)^2 + (y_Q-y)^2 + (Z_Q)^2]^{3/2}}$$

Separating these into i, j, and k components,

$$\delta \overline{V}_{Q,p} = \frac{\Gamma p}{4\pi} \frac{\{-r(y_Q-y)\sin\theta d\theta \overline{k} + rZ_Q \sin\theta d\theta \overline{j} - r(X_Q-X)\cos\theta d\theta \overline{k}}{[(X_Q-X)^2 + (y_Q-y)^2 + z_Q^2]^{3/2}}$$

$$\frac{+rZ_Q \cos\theta d\theta \overline{i} - k(X_Q-X)d\theta \overline{j} + kd\theta(y_Q-y)\overline{i}\}}{}$$

Finally,

$$\delta \overline{V}_{Q,p} = \frac{\Gamma p}{4\pi} \frac{\{\overline{i}[k(y_Q-y)+r(Z_Q)\cos\theta]d\theta + \overline{j}[-k(X_Q-X)+rZ_Q\sin\theta]d\theta}{[(X_Q-X)^2 + (y_Q-y)^2 + (Z_Q)^2]^{3/2}}$$

$$\frac{+\overline{k}[-r(y_Q-y)\sin\theta - r(X_Q-X)\cos\theta]d\theta\}}{}$$

This expression represents the velocity induced at point P due to infinitesmal vortex filament Q. The velocity at Q induced by an entire horseshoe vortex P is

$$\overline{V}_{Q,p} = \frac{\Gamma p}{4\pi} \int_{-\infty}^{0} \frac{\{\overline{i}[k(y_Q - r\sin\theta) + r(Z_Q + k\theta)\cos\theta]d\theta + \overline{j}[-k(X_Q - r\cos\theta)}{[(X_Q - r\cos\theta)^2 + (y_Q - r\sin\theta)^2 + (Z_Q + k\theta)^2]^{3/2}}$$

$$\frac{+r(Z_Q + k\theta)\sin\theta]d\theta + \overline{k}[-r(y_Q - r\sin\theta)\sin\theta - r(X_Q - r\cos\theta)\cos\theta]d\theta\}}{[(X_Q - r\cos\theta)^2 + (y_Q - r\sin\theta)^2 + (Z_Q + k\theta)^2]^{3/2}}$$

     This is integrable if x and y are zero.  For all other cases, a numerical solution to the integration is required.

## Appendix D – Blade Element Method

The blade element method uses airfoil data to predict the performance of a propeller configuration.

Lift and drag coefficients are obtained by assuming that the induced flow past a blade element is the same as past a wing of aspect ratio 6 (Ref 7). The forces on the blade element of width dr and chord c are shown in Fig 6.

The thrust due to the element is equal to the sum of the lift and drag forces perpendicular to the plane of rotation. From Fig. 6,.

$$dT = dL \cos \phi - dD \sin \phi$$

$$= \tfrac{1}{2} \rho V_{TOT}^2 \, c \, dr \, (C_L \cos \phi - C_D \sin \phi)$$

Similarly, the torque due to the element is equal to the sum of the lift and drag forces in the plane of rotation multiplied by the mean element radius, or

$$dQ = r(dL \sin \phi + dD \cos \phi)$$

$$= \tfrac{1}{2} \rho V_{TOT}^2 \, c \, r \, dr \, (C_L \sin \phi + C_D \cos \phi)$$

Since efficiency is defined as output (thrust) power divided by input (torque) power,

$$\eta = \frac{U_\infty \, dT}{2\pi n \, dQ}$$

$$= \frac{U_\infty}{2\pi nr} \cdot \frac{C_L \cos \phi - C_D \sin \phi}{C_L \sin \phi + C_D \cos \phi}$$

The values of dT and dQ must be found at every element in order to find total thrust (T), total torque (Q), and hence input power (P) for the configuration. These quantities are found using the equations

$$T = \int BdT = B\int_{r_{HUB}}^{r_{TIP}} \tfrac{1}{2} \rho V_{TOT}^2 \; c(C_L\cos\phi - C_D\sin\phi)dr$$

$$Q = \int BdQ = B\int_{r_{HUB}}^{r_{TIP}} \tfrac{1}{2} \rho V_{TOT}^2 \; c(C_L\sin\phi + C_D\cos\phi)r \; dr$$

The integrations are normally performed graphically.

In Ref 8, Cooper presents a methodology for using the blade element theory to calculate blade performance. For the cases analyzed, many of the parameters used by Cooper are not applied. In an effort to simplify the calculations, a modified version of his worksheet is used.

The worksheet utilizes user inputs which require some knowledge of the airfoil/propeller that is being analyzed. As an example, the zero-angle-of-attack lift coefficient $(C_{1i})$ is an input parameter (this is zero for the flat plate). The input parameters are used to generate a spanwise distribution of thrust and torque. Empirical data are used to translate the inputs into performance data. The lift coefficient correction curve for three-dimensional (aspect ratio) effects is shown in Fig 21. Corrected lift coefficient is the least manipulated performance parameter

59

in the procedure, therefore it is used for comparison with
the results from the vortex lattice method.

# Appendix E - Momentum Theory

One of the analytical aspects which is peculiar to propellers that is not covered in this thesis is the influence of wake extension due to flow acceleration through the propeller. In this model, the wake is presumed to be a helix with a helix angle independent of axial location. Since the shape of the wake is dependent upon the relationship between axial and rotational velocity, the previously mentioned change in axial velocity becomes important in finding the actual wake shape. An approximation for change in axial velocity is predicted by the momentum equation (Ref 9).

The Rankine-Froude momentum theory for propellers assumes that the propeller disk may be physically replaced by an actuator disk that has an infinite number of blades and that is capable of producing a uniform change in velocity of the air stream passing through the disk. The momentum theory is useful in determining theoretical maximum efficiencies, but tells nothing about the effects of a finite number of blades of finite thickness.

In developing the momentum theory, a perfect incompressible fluid in a constant energy (irrotational) flow is assumed in front of and behind the disk, but not through the disk itself. The streamlines of the flow past the disk are shown in Fig 11.

Referring to Fig 13, the pressure in the freestream is

p and the velocity is V. As the air stream approaches the front disk face, the velocity increases until it achieves a value V+v through the disk and at the same time, the pressure drops off to a value p'. At the disk, energy is added in the form of an increase in pressure p. Aft of the disk, the pressure drops to the freestream value, and far behind the disk, the air has a velocity V+vl. The high-velocity stream of air behind the propeller is referred to as the slip-stream or wake.

Although Bernoulli's equation does not hold for flow through the disk, it does hold for the flow in front of and behind the disk; thus we may write

total head in front of disk = H

$$= p + \frac{\rho V^2}{2} = p' + \frac{\rho (V+v)^2}{2} , \qquad \text{E-1}$$

total head behind the disk = $H_1$

$$= p' + \Delta p + \frac{\rho (V+v)^2}{2} = p + \frac{\rho (V+v_1)^2}{2} \qquad \text{E-2}$$

The change in pressure across the disk must be equal to the change in head, or, using the second evaluation for $H_1$ in Eq E-2 and the first evaluation for H in Eq E-1,

$$\Delta p = H_1 - H = p + \frac{\rho (V+v_1)^2}{2} - (p + \frac{\rho V^2}{2})$$

$$= \rho (V+v_1/2) v_1 \qquad \text{E-3}$$

where $\Delta p$ is the average change in pressure over the disk.

The thrust acting on the disk is

$$T = A\Delta p$$

where A = disk area; or, from Eq E-3,

$$T = A\rho (V + \frac{v_1}{2}) v_1 \qquad \text{E-4}$$

To obtain a relationship between $v_1$ and $v$ it is neces-
sary to write another equation for thrust.  This may be done
by considering the change in momentum of the air produced by
the disk.  Newton's second law,

$$T = ma = \frac{mdV}{dt}$$

states that the thrust is equal to the change in axial momen-
tum per unit time.  The mass per unit time is the mass flow
through the disk,

$$Q = A\rho (V+v)$$

and

$$dV = v_1$$

so that

$$T = \frac{mdV}{dt} = A\rho (V+v) v_1 \qquad \text{E-5}$$

Equating Eq E-4 to Eq E-5 we have

$$A\rho (V + \frac{v_1}{2}) v_1 = A\rho (V+v) v_1$$

and so

$$v_1 = 2v$$

Thus, the momentum theory states that one-half the

velocity increase occurs in front of the disk and one-half behind the disk.

The momentum theory shows how the velocity in the slip stream can be significantly greater than the freestream velocity (particularly for heavily loaded propellers). This can consequently stretch the wake a great deal. Remembering that the Biot-Savart Law has an inverse-squared distance term, it becomes apparent that the positioning of the wake filaments could become significant for the case of the heavily loaded propeller.

The model used in the current analysis uses flight speed as the axial component of velocity. As a next step, an iterative solution would be required to get a better representation of the wake location, and consequently a more accurate solution.
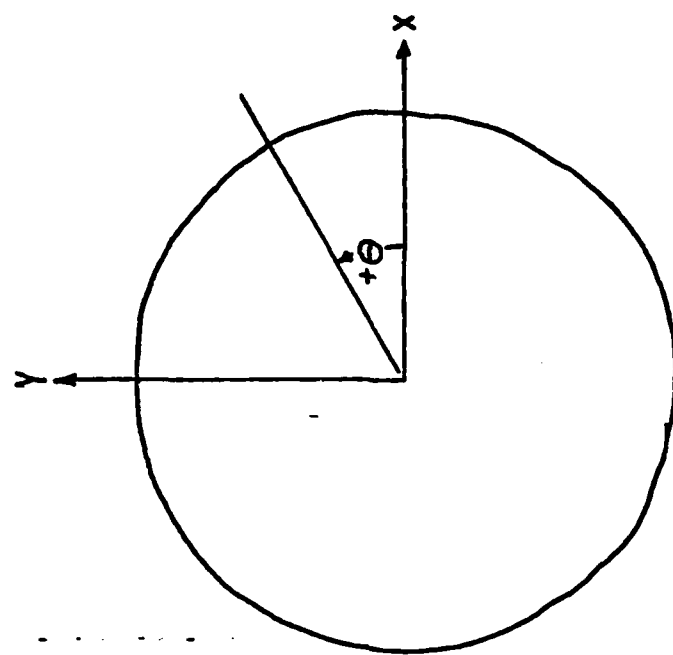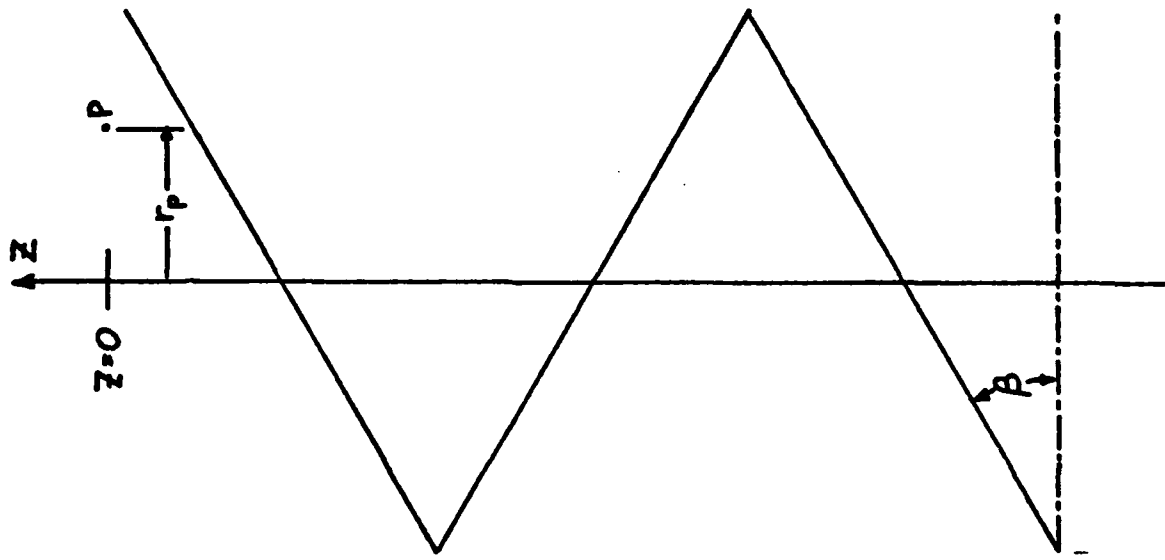
Fig 1. Diagram of Helix Model

65

FLAT PLATE AT
ANGLE OF ATTACK

$U_\infty \longrightarrow$

$\alpha$

ACTUAL CONDITION
curved wake, asymptotically
becomes parallel to $U_\infty$.

$U_\infty \longrightarrow$

$\alpha$

MODELED CONDITION
straight wake, follows
chord line.

$U_\infty$

W

Boundary Condition
no flow through the
control point.

CONTROL
POINT
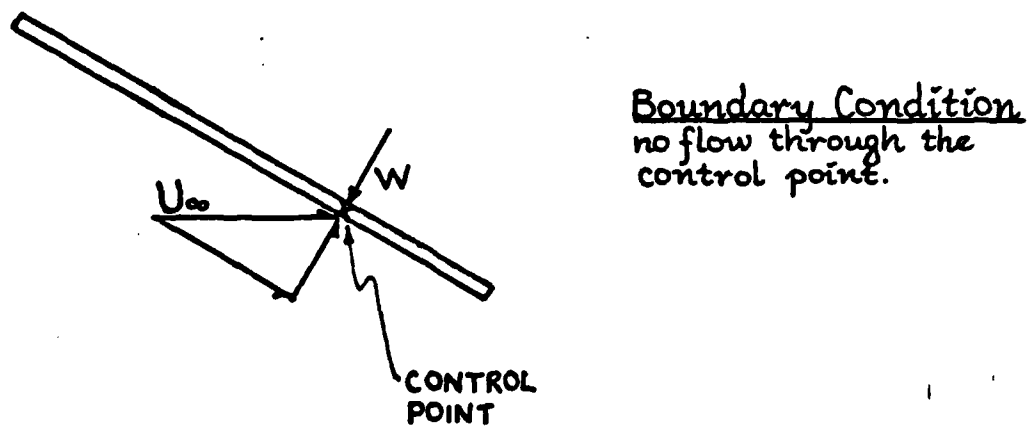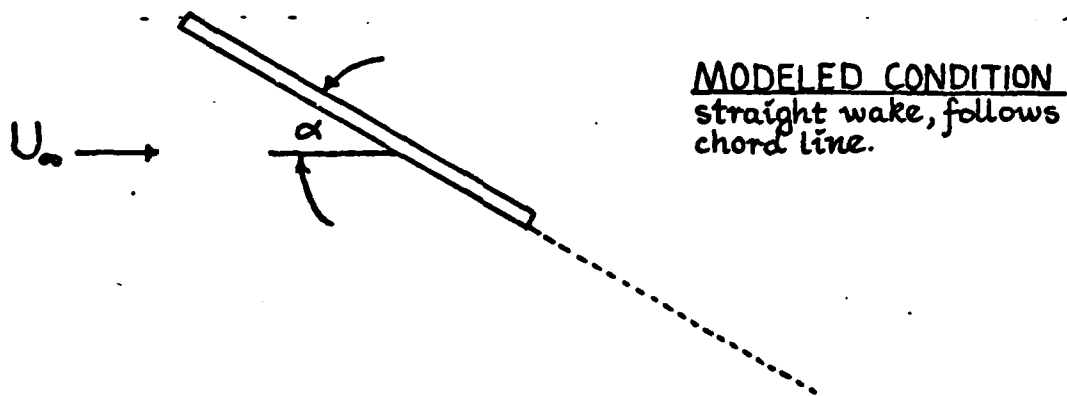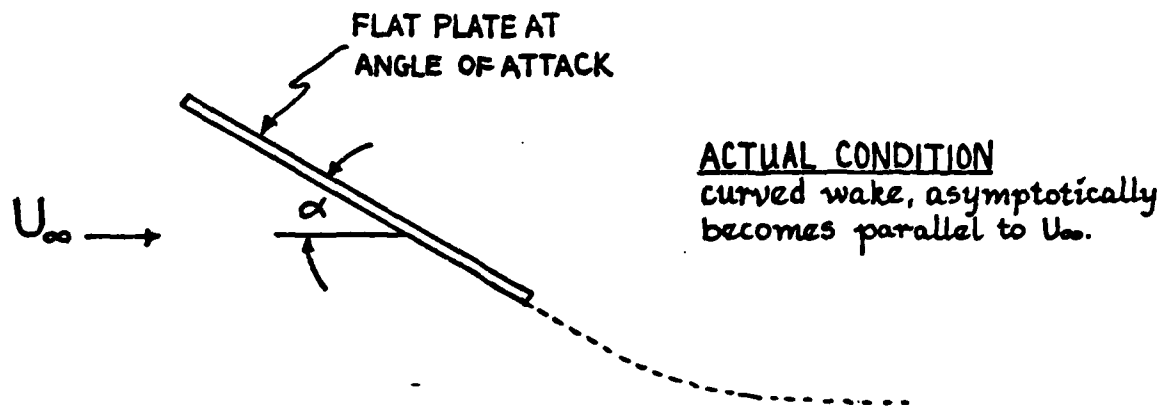
Fig 2.   Wake Models and Boundary Condition for Wing

66
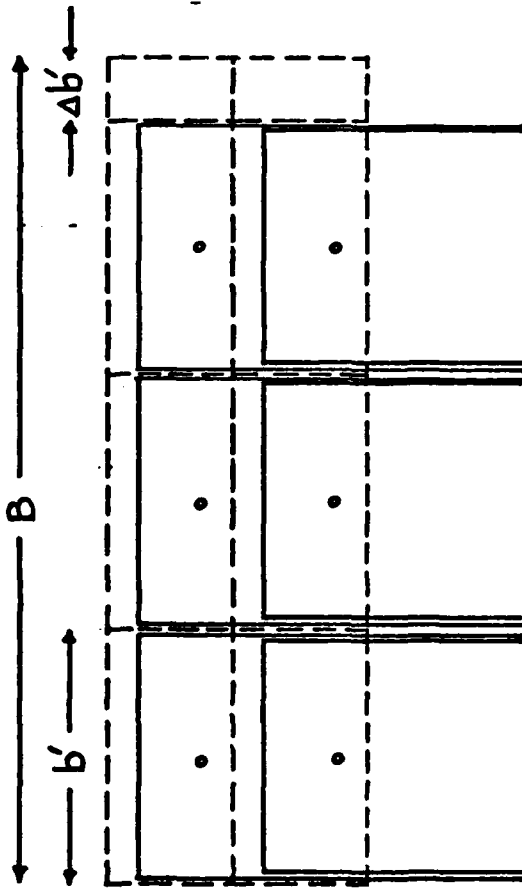
Fig 3. Lattice Configuration with Tip Inset
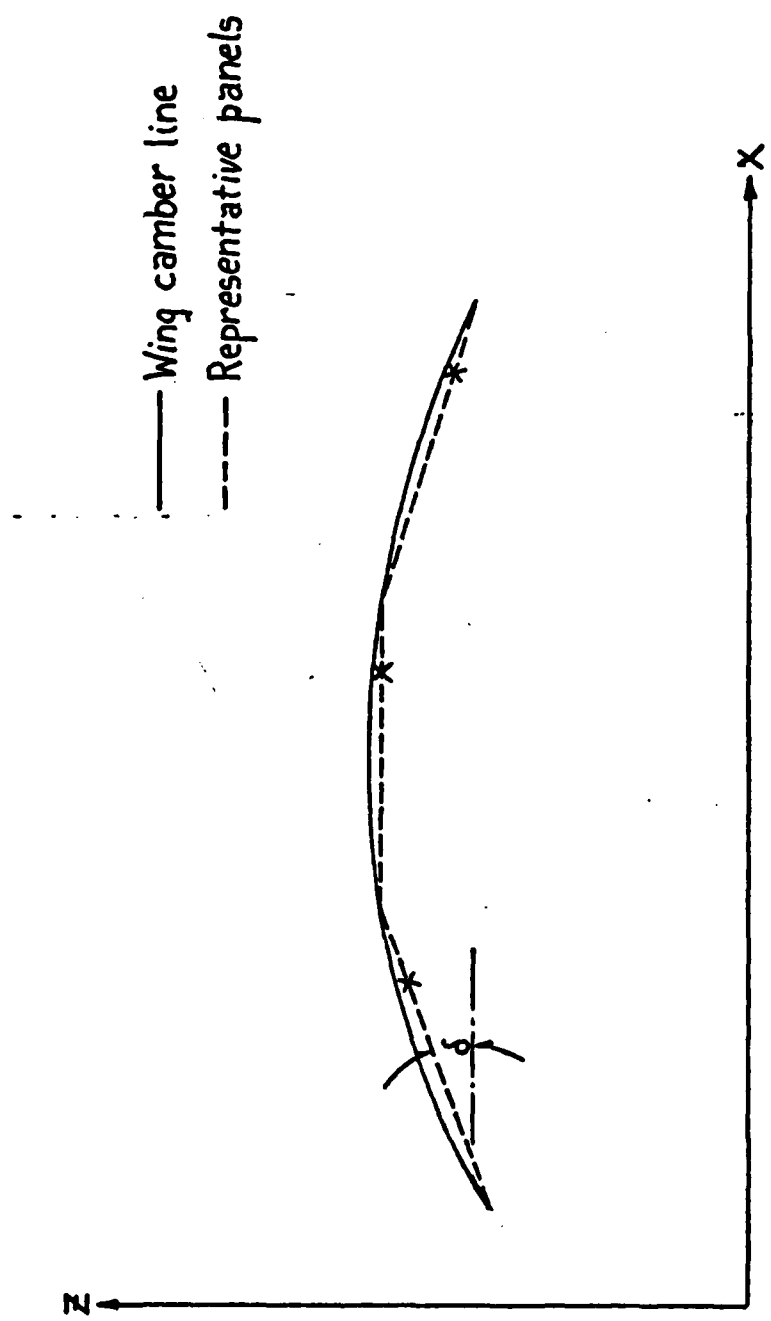
Fig 4. Paneled Representation of a Cambered Airfoil
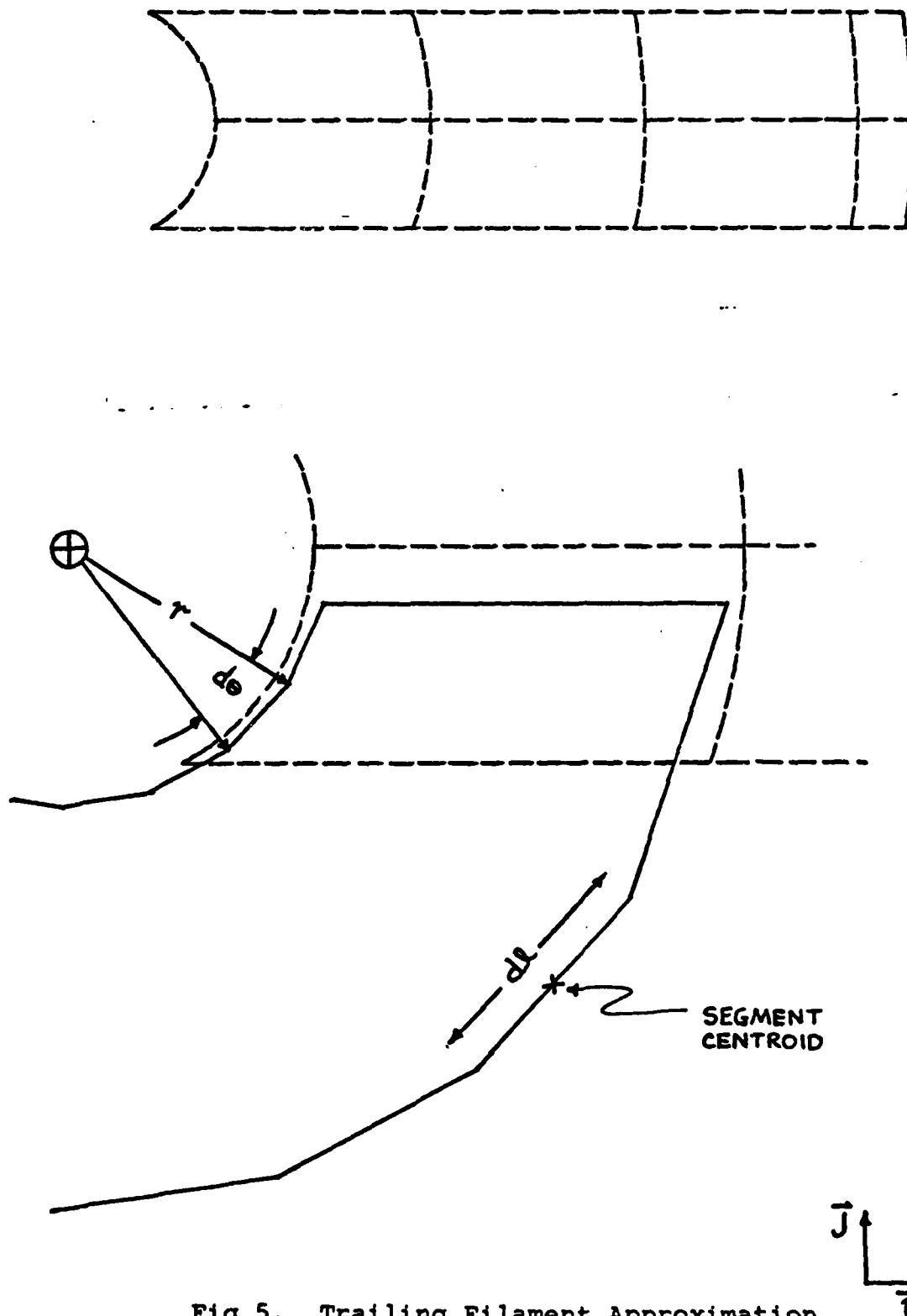
Fig 5.   Trailing Filament Approximation

69
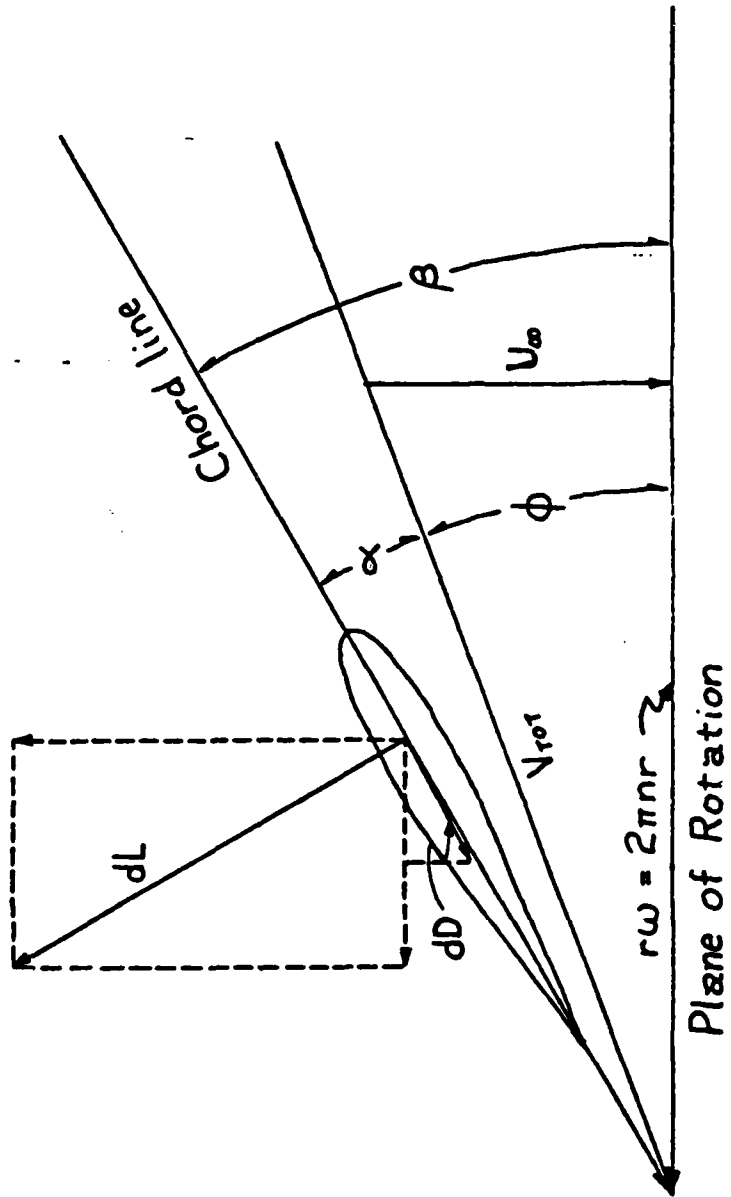
Fig 6. Propeller Nomenclature Diagram

Fig 7. Propeller Run to Simulate a Wing
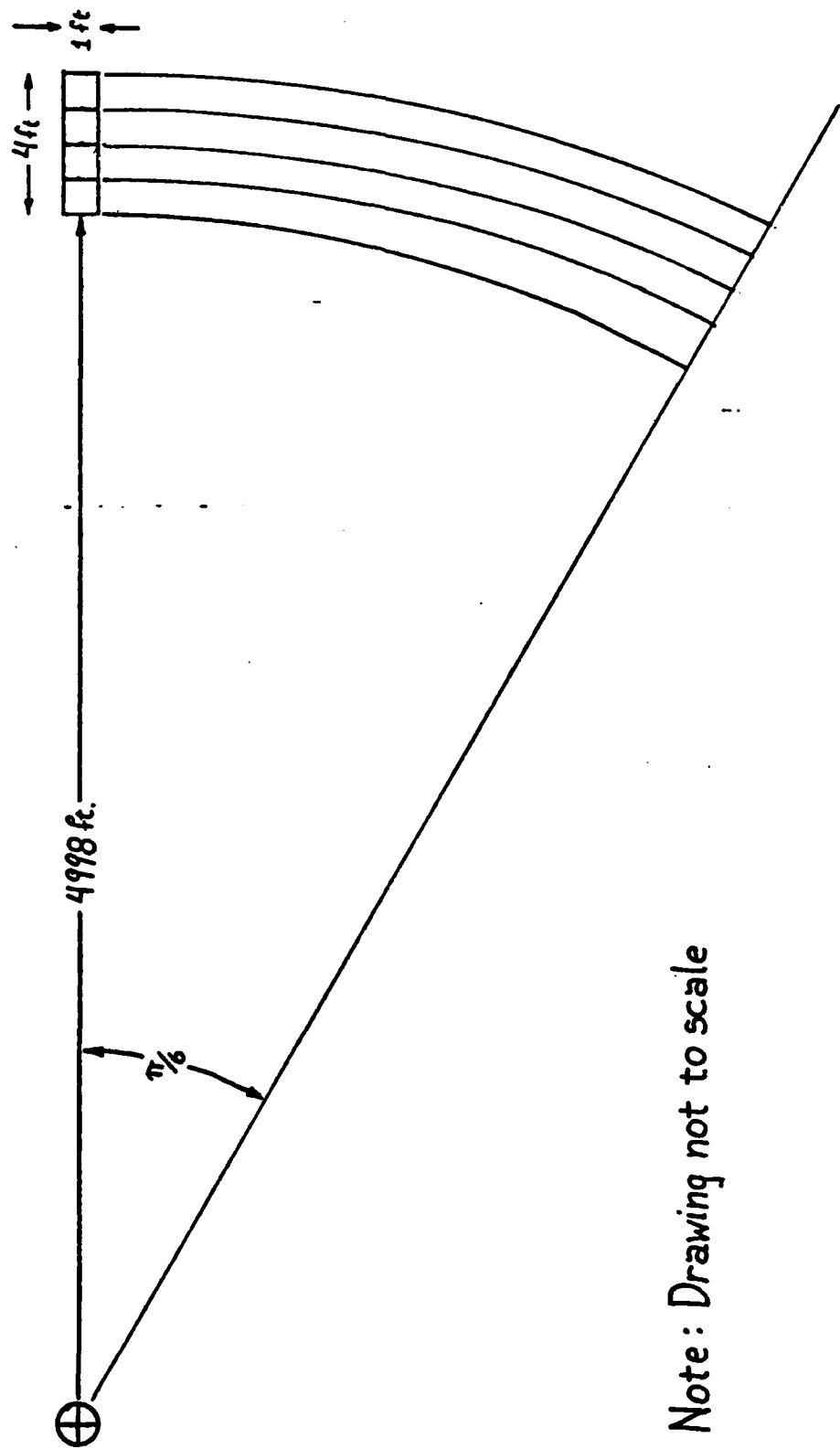
Note: *Drawing not to scale*

1 ft

4 ft

4998 ft.

$\pi/6$
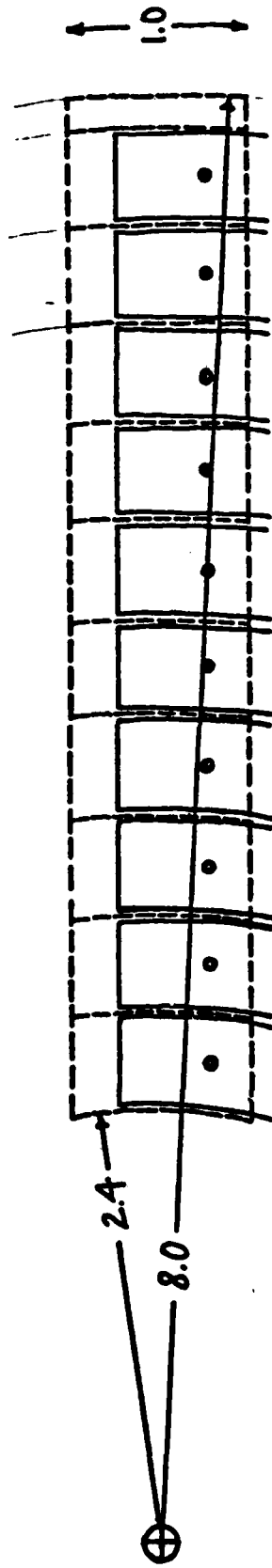
Fig 8. Propeller Configuration Used for Comparison

# VLM CASE #1
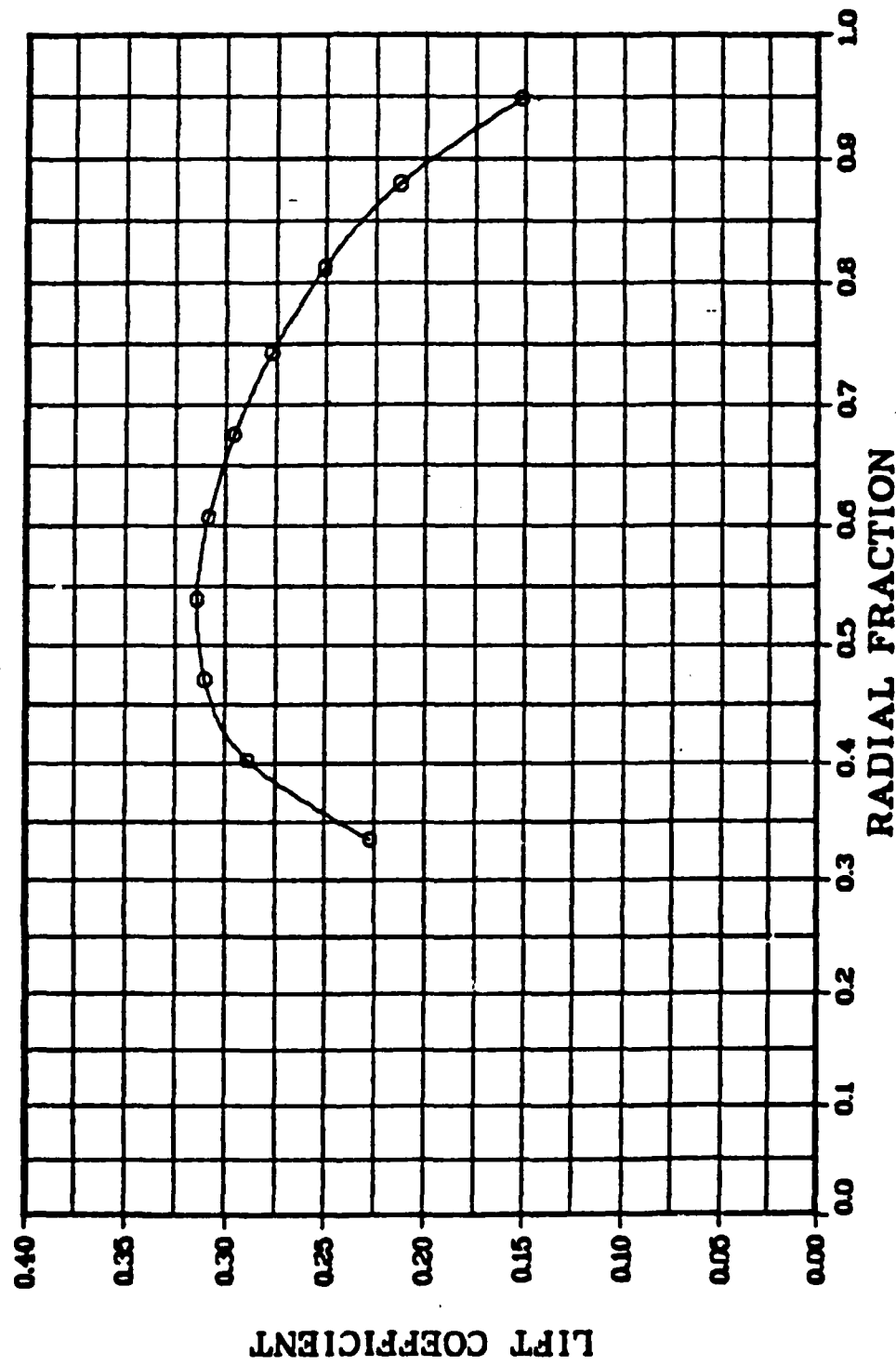


Fig 9a. Vortex Lattice Method Test Case #1

73
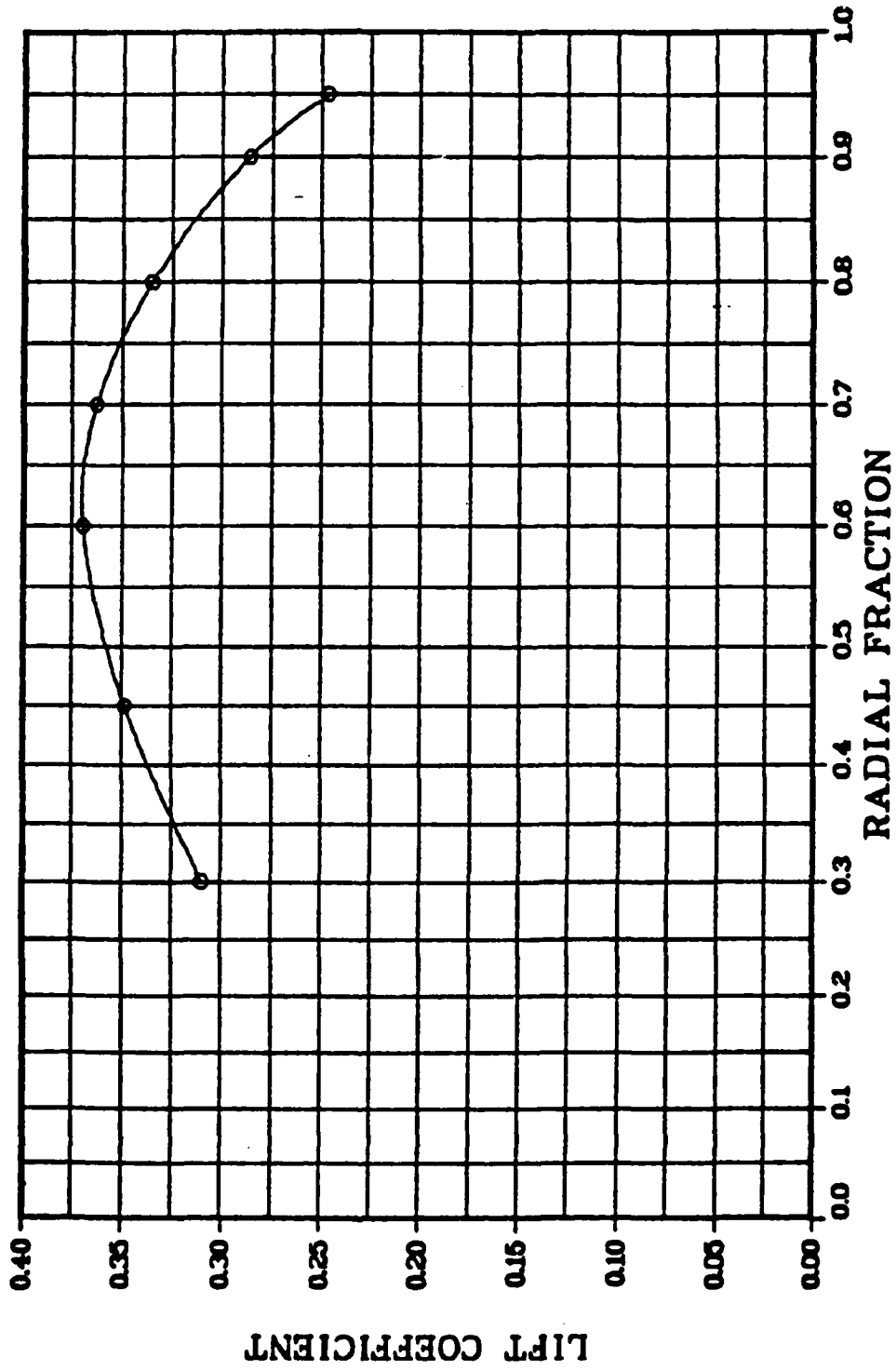
# BEM CASE #1



Fig 9b.  Blade Element Method Test Case #1

74
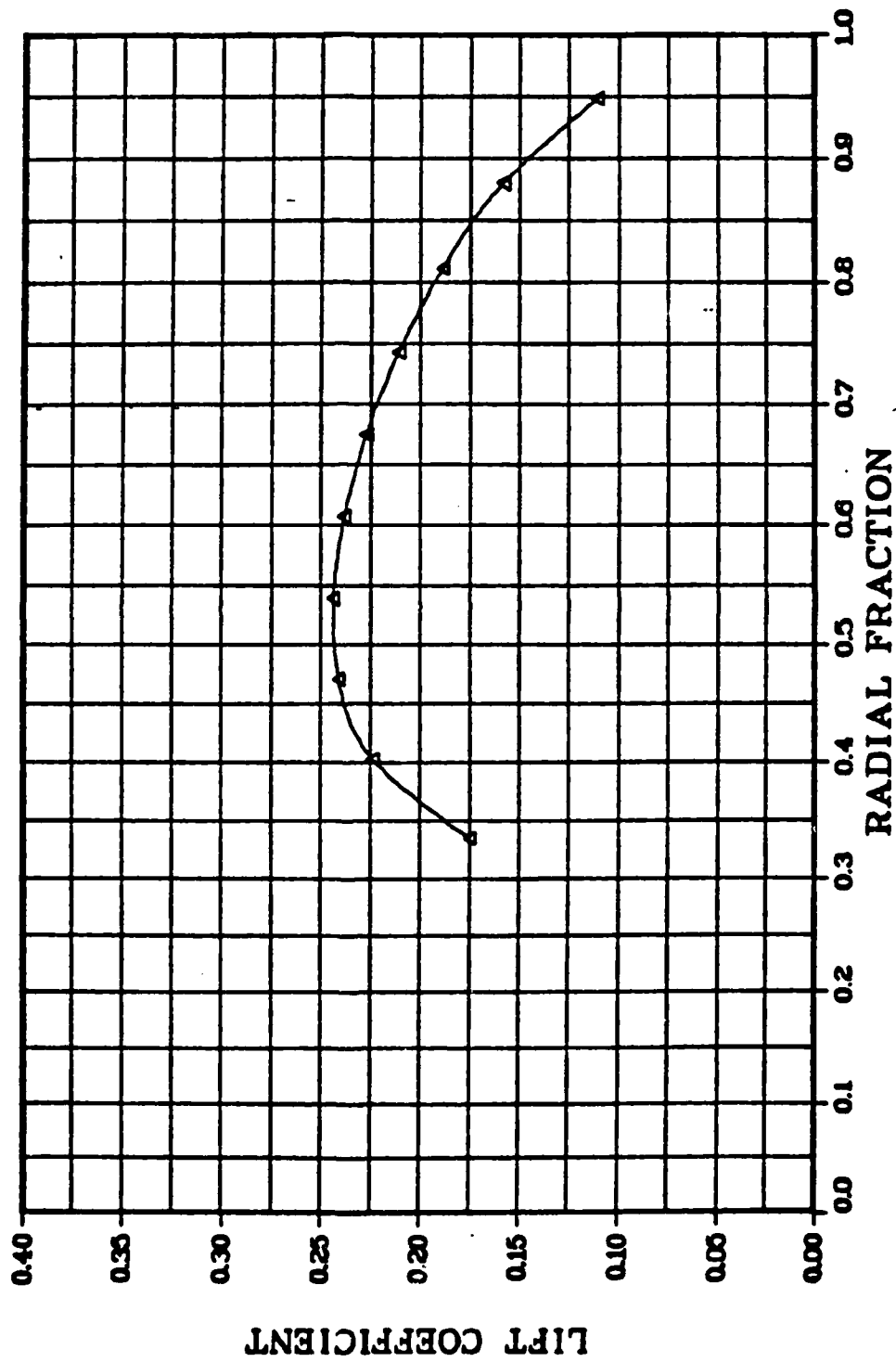
Fig 9c. Vortex Lattice Method Test Case #2

75
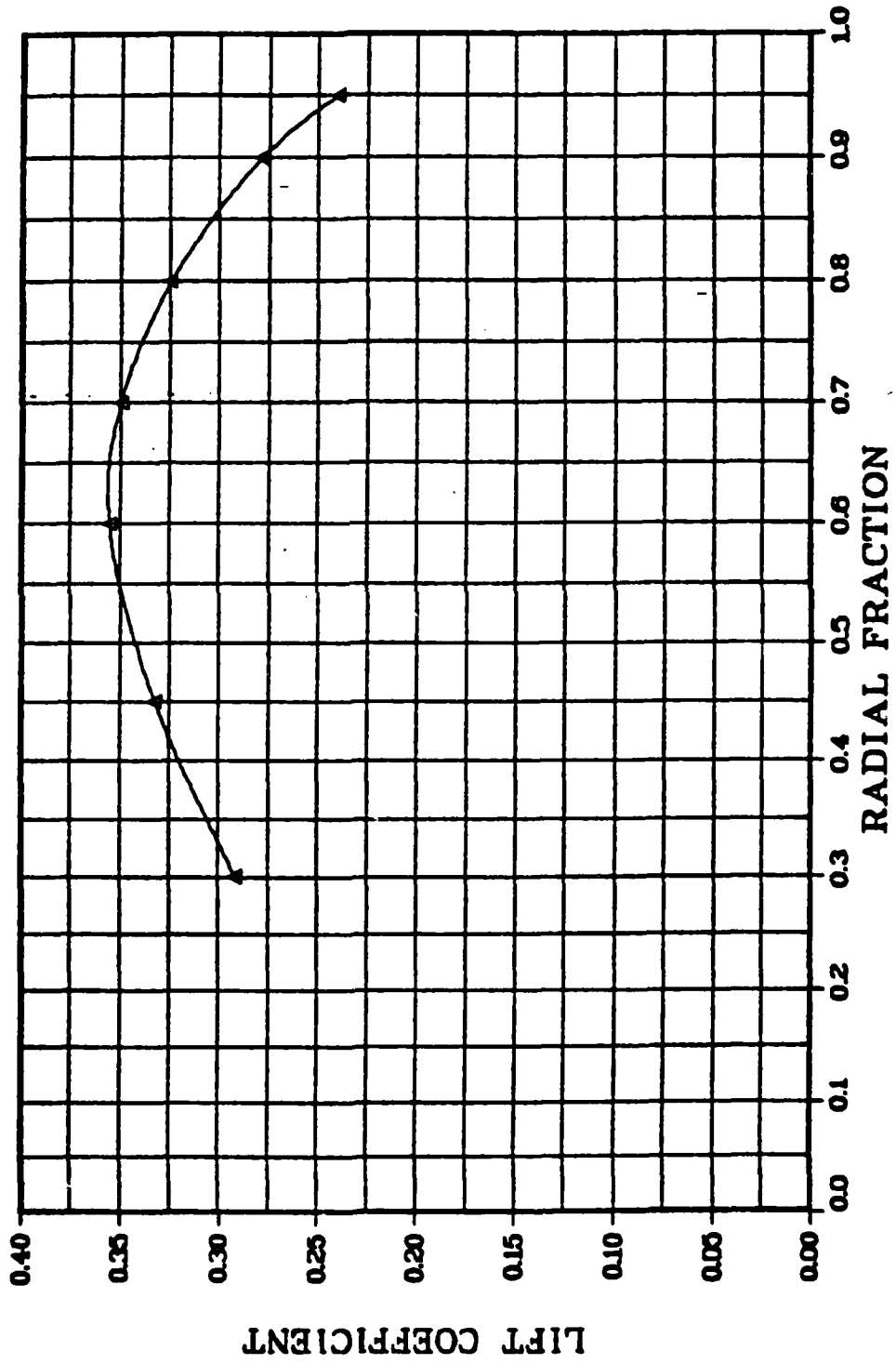
# BEM CASE #2



Fig 9d.  Blade Element Method Test Case #2

LIFT COEFFICIENT

RADIAL FRACTION

76
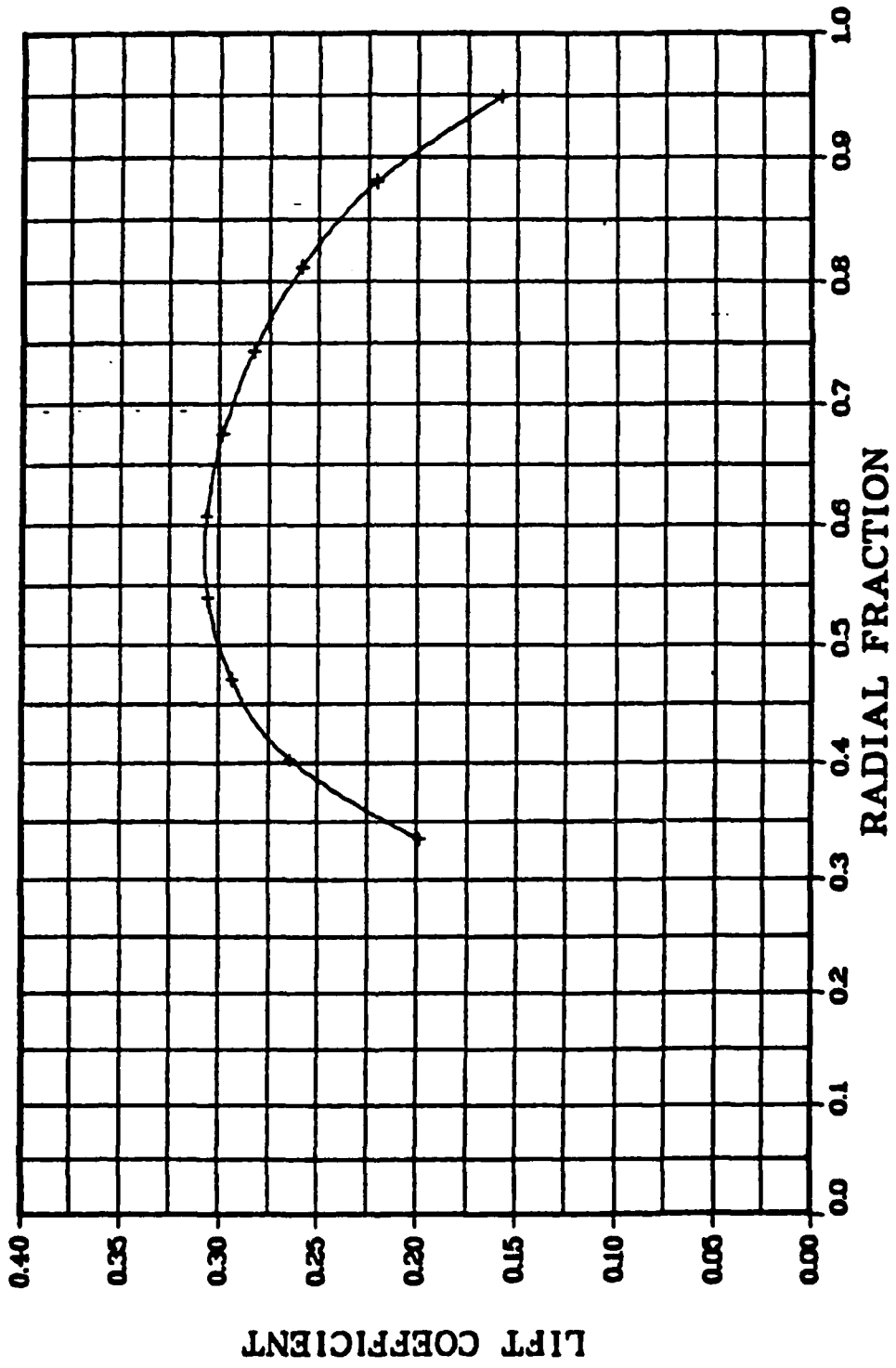
# VLM CASE #3

Fig 9e.  Vortex Lattice Method Test Case #3

77
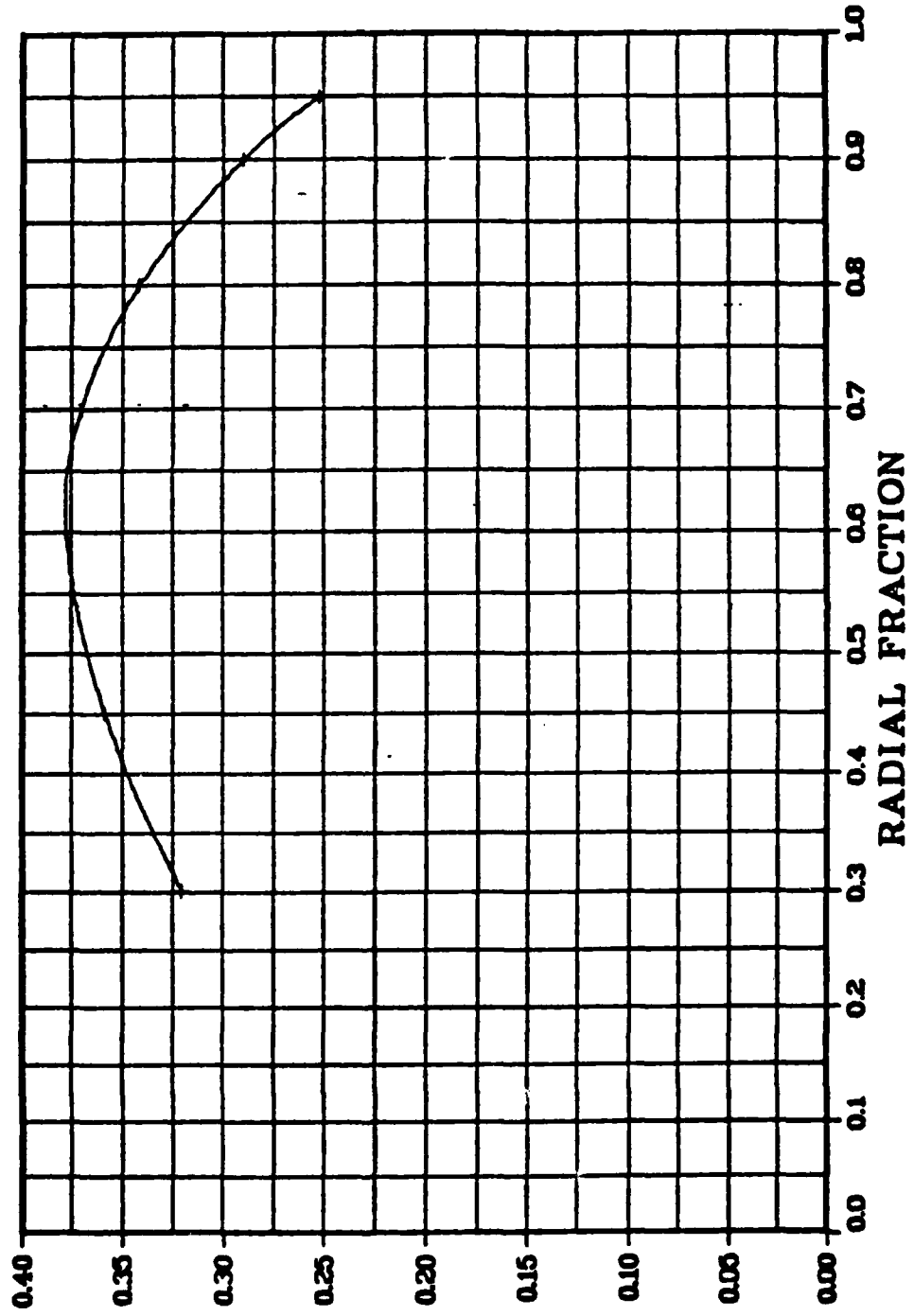
# BEM CASE #3



Fig 9f. Blade Element Method Test Case #3

78
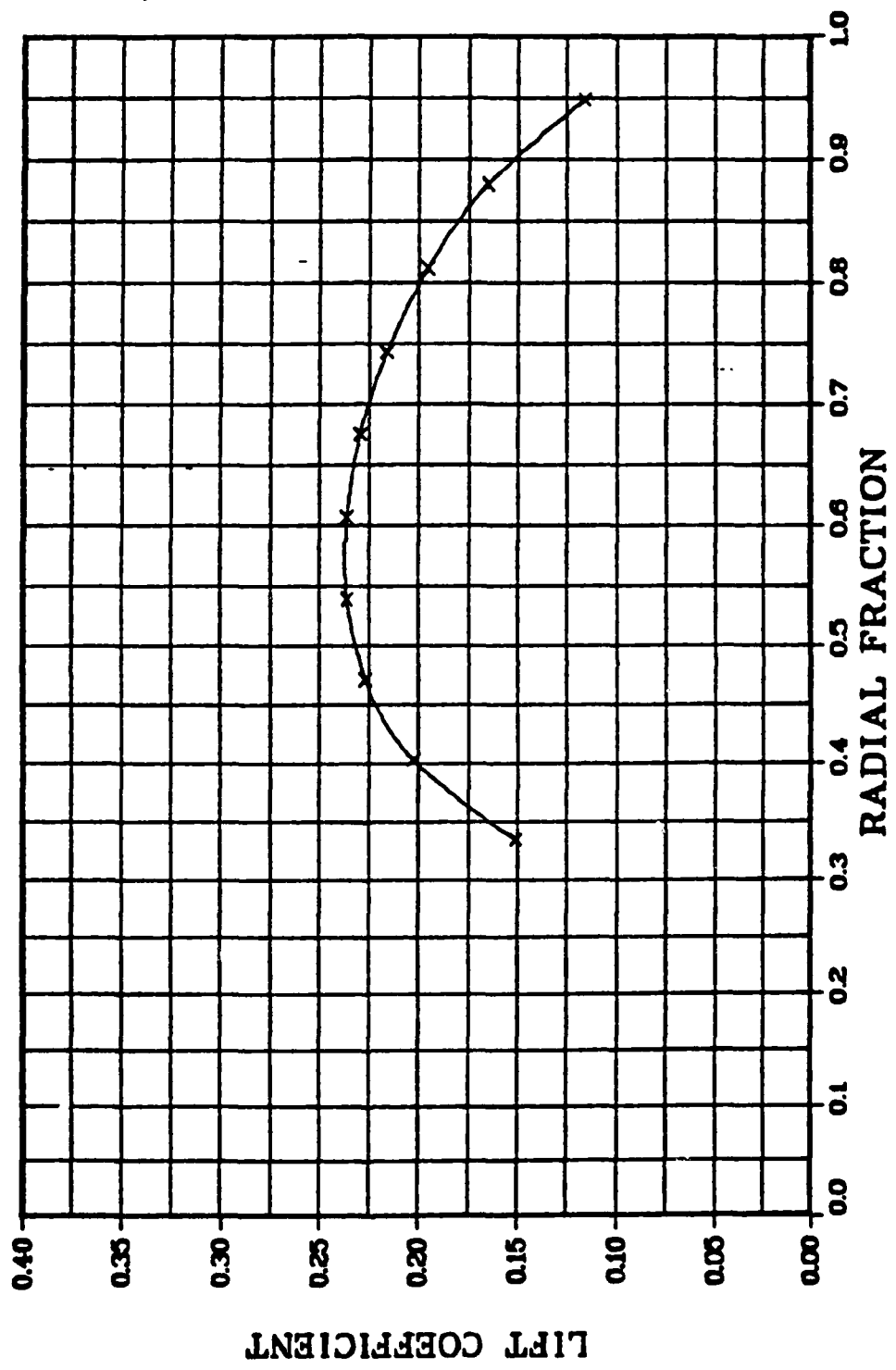
# VLM CASE #4



Fig 9g. Vortex Lattice Method Test Case #4

79
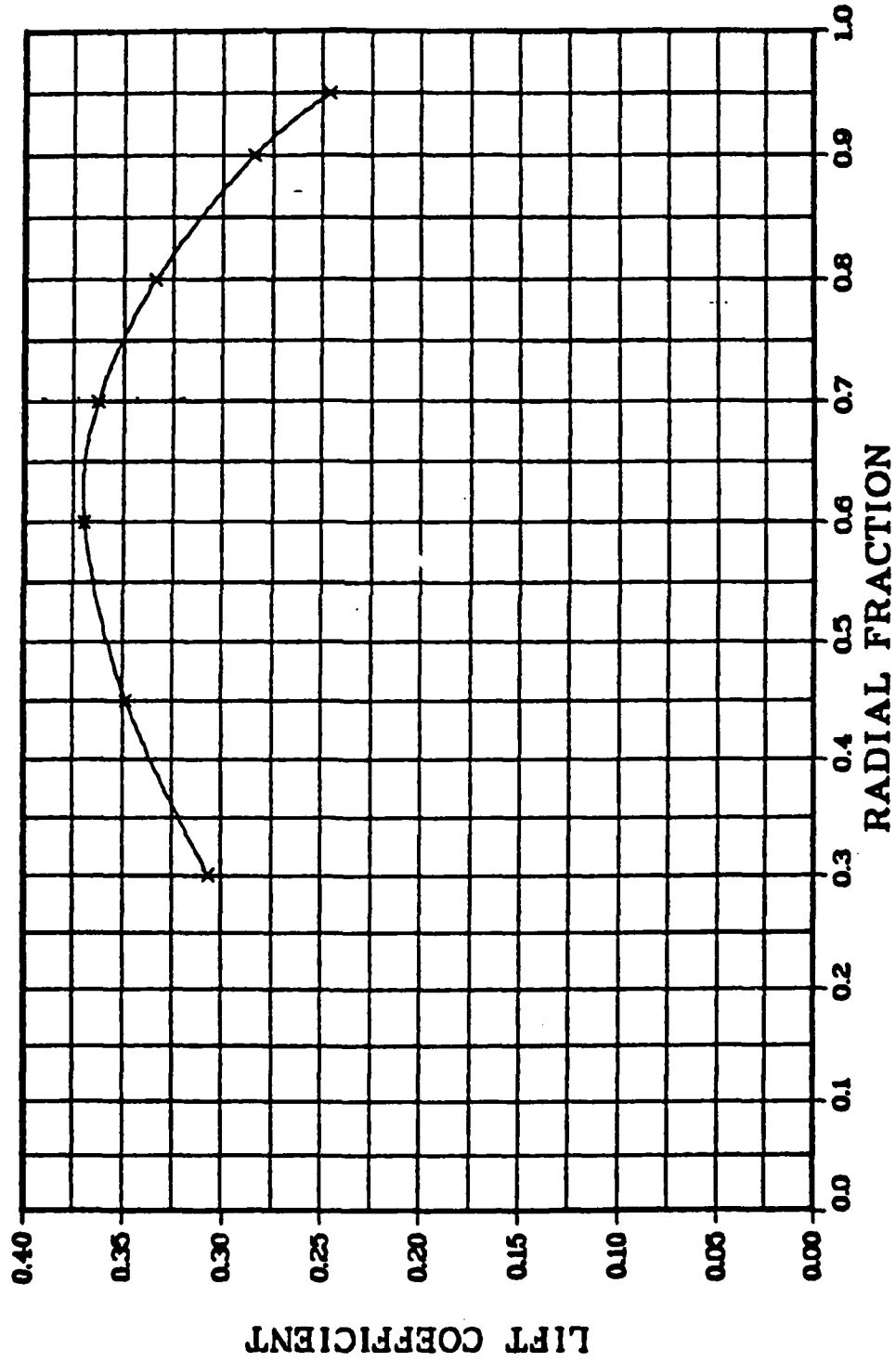
Fig 9h. Blade Element Method Test Case #4

# VLM CASE #5
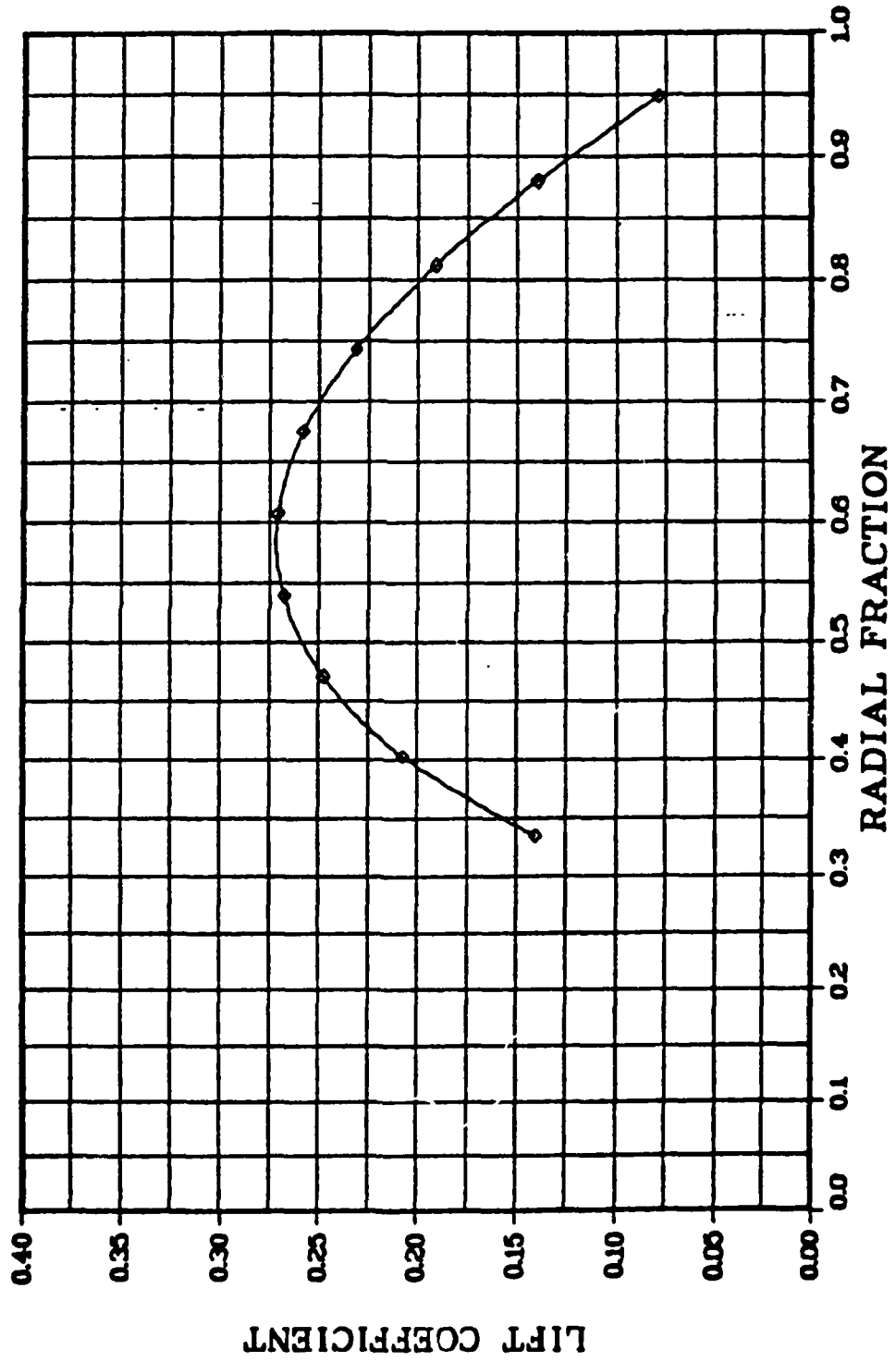


Fig 91.  Vortex Lattice Method Test Case #5

81
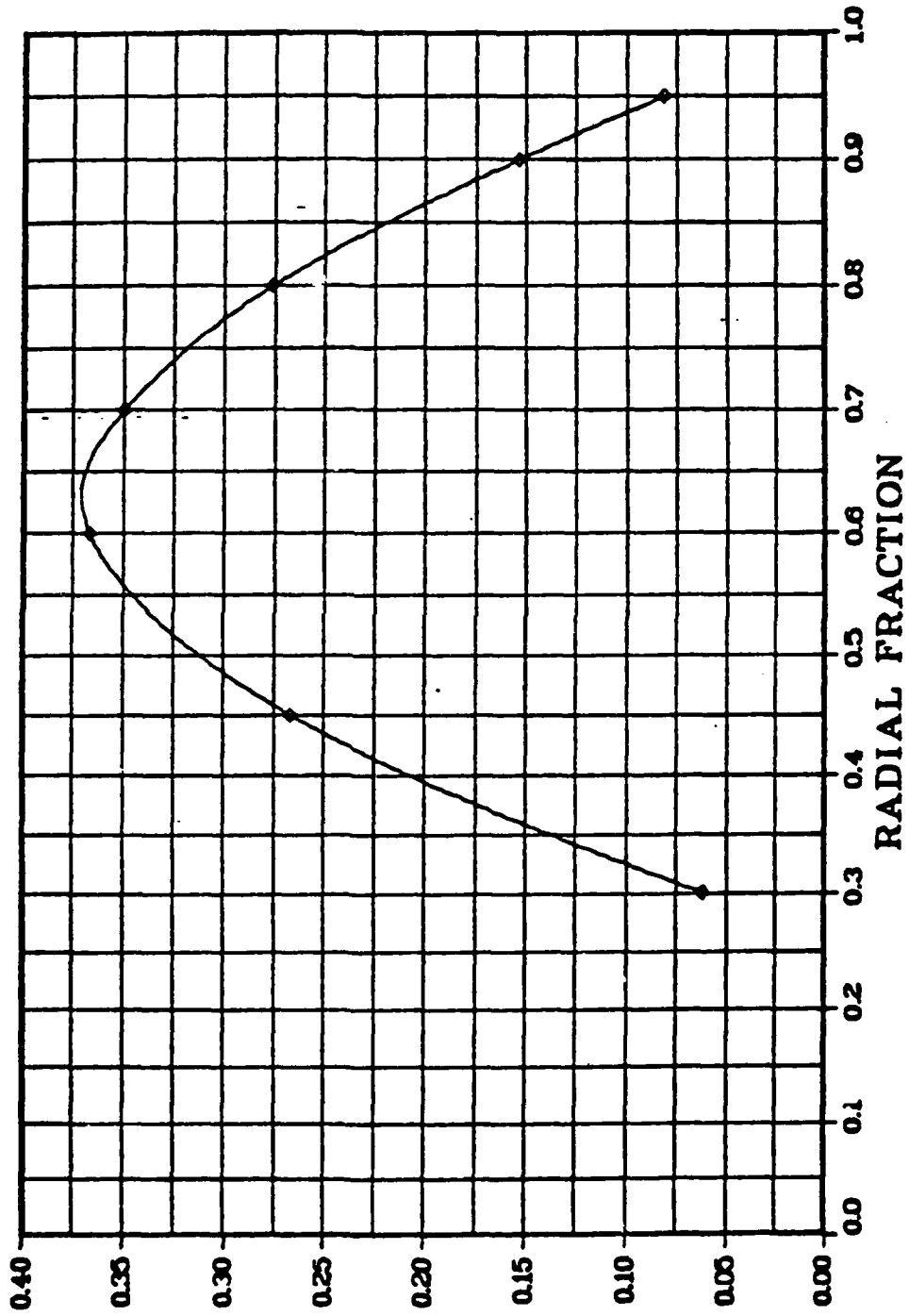
# BEM CASE #5



Fig 9j. Blade Element Method Test Case #5

82
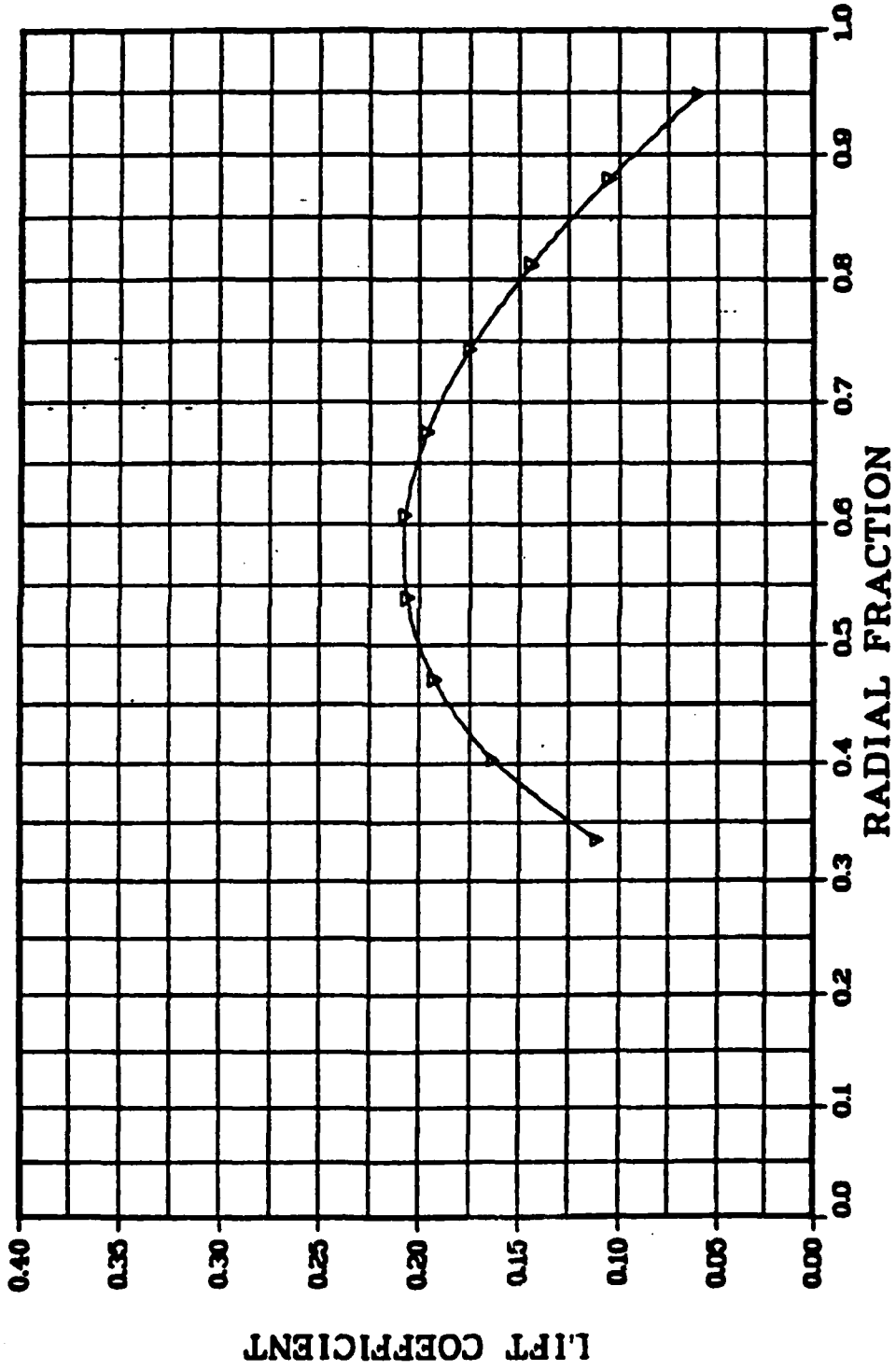
# VLM CASE #6



Fig 9k.  Vortex Lattice Method Test Case #6
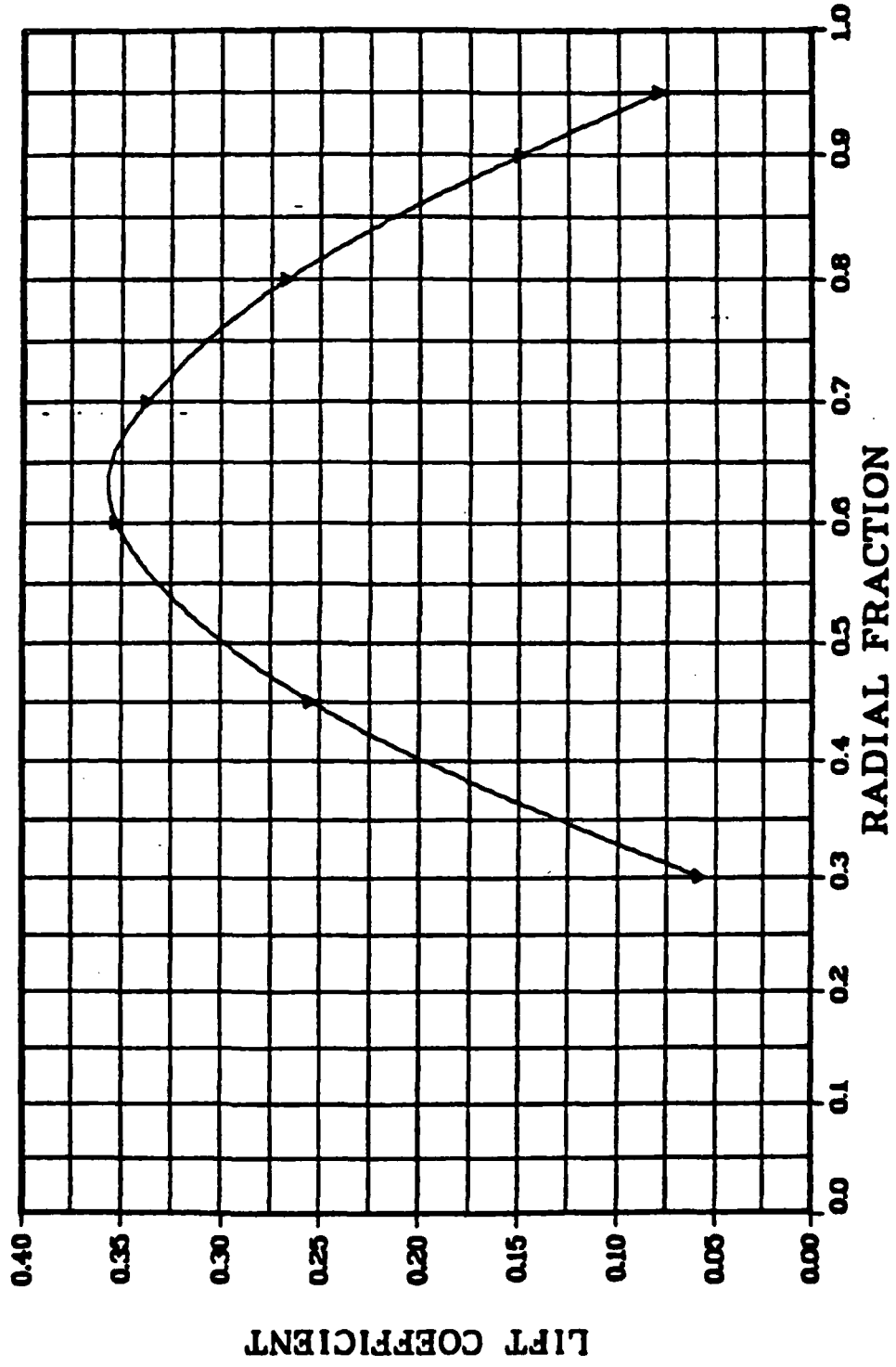
Fig 91. Blade Element Method Test Case #6

# VLM CASE #7
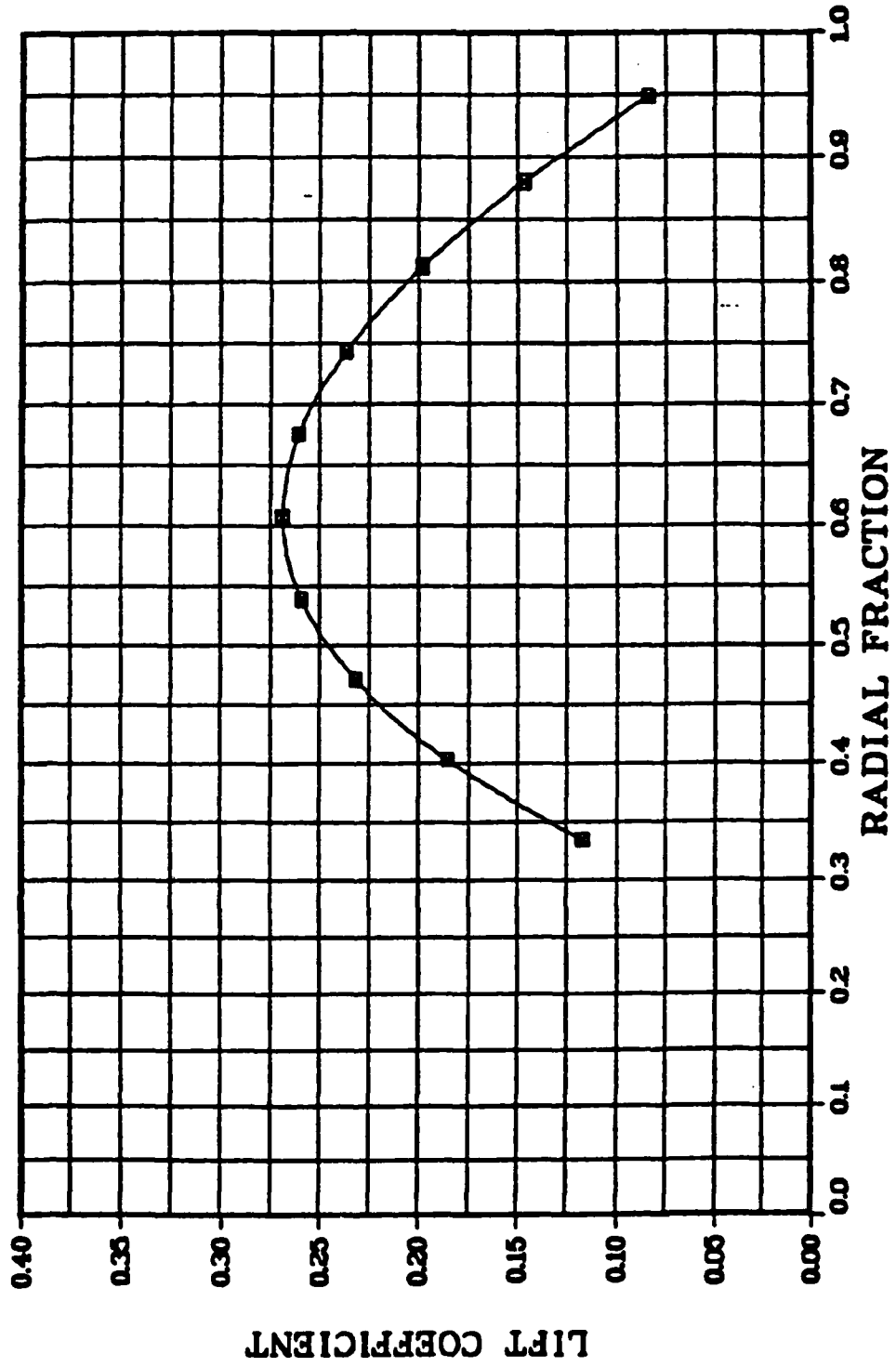
Fig 9m. Vortex Lattice Method Test Case #7

85
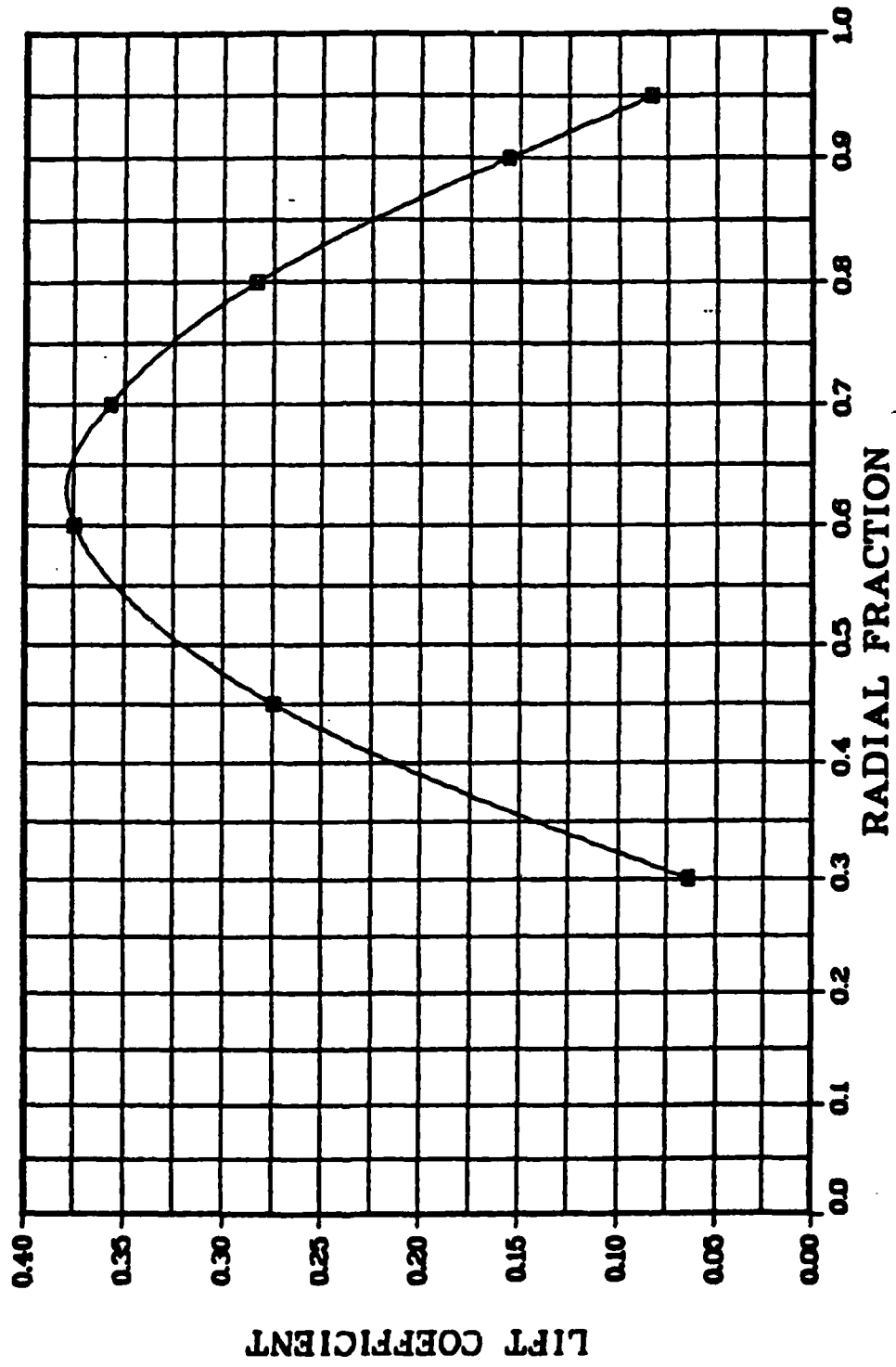
# BEM CASE #7



Fig 9n. Blade Element Method Test Case #7

# VLM CASE #8
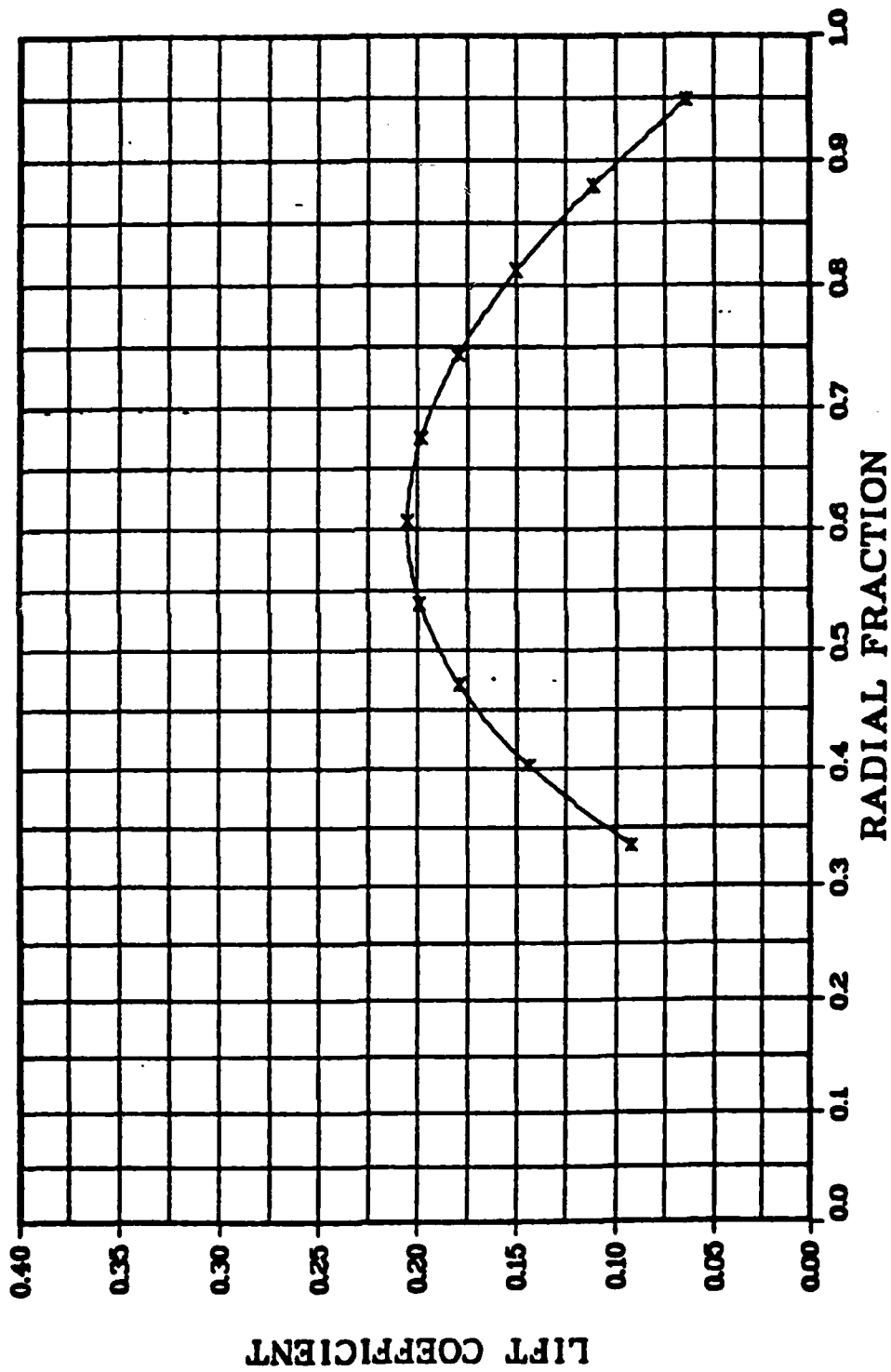


Fig 90. Vortex Lattice Method Test Case #8

87

# BEM CASE #8
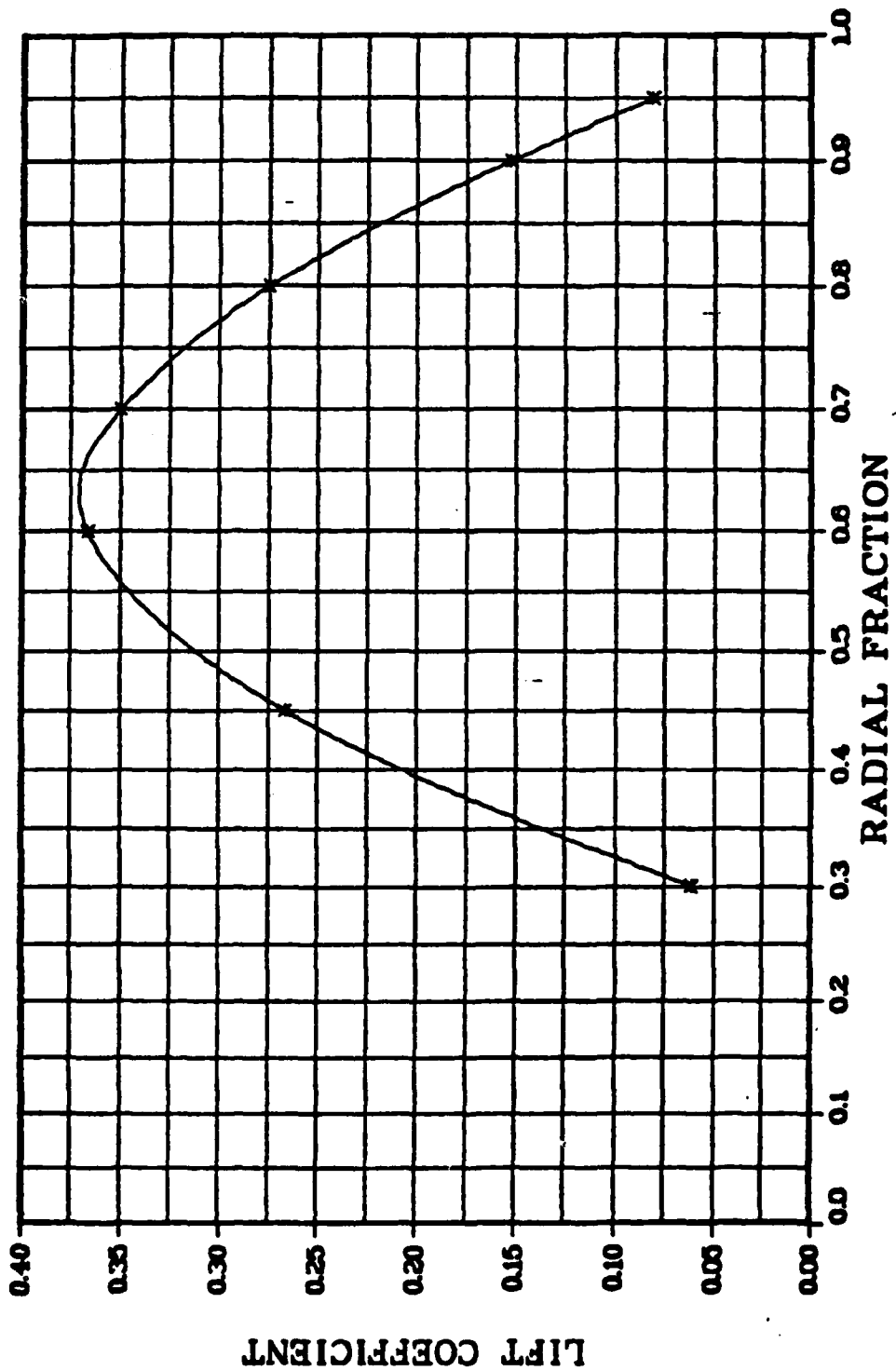


Fig 9p.  Blade Element Method Test Case #8
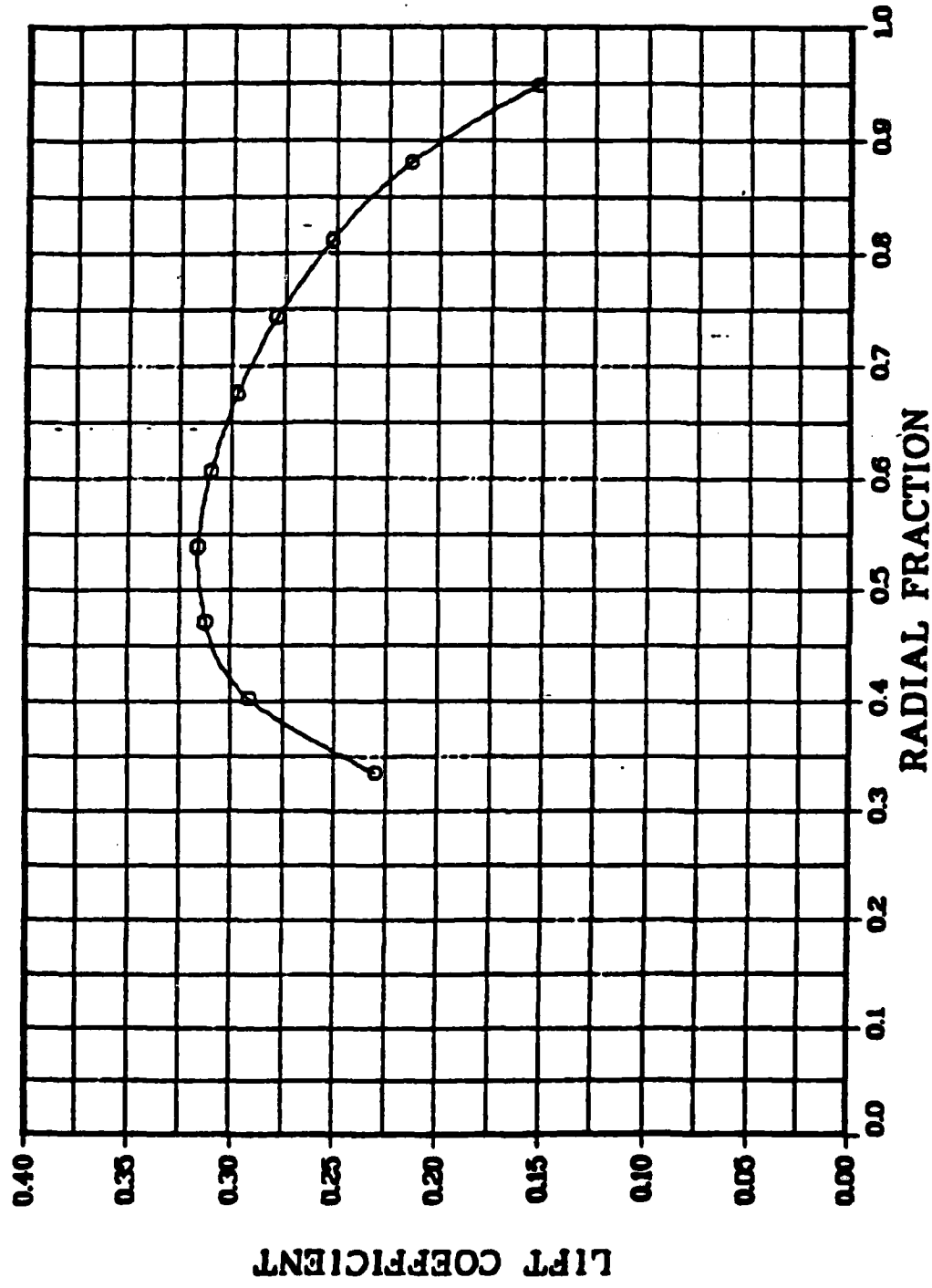
Fig 10.  5 x 10 Chord-Averaged Lift Coefficient
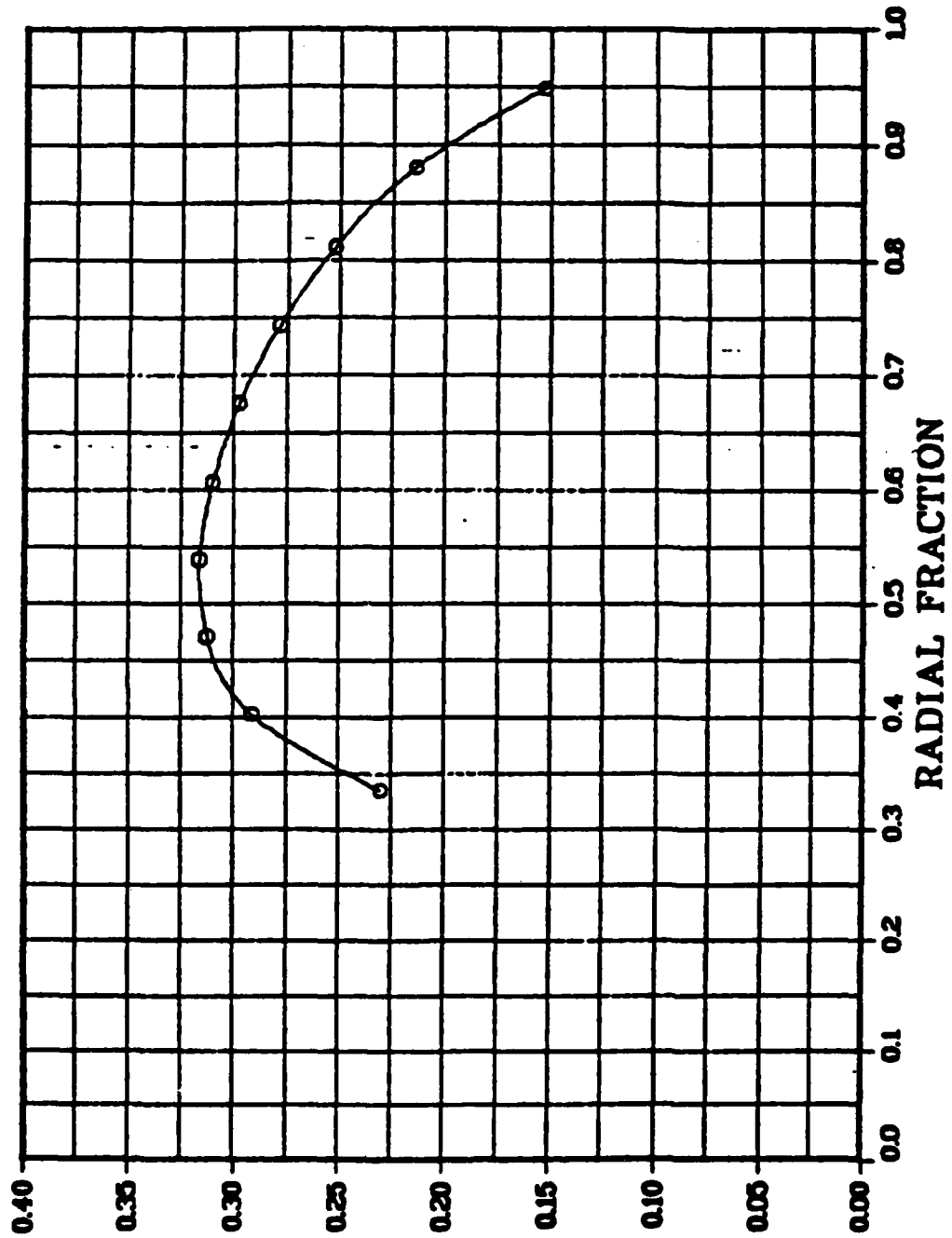
Fig 11. 10 x 10 Chord-Averaged Lift Coefficient

# 10 X 10 TEST CASE
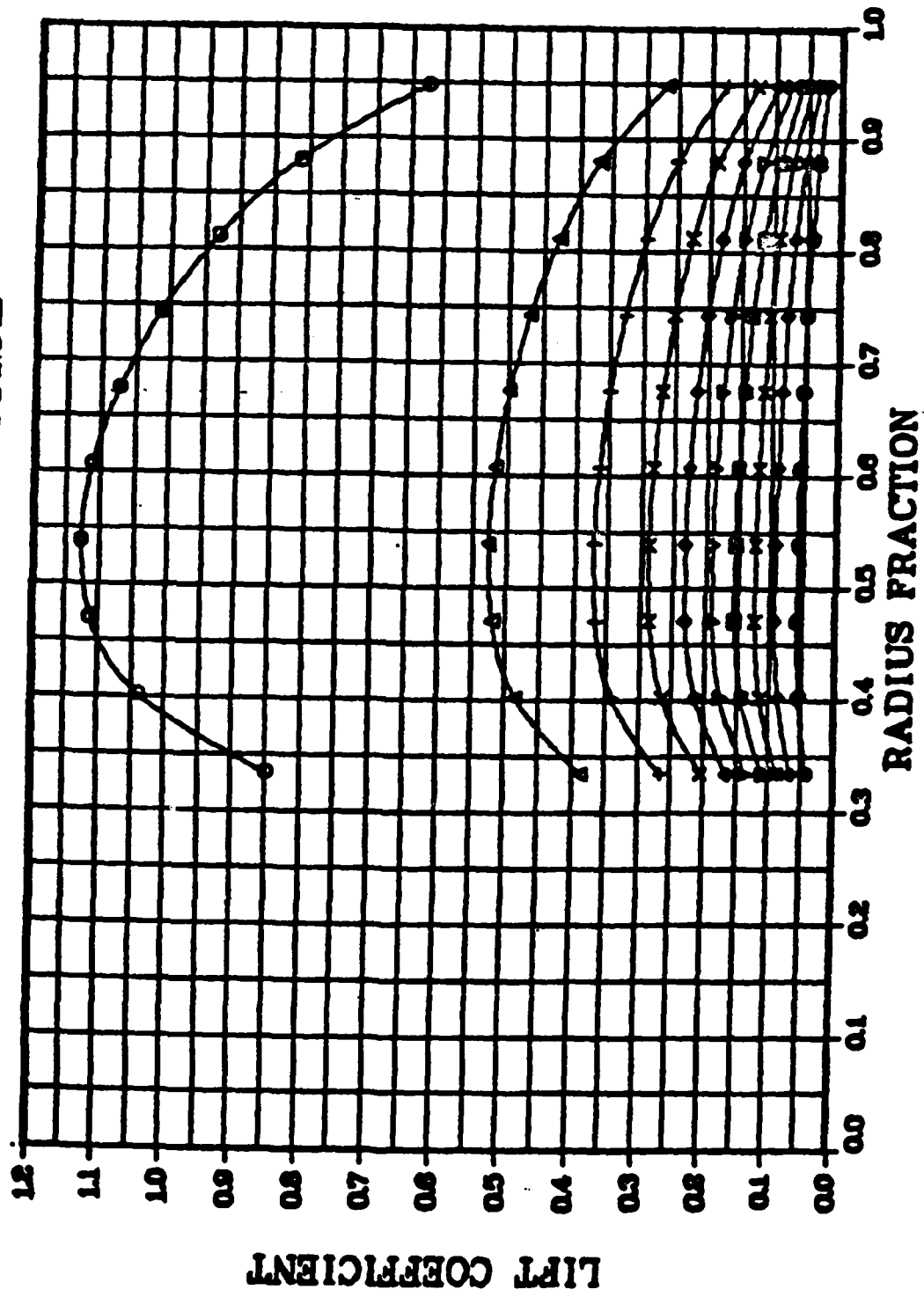


Fig 12a. 10 x 10 Spanwise Lift Coefficient

RADIUS FRACTION

LIFT COEFFICIENT

91

# 10 X 10 CHORDWISE DISTRIBUTION
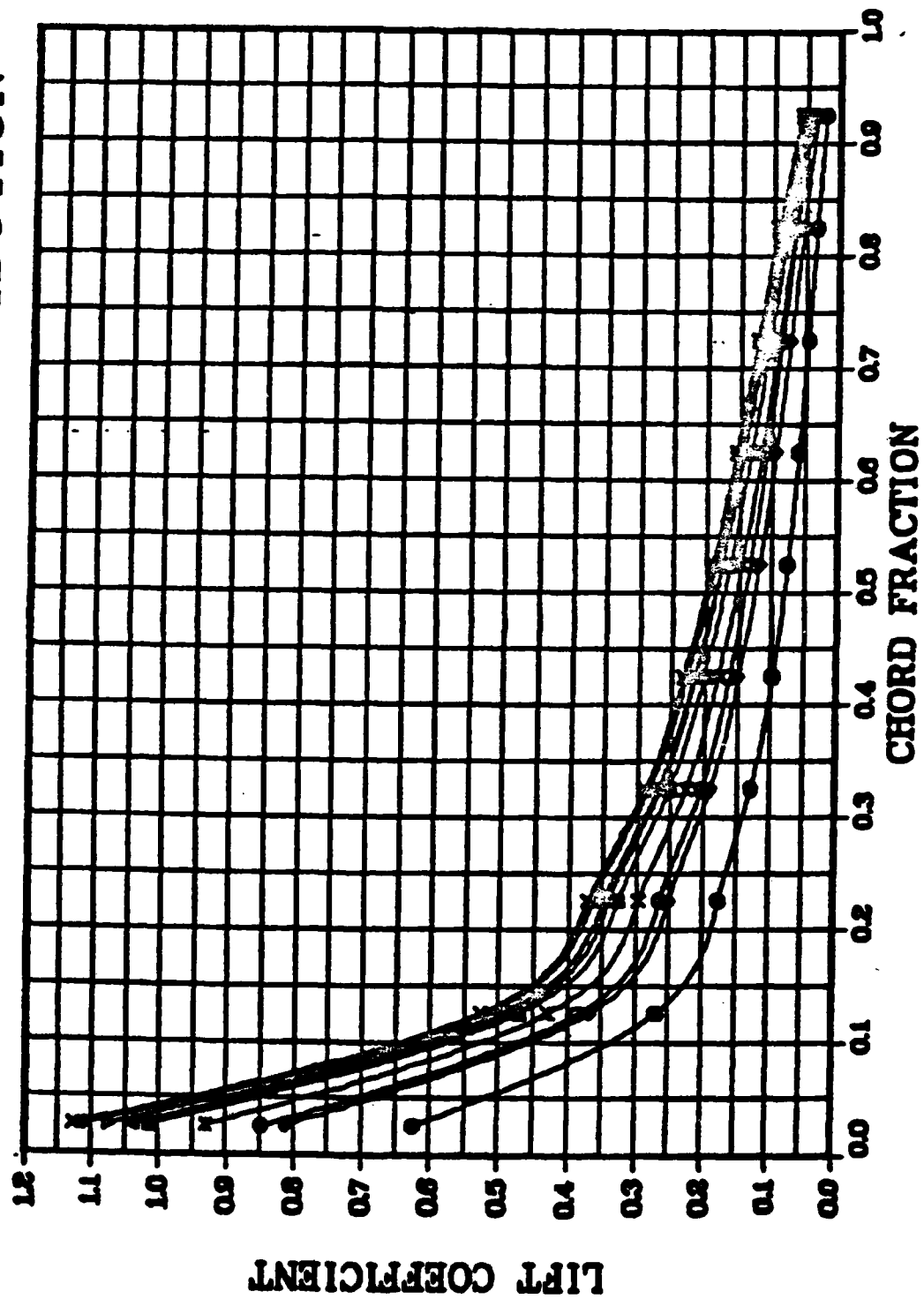


Fig 12b. 10 x 10 Chordwise Lift Coefficient
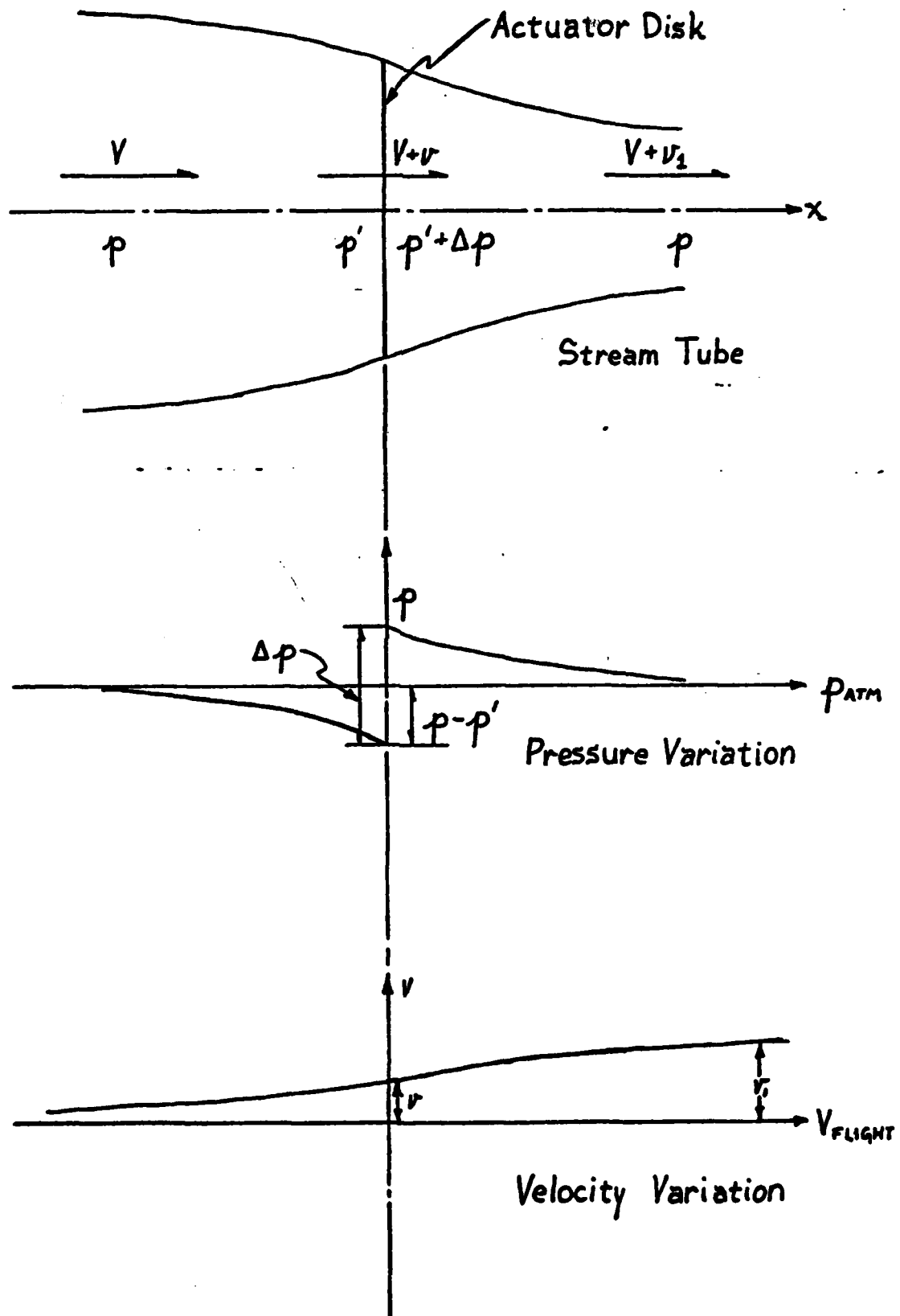
**Fig 13.   Momentum Theory Flow Conditions**

93
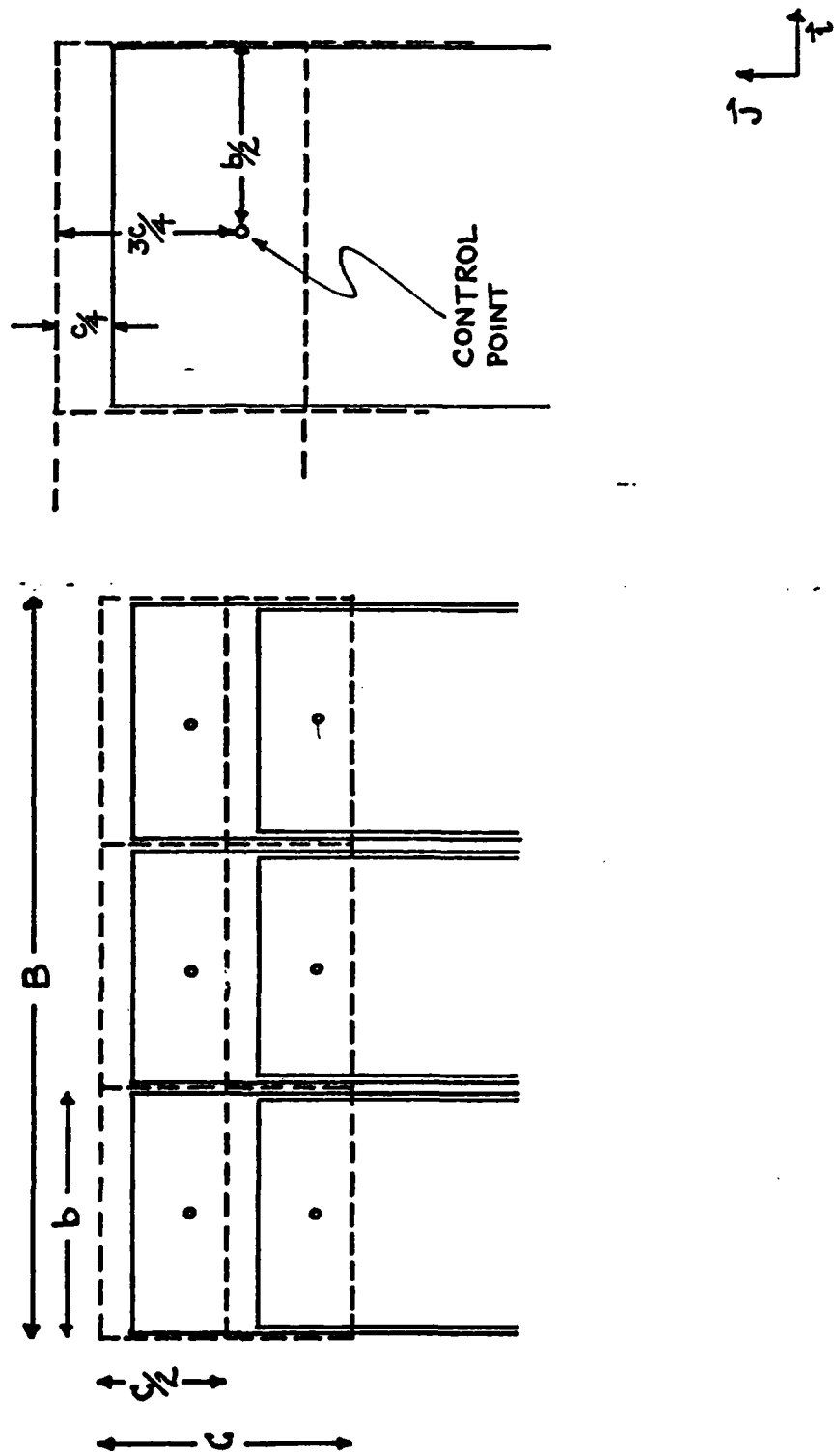
Fig 14. Lattice Configuration for 3 x 2 Panel Distribution

94
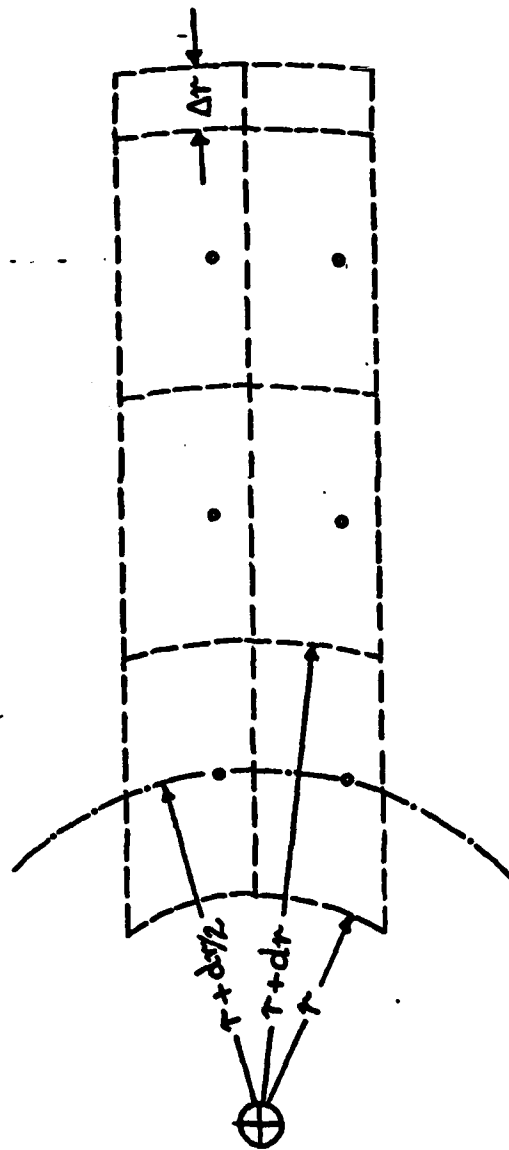
Fig 15. Lattice Configuration for Propeller
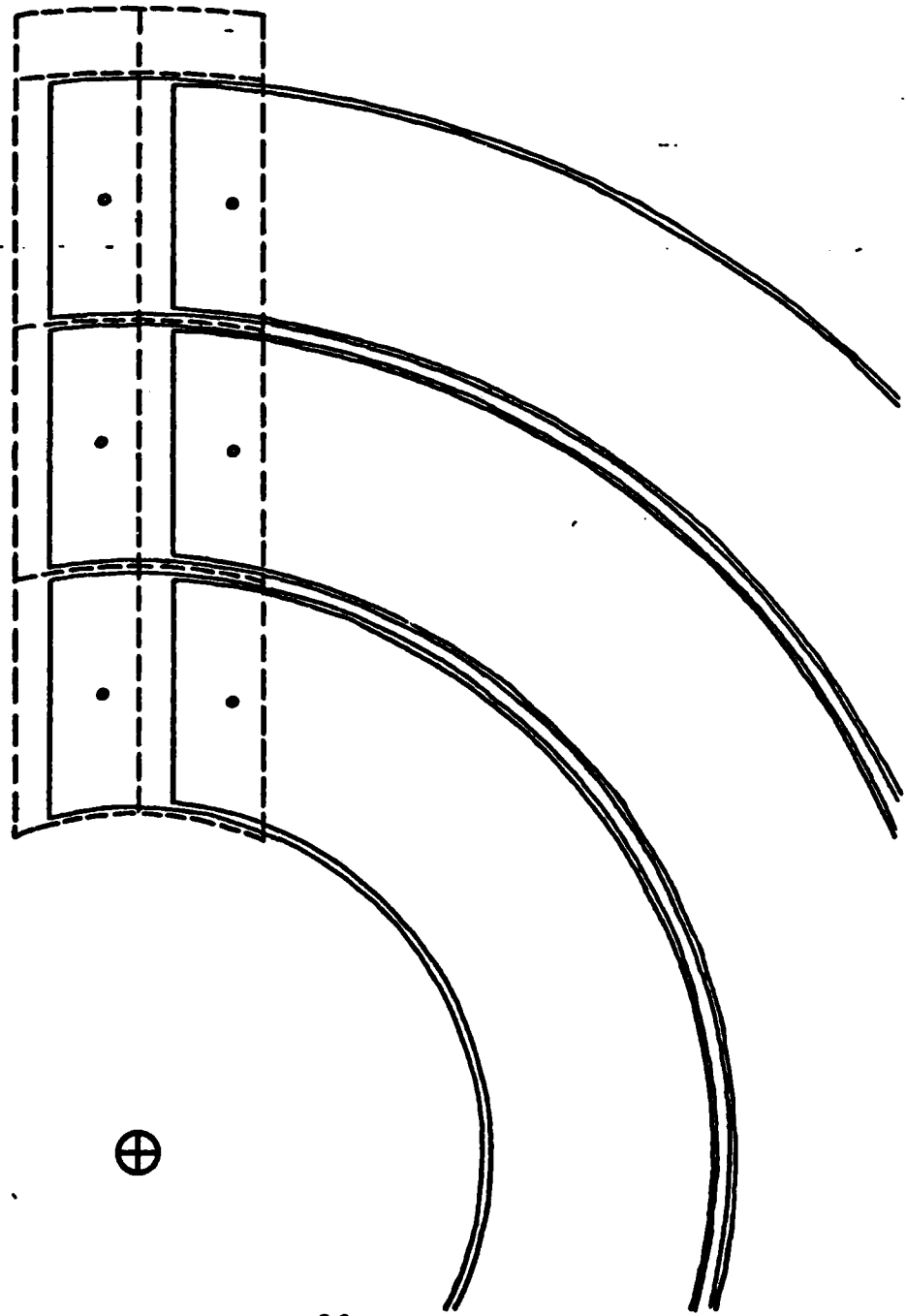
Fig 16.  Lattice Configuration and Trailing Filaments for Propeller

96

Axis of Rotation

Blade section at angle
of attack

$V_{TOT}$

$\alpha$

$U_\infty$

$r\omega$
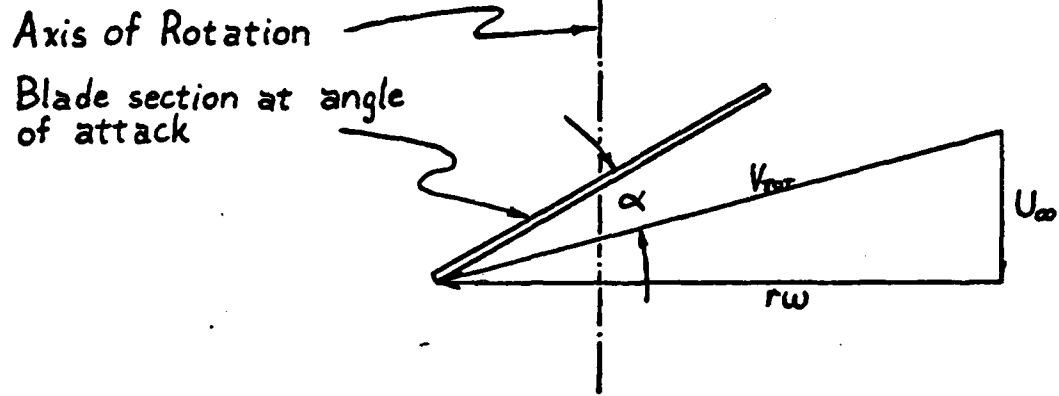
MODELED CONDITION
Straight wake, parallel to
total velocity vector

$\alpha$
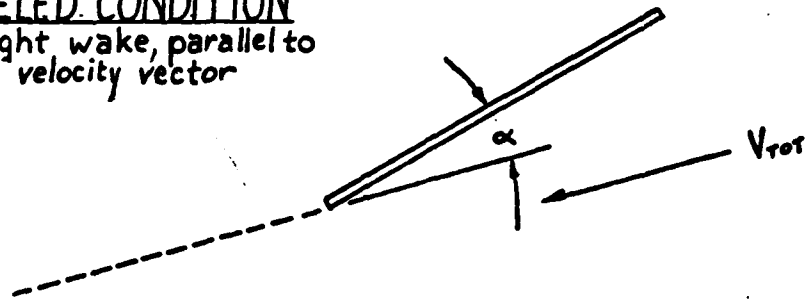
$V_{TOT}$

ACTUAL CONDITION
Curved wake, asymptotically
becomes parallel to $V_{TOT}$ vector

$V_{TOT} \cdot \cos\alpha$

$\alpha$

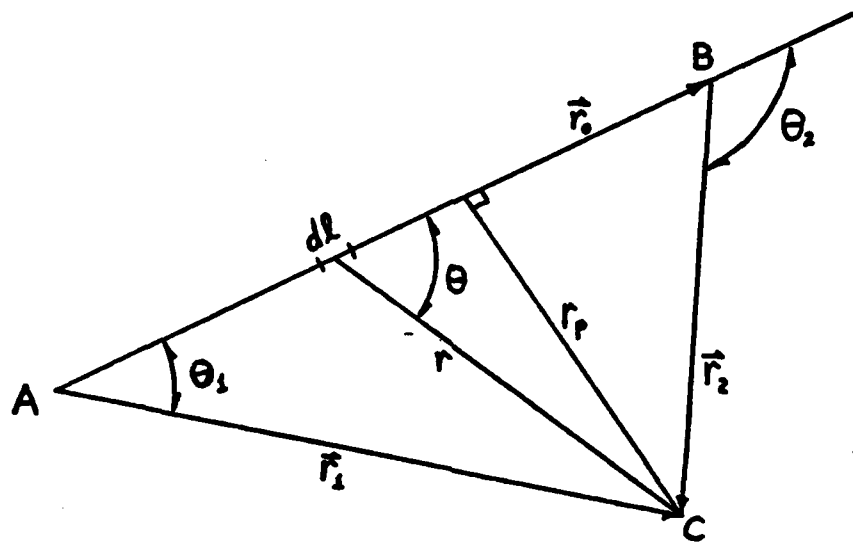$V_{TOT}$

$\vec{k}$

$\vec{j}$
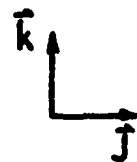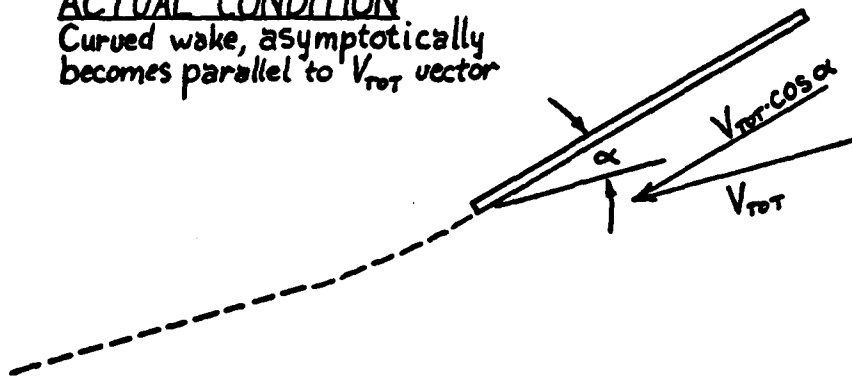
Fig 17. Wake Model for Propeller
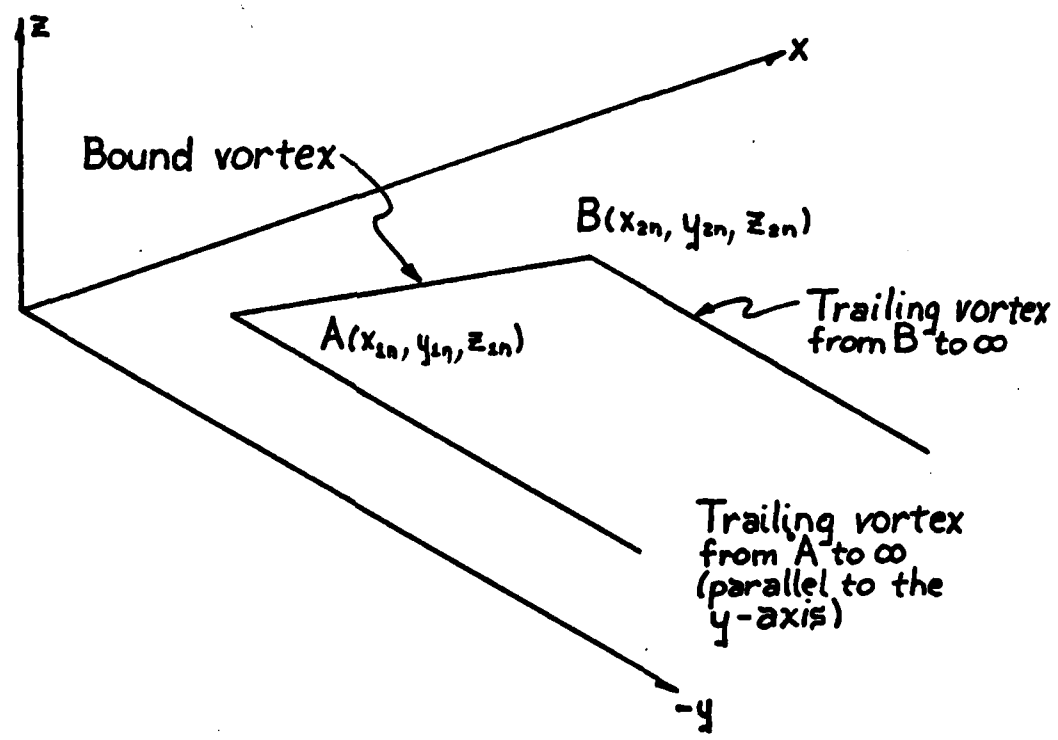
Fig 18.   Nomenclature for a Finite Length Vortex Segment

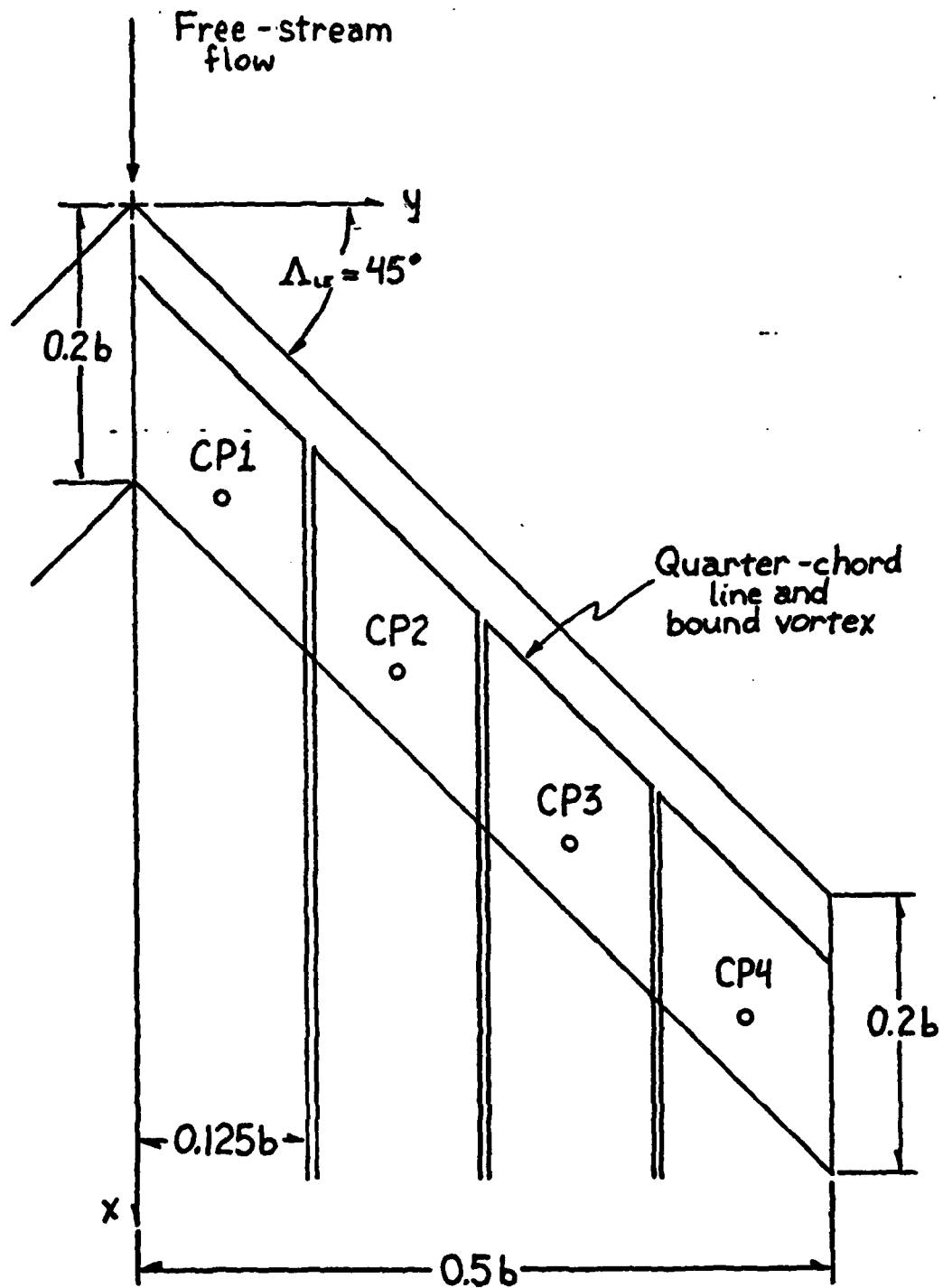**Fig 19.   Four-Panel Representation of a Swept, Planar Wing**

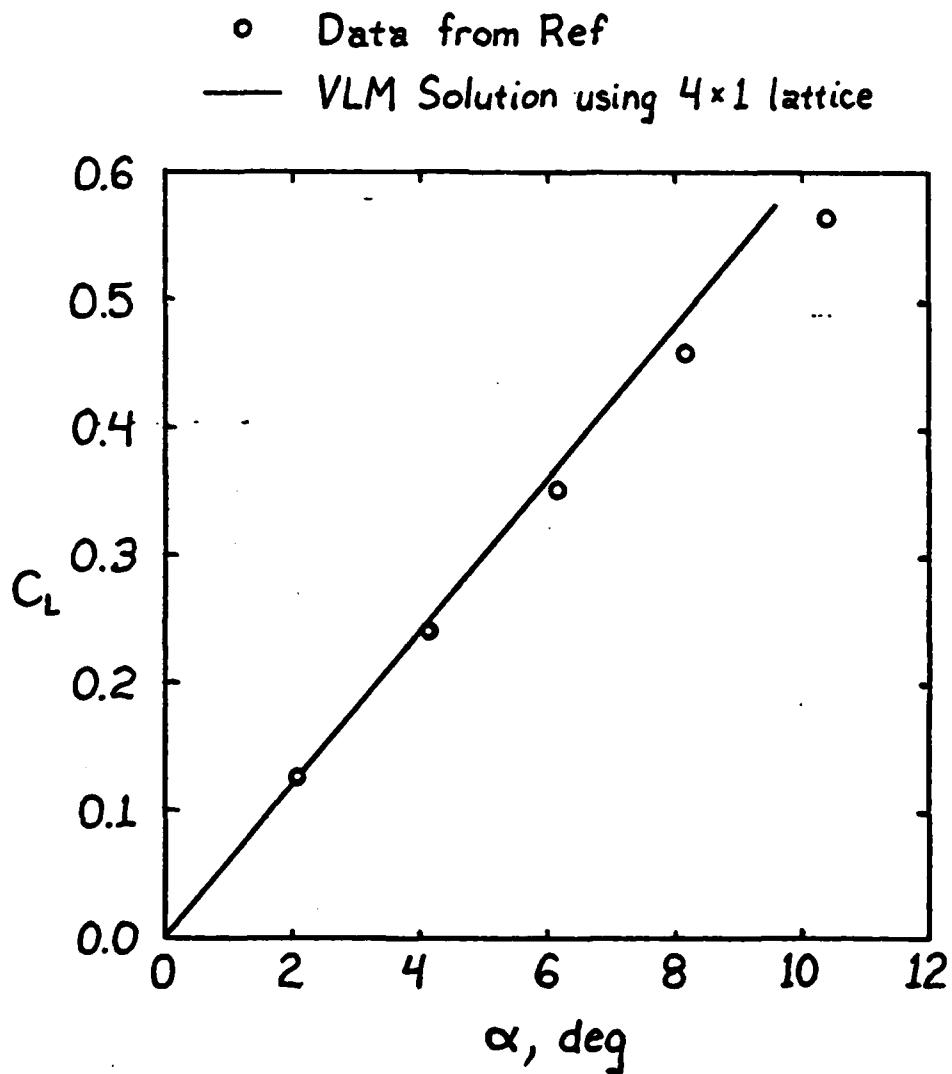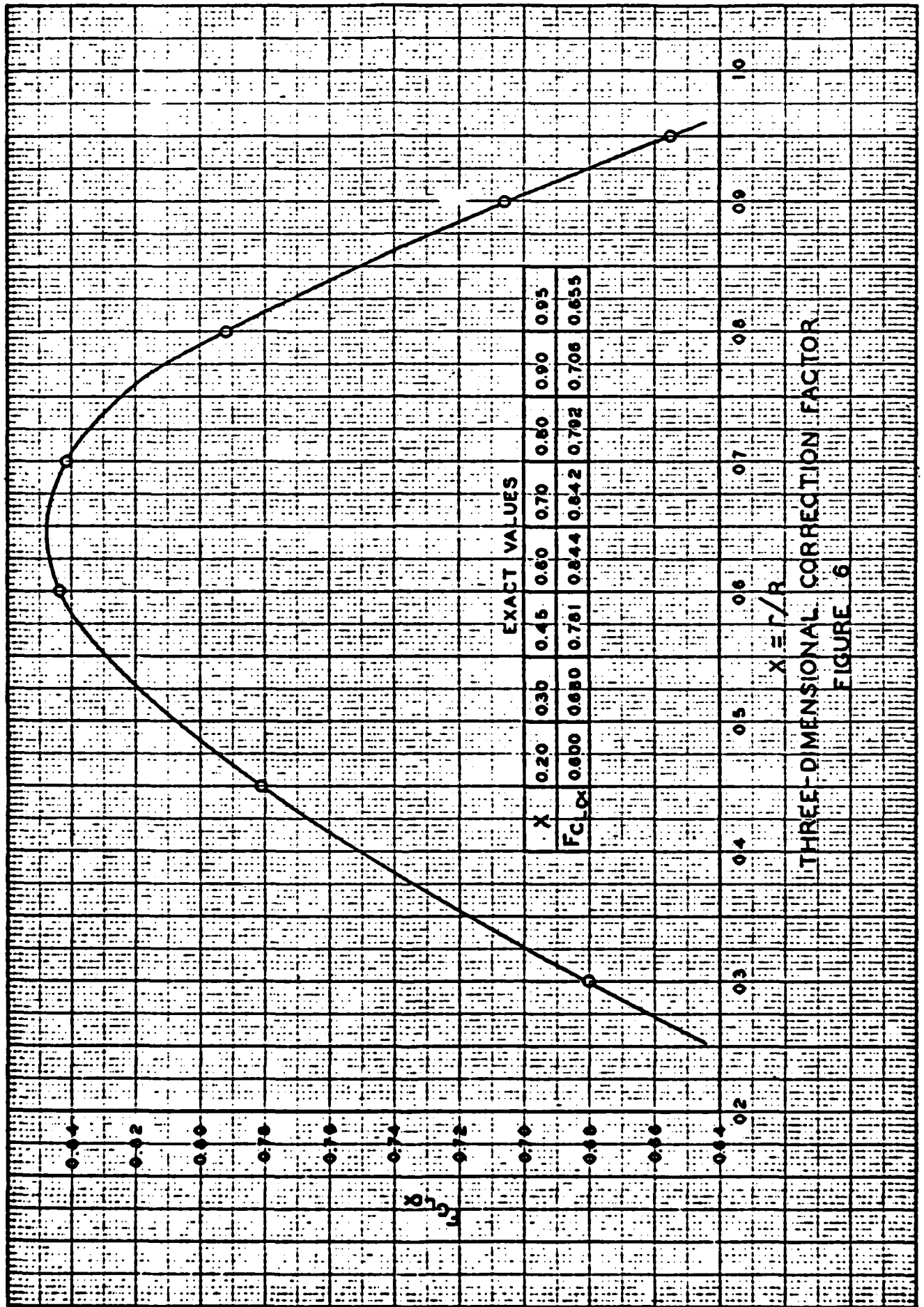Fig 20. Theoretical vs. Experimental Lift Coefficients for the Wing of Fig 19

| X | 0.20 | 0.30 | 0.45 | 0.60 | 0.70 | 0.80 | 0.90 | 0.95 |
|---|------|------|------|------|------|------|------|------|
| $F_{CL_\alpha}$ | 0.600 | 0.650 | 0.701 | 0.844 | 0.842 | 0.792 | 0.706 | 0.655 |

EXACT VALUES

$X = r/R$

THREE-DIMENSIONAL CORRECTION FACTOR

FIGURE 6

Fig. 21. Lift Coefficient Correction Factor

101